ENERGY OPTIMAL PATH PLANNING OF AN UNMANNED SOLAR POWERED AIRCRAFT

A THESIS SUBMITTED TO
THE GRADUATE SCHOOL OF NATURAL AND APPLIED SCIENCES
OF
MIDDLE EAST TECHNICAL UNIVERSITY

BY

ERDEM EMRE PINAR

IN PARTIAL FULFILLMENT OF THE REQUIREMENTS
FOR
THE DEGREE OF MASTER OF SCIENCE
IN
MECHANICAL ENGINEERING

JANUARY 2013

Approval of the thesis:

ENERGY OPTIMAL PATH PLANNING OF AN UNMANNED SOLAR POWERED AIRCRAFT

submitted by **ERDEM EMRE PINAR** in partial fulfillment of the requirements for the degree of **Master of Science in Mechanical Engineering Department, Middle East Technical University** by,

Prof. Dr. Canan Özgen _____
Dean, Graduate School of **Natural and Applied Sciences**

Prof. Dr. Suha Oral _____
Head of Department, **Mechanical Engineering**

Assoc. Prof. Dr. Derek K. Baker _____
Supervisor, **Mechanical Engineering Dept., METU**

Assist. Prof. Dr. Eray Uzgören _____
Co-Supervisor, **Mechanical Eng. Dept., METU-NCC**

Examining Committee Members:

Prof. Dr. Reşit Soylu _____
Mechanical Engineering Dept., METU

Assoc. Prof. Dr. Derek K. Baker _____
Mechanical Engineering Dept., METU

Assoc. Prof. Dr. Nurdan Sankır _____
Mat. Sc. and Nanotechnology Engineering Dept., TOBB-ETU

Assist. Prof. Dr. Eray Uzgören _____
Mechanical Engineering Dept., METU-NCC

Instructor Dr. Özgür Bayer _____
Mechanical Engineering Dept., METU

Date: 18 – 01 – 2013

I hereby declare that all information in this document has been obtained and presented in accordance with academic rules and ethical conduct. I also declare that, as required by these rules and conduct, I have fully cited and referenced all material and results that are not original to this work.

Name, Last name : Erdem Emre PINAR

Signature :

ABSTRACT

ENERGY OPTIMAL PATH PLANNING OF AN UNMANNED SOLAR POWERED AIRCRAFT

Pınar, Erdem Emre

M.Sc., Department of Mechanical Engineering

Supervisor: Assoc. Prof. Dr. Derek K. Baker

Co-Supervisor: Assist. Prof. Dr. Eray Uzgören

January 2013, 98 pages

In this thesis, energy optimal route of an unmanned solar powered air vehicle is obtained for the given mission constraints in order to sustain the maximum energy balance. The mission scenario and the constraints of the solar powered UAV are defined. Equations of motion are obtained for the UAV with respect to the chosen structural properties and aerodynamic parameters to achieve the given mission. Energy income and loss equations that state the energy balance, up to the position of the UAV inside the atmosphere are defined. The mathematical model and the cost function are defined according to the mission constraints, flight mechanics and energy balance equations to obtain the energy optimal path of the UAV. An available optimal control technique is chosen up to the mathematical model and the cost function in order to make the optimization. Energy optimal path of the UAV is presented with the other useful results. Optimal route and the other results are criticized by checking them with the critical positions of the sun rays.

Keywords: Solar Energy Utilization, Unmanned Air Vehicle, Energy Optimization, Flight Mechanics, Flight Path Planning, Optimal Control.

ÖZ

GÜNEŞ ENERJİSİNDEN FAYDALANAN BİR İNSANSIZ HAVA ARACININ OPTİMUM ENERJİYİ SAĞLAYACAK ROTA PLANLAMASI

Pınar, Erdem Emre

Yüksek Lisans, Makina Mühendisliği Bölümü

Tez Yöneticisi: Doç. Dr. Derek K. Baker

Ortak Tez Yöneticisi: Yrd. Doç. Dr. Eray Uzgören

Ocak 2013, 98 sayfa

Bu çalışmada, Güneş Enerjisi ile çalışan bir insansız hava aracının, verilen görevi en yüksek enerji dengesi ile tamamlamasını sağlamak üzere rota planlaması yapılmaktadır. Güneş Enerjisi ile çalışan İHA'nın görev senaryosu ve kısıtları belirlenmiştir. Belirlenen görev kısıtlarına göre yapısal özellikleri ve aerodinamik değiştirgeleri seçilen İHA için uygun hareket denklemleri çıkarılmıştır. İHA'nın atmosferdeki pozisyonuna göre enerji dengesini belirleyecek enerji kazancı ve enerji kaybı denklemleri türetilmiştir. Belirtilen görev kısıtları, uçuş mekaniği ve enerji dengesi denklemlerine göre İHA'nın enerji dengesini en çoklayacak matematiksel model ve amaç fonksiyonu oluşturulmuştur. Oluşturulan bu matematiksel model ve amaç fonksiyonuna göre uygun bir optimal kontrol tekniği belirlenmiş ve eniyileme çalışması yürütülmüştür. Görev şartları ve yapısal özellikleri belirlenen İHA için görev sonu depolanacak enerjiyi en çoklayacak uçuş rotası belirlenmiştir. Planlanan uçuş rotası ve elde edilen diğer sonuçlar sunulmuştur. Belirlenen rota ve diğer sonuçlar, Güneş ışınlarının kritik geliş açılarına göre irdelenmiştir.

Anahtar kelimeler: Güneş Enerjisi Çevrimi, İnsansız Hava Aracı, Enerji En İyilemesi, Uçuş Mekaniği, Rota Planlaması, Optimal Kontrol.

Dedicated to the Memory of
Necmiye Erdem…

ACKNOWLEDGEMENTS

First, I express my sincere appreciation to my thesis supervisor Assoc. Prof. Dr. Derek BAKER and co-supervisor Assist. Prof. Dr. Eray UZGÖREN. Their guidance, encouragement and advices for the entire progress of this thesis study, keep me going.

I would like to thank my family for having supported me throughout my life with patience and love. In addition to my family, I must thank to my sincere friends Çağlar ULUKAN and Samet KONU for backing up me in any case.

This thesis would not have been possible without the great support of my company so I gratefully acknowledge ASELSAN Inc.

I am greatly indebted to my design leader Suphi YILMAZ and manager Tahir FİDAN for their high patience and support for the entire thesis study.

Additionally, I would like to state my thanks to Zafer ERKAL for assisting me about academic writing with his valuable experience, Mert ATASOY for helping me in the critical stages of coding and Ali OKUŞLUĞ for revealing me working on solar powered aircrafts and dynamic programming.

I can never forget the help of Koray TAŞTANKAYA who accompanied my studies on solar energy conversion also contribution of Yusuf Okan PEKEL and Serkan KAYMAK with their high knowledge on flight mechanics.

I am also appreciated to my colleagues, Cengiz ALEMDAROĞLU, Okan ÇINAR, Duygu ÜRÜN, Süha Doruk KADIOĞLU, Kerem Furkan ÇİÇEK and Sercan SOYSAL for their understanding and help.

Finally, I would like to state my deepest gratitude to Mustafa Kemal ATATÜRK since inspiring me and my studies with his immortal idea.

TABLE OF CONTENTS

LIST OF TABLES

TABLES

LIST OF FIGURES

FIGURES

LIST OF SYMBOLS

a	acceleration (m s^{-2})
b	wing span (m)
a_{sc}	area of the solar cells (m^2)
C_l	coefficient of lift
C_d	coefficient of drag
$C_{D\text{afl}}$	airfoil drag coefficient
$C_{D\text{par}}$	parasitic drag coefficient
D	drag force (N)
e	Oswald's efficiency factor
F	force (N)
F_r	centrifugal force (N)
G	solar irradiance (W)
G_{sc}	solar constant (W m^{-2})
g	gravitational acceleration (m s^{-2})
J	performance measure
h	terminal performance measure
I_{max}	maximum irradiance (W m^{-2})
k_{bat}	energy density of lithium-ion
k_{sc}	mass density of solar cells
k_{enc}	mass density of encapsulation
k_{mppt}	mass to power ratio of MPPT
k_{prop}	mass to power ratio of propeller
k_{af}	structural mass constant
K	repeating times of the half of a full tour between two grid points
L	lift force (N)
m	mass (kg)
n	day of the year
P	power (W)
Q	positive weighting matrix
r	desired state
R	turning radius of the aircraft (m)
S	area of the wings (m^2)
t	time (s)
t_{tr}	travel time (s)
T	thrust force (N)
u	control parameter
W	weight (N)
x	position (m)
x_g	length between two grid points
x_t	the distance that aircraft travels between two grid points
X	x coordinate
V_∞	velocity of the aircraft (m s^{-1})
Y	y coordinate

Z	z coordinate

Greek Symbol

α_s	solar altitude angle
β	angle of slope for solar panels
γ	surface azimuth angle
γ_s	solar azimuth angle
δ	solar declination angle
ε	angle that aircraft travels between two grid points
η	efficiency
η_{wthr}	irradiance margin factor
θ	solar incidence angle
θ_Z	zenith angle
Θ	pitch angle
ρ	air density (kg m^{-3})
ω	hour angle
ϕ	latitude
Φ	roll angle
ψ	surface azimuth angle
Γ	dihedral angle

Subscripts

01	single stage decision problem
av	auto pilot system
aver	average
b	beam
bec	step down converter
B	body
c	central wing
cbr	curved solar panels
chrg	battery charge
ctrl	controller
dchrg	battery discharge
d	diffuse
f, 1	final
i, 0	initial
in	income
E	earth
grb	gear box
k	aerodynamic ratio
l	left wing
mot	motor
out	consumption
pld	payload
pr	propeller
r	right wing
sc	solar cells

Abbreviations

AR	aspect ratio
ERAST	environmental research aircraft sensor technology
IC	inner cost
IT	inner time
MPPT	maximum power point tracker
NASA	national aeronautics and space administration
NC	nodal cost
PV	photovoltaic
ST	solar time
UAV	unmanned air vehicle

CHAPTER 1

INTRODUCTION

Internal combustion engines and gas turbines have always been the main power suppliers of modern aircrafts. Improvements in gas turbine technology after the Second World War had significant effects on the performance of air vehicles. In recent years, the possibility of utilizing unconventional energy in aviation field has been evaluated as an alternative to hydrocarbon consuming aircrafts by several research groups and inventors.

In this thesis, energy optimal path planning of an unmanned solar powered air vehicle is analyzed. Particularly, the possibility of improving the range of the aircraft by making an optimization between mission and time constraints is researched rather than examining improvements on sub-systems or components of the air vehicle.

Motivation for the thesis study will be explained in the beginning of this chapter. A brief history of solar energy utilization in the aviation field will be summarized in the literature survey sub-section of this chapter. Moreover, general information about the studies on sub-system design, potential missions and improvements will be given in the literature survey. Relevant studies which are focused on energy optimal path planning of the solar powered aircrafts are also summarized in the literature review. The objective and scope of the thesis are given at the end of the chapter.

1.1 Motivation

Although some attempts have been made by different research groups, unconventional energy sources have never been perceived as a serious alternative to traditional energy sources for aviation up to the early 1990's. As Nam et al. [1] state, "Only a few attempts have reminded the aerospace community of the obvious but not always apparent fact that aircraft can be powered by different energy sources or different power generation devices".

In the recent years, as a result of attention on the renewable and sustainable energy sources, unconventional energy applications like solar powered aircrafts have become an interesting research field for aviation. Revolutionary structural designs have been coupled with solar cells or fuel cells. Pioneering electrical system design and advanced technology electronic devices have equipped solar powered aircrafts with high capacity batteries. Also, various design, estimation, analysis and simulation methods have been developed which specialize on unconventional energy consuming aircrafts like solar powered

aircrafts. These methods generate the scientific base for advanced solar powered aircrafts which have more structural strength, higher efficiency and longer endurance relative to former ones. To sum up, it is very clear that, solar powered aircrafts have gained a strong position in the aviation field in the last thirty years and promise a bright future.

Design and development of solar powered aircraft have become an interesting issue due to increasing environmental consciousness and improvements in solar powered energy conversion. It is very critical to achieve the integration of the solar energy in aerospace industry in long term future to reduce carbon emissions since aerospace industry has a significant role in global fossil fuel consumption. In addition to the environmental benefits, possibility to accomplish some extreme missions is going to be realized due to the use of solar energy in aviation. Solar powered aircrafts have a chance to sustain 24 hour flight with optimum power system, mission and aircraft design. Also, since non-air breathing solar powered engines do not have any exhaust gases, it is very hard to be fixed by thermal sensors and is more convenient to work together with the measuring systems on atmospheric test airplanes. From this point of view, it is convenient to state that, the connection of the solar power conversion systems with aerospace vehicles is going to be an area undergoing rapid development in the aviation field in the future.

As mentioned, the most significant advantage of using unconventional energy sources, like solar energy in aerospace industry is its considerable effect on reducing carbon dioxide emissions. Although it does not seem to be feasible to apply solar energy systems in commercial airplanes in mid-term future, promising developments in solar powered aircrafts in last twenty years give hope about long-term future applications [1]. Apart from environmental benefits, utilizing solar power energy in aircrafts is going to present various advantages in near-term future. Especially unmanned solar powered aircrafts are suitable to use in many different commercial and non-commercial applications as well as offering innovations in existing applications.

According to Landis et al. [2] efficient and low-cost solutions for scientific missions can be supplied by solar-powered aircrafts. An eternal flight theoretically could be achieved by solar powered aircrafts and this factor makes solar powered aircrafts a prime choice for long duration missions. Additionally, solar powered aircrafts could be an ideal alternative for military applications which are presently done by hydrocarbon fueled unmanned aircrafts. Since a solar powered aircraft can theoretically keep flying all day long; there is no fuel cost, noise limitations of electrical engines are very low and there is no exhaust gas which may be fixed by thermal sensors, it appears as a perfect platform for intelligence missions and some other military applications.

1.2 Literature Review

Although, there were some studies related with utilizing solar energy in aviation before the 1980's, most of the important researches that focus on this subject have occurred over the last thirty years.

The National Aeronautics and Space Administration (NASA) is one of the major associations which is related with solar energy utilization in aerospace vehicles starting from the 1960's since their satellite projects involved solar energy utilization. After the 1990's, studies of NASA continued with researches on designs of solar powered aircrafts

which are able to flight on Venus, Mars and Earth. As a result, NASA has many publications about the design, analysis and applications of solar power energy usage in the aerospace field [2]. Additionally, universities mostly from the United States, Switzerland and the European Union have several significant studies about solar energy applications in the aero-space field [3]. Although most of these studies are related with the design of solar powered airplanes, some also address energy optimal path planning of various flight scenarios [4]. Furthermore, some studies are related with interesting commercial and non-commercial applications of solar powered aircrafts [5].

Although, there had been some electrically powered flight attempts before, the use of solar power in small scale model planes started with the birth of photovoltaic technology in 1954, at Bell Telephone Laboratories. Trailblazer model solar powered aircrafts "Sunrise I" and "Sunrise II" from the United States made their first flights in the first half of the 1970's. The dream of solar powered flight continued in Europe with the flight of "Solaris" in August 1976. The duration of the solar powered flight has been risen rapidly with the further solar aircrafts like "Solar Solitude" and "Solar Excel" [3].

With the proven feasibility of small scale unmanned model aircrafts, researches on manned solar powered flight have started to become widespread in the aviation field. "Solar Riser" achieved a manned flight with solar energy utilization in April 1979. On the other hand, energy of the sun was not sufficient to manage the flight of "Solar Riser" without the help of the nickel-cadmium batteries. This milestone was achieved with the "Gossamer Penguin" in May 1980. The flight of the "Gossamer Penguin" is shown in the Figure 1.1 and it is accepted as the first manned solar energy powered flight [3].

Development of the manned and solar powered airplanes continued with the "Solar Challenger" achieved to fly from Paris to London on July 1981 without any energy storage system. "Sunseeker", "Icaré 2" and "Solair II" were the other significant solar powered aircraft designs at the end of the 1980's [3].

Apart from the manned flight attempts for solar powered aircrafts, high altitude long endurance eternal flights are aimed to get realized by solar powered aircraft designers and especially by NASA. The solar powered aircrafts "Pathfinder", "Pathfinder Plus", "Centurion" and "Helios" were built by NASA for the program of Research Aircraft Sensor Technology (ERAST). "Helios" was the last plane in NASA solar powered aircraft series and was made to achieve two essential aims. The first was making a sustained flight at 30,480 m, and the second was to fly non-stop for 24 hours. "Helios" achieved her first goal, but was unable to achieve her second mission because of structural failures. One of the successful flights of the "Helios" is shown in the Figure 1.2 [3].

Figure 1.1 Gossamer Penguin **[3]**

Figure 1.2 Helios **[3]**

The second goal of "Helios" was later achieved by another unmanned solar powered aircraft "Solong" by making a 24 hours and 11 minutes flight. After this first 24 hours flight, the "Zephyr" broke the longest sustained unmanned solar powered flight record by flying for 54 hours in September 2007 [3].

An important goal for solar powered aircrafts has always been to achieve a continuous flight for 24 hours with a manned aircraft. The Swiss aircraft, "Solar Impulse" has shown that a solar powered air vehicle is capable of making an all-night flight by flying for 26 hours in June 2010. New goal for "Solar Impulse" is to fly around the world [6].

Figure 1.3 Solar Impulse **[6]**

A brief history of solar power energy applications in aviation has been presented. As a more relevant subject to the objective of this thesis, three studies about "energy optimal path planning" of different mission scenarios for solar powered aircrafts are published ([4], [7], [8]).

Klesh and Kabamba [4] published a forerunner paper about "Energy-Optimal Path Planning for Solar-Powered Aircraft in Level Flight" in 2007. The study mainly indicates the role of the banking angle on the energy balance of a solar powered aircraft and the effect of the bank angle on the aircraft kinematics is examined in order to reach the optimal path of the solar powered aircraft. An aircraft kinematic model, energy collection model and energy loss model are examined. The mission is described; optimization problem is presented and the equations required to provide the optimal paths are derived. The problem is divided into small parts to get a numerical approximation and graph of the energy optimal path is drawn. The paper concludes by giving the experimental connection of the power-ratio with energy-ratio and a summary of extreme paths. According to the

authors, the most important result of this study is showing the increase of energy collection by both efficient design and optimal path planning for a solar powered aircraft.

Another study of Klesh and Kabamba [7] is related with "Energy-Optimal Path Planning and Perpetual Endurance". The selected solar powered aircraft design concept is the same as the plane in the former paper. It is an unmanned solar powered aircraft which has solar cells on the wings. As a difference from the former study, this paper is interested in two different missions. The first is traveling between two different points within an allowed duration while maximizing the final energy and the second is to loiter perpetually over a given position. Again, relation with energy balance and aircraft kinematics is used for optimization. Although general sections of paper which form the optimization process are very similar with the former study, some modifications are done in order to enable the optimization of two different missions. Also, the difference in total energy balance between the optimal flight trajectory and direct flight is estimated in this paper. As a major addition, a comparison of the design requirements between Earth and Mars is made.

Spangelo et al. [8] studied "Periodic Energy-Optimal Path Planning for Solar-Powered Aircraft". As an important difference with the other two papers, altitude is taken into account in this paper. In the former two studies altitude is constant so the flight path is on a plane without ascending and descending. In this study, the solar powered aircraft flies along the surface of a vertical cylinder. Prior to this study, authors have not studied pitching maneuvers of aircraft. The main contribution of this paper is developing a new "spline-based optimization" process in periodic and cylindrical constraints. Another important contribution of this thesis to the literature is the analysis of flight angles, velocity, forces and power in time. On the other hand, air-density and the position of the sun is assumed to be constant in this study although air-density changes with altitude and the position of the sun changes continuously in the sky with time.

An important common point for these three papers related with energy optimal path planning is presenting a very useful literature survey. This literature survey sheds light on the history of energy related studies on solar powered aircrafts. Apart from energy related studies, a significant database of knowledge and know-how has been developed about solar powered aircrafts which are related with their design, analysis, optimizations and different applications.

Rizzo and Frediani [9] developed a preliminary design model of a high altitude long endurance solar powered aircraft. They aimed to form a mathematical model for the preliminary design of this solar powered aircraft which was also useful to compare the following four different aircraft configurations flying wing; conventional aircraft; twin boom aircraft; and biplane aircraft. They validated their mathematical model according to the Helios platform of NASA. After validation, they used their validated mathematical model in order to compare four different aircraft configurations.

Colozza [10] worked on the "Effect of Power System Technology and Mission Requirements on High Altitude Long Endurance Aircraft" in 1993. His aim in this study was determining the effect of the different power system components and mission requirements on the sizing of solar powered long endurance aircraft. The scheme of the propulsion and the power system has been shown clearly and then a weight estimation of all components was done. Changes in wing area and wing span by aspect ratio are given

for different fuel cells and photovoltaic cells at different altitudes are given in graphs as a result of this study. This paper is very useful to examine the effect of PV cells and fuel cells on structural parameters of a solar powered aircraft.

In 1998, Colozza et al. [11] examined the application of a specific type of space solar cells in solar powered aircrafts. The authors mentioned about the aircraft design, material selection, flight tests (in order to determine flight worthiness) and the remote control system of this aircraft in the paper. Furthermore, the performance of the solar array and power system (which consists of an 11 cell nickel-cadmium battery and solar array) are examined. Authors mentioned about the solutions for condensation problems related with solar arrays.

In addition to the design and the analysis of solar powered aircrafts and its sub-systems, also some specific issues like the effects of flight types on endurance have been examined by researchers. For instance, Chichka and Speyer [12] investigated the positive effect of formation flight on solar powered aircrafts for sustained endurance. According to them, "it is theoretically possible to create a formation flight system that is capable of truly infinite endurance". With this study they mainly indicated the important effect of high aspect ratio wings and formation flight on decreasing the effect of induced drag for aircrafts.

As a different example of interesting issues which have been studied by solar powered aircraft researchers, a commercial application of a solar powered unmanned aircraft is examined by Herwitz et al. [5]. They used the "Pathfinder Plus" in order to help precision agriculture activities. A real time imaging system which was mounted on a solar powered aircraft guides mechanical harvesters in this application. Although telemetry system and image analysis were primarily studied, some structural issues like payload tests and structural properties are examined in some parts of this study.

Atmospheric risks such as turbulence, cloud cover, runway winds and excess wind drift at altitudes aloft are experienced for the flights of the "Pathfinder", "Pathfinder Plus" and "Helios" and analyzed in the paper of Ehernberger et al. [13]. They also gave the record of weather events from June 1997 to June 2003 according to altitudes. According to the authors, "results of this tests and analyses, advance in airframe design, solar cell efficiency, batteries and fuel cells are demonstrating new approaches to high-altitude long-endurance aircraft for applications to earth observations, communications and atmospheric sciences".

In 2008, Noth [3] studied solar powered airplanes for continuous flight. He developed mathematical models for requirements of daily electrical energy, daily solar energy gain, and mass predictions of components and studied "Sky-Sailor" which is aimed to fly over 24 hours for any day over 3 months period in summer. Also, real time simulation environment model of solar flight is examined. Transition from preliminary design to detailed design is the general scope of this section with manufacturing and validations by tests. Structure details, airfoil selection, propulsion group (propeller, motor, gearbox and motor controller), control surface actuators, battery, solar generator, control and navigation system and ground control station are all designed comprehensively in this thesis study. Results from a continuous 27 hours test flight is presented and used to validate the theoretical parts of this research.

Figure 1.4 Sky-Sailor **[3]**

As into solar powered aircrafts has increased rapidly with time, the necessity for specialized design, analysis and estimation methods have increased. Nam et al. [1] developed a power based sizing method which is more suitable for unconventional energy consuming aircrafts. Before this study, traditional sizing methods for aircrafts were most suitable for hydrocarbon fuel consuming aircrafts. One of the major differences between hydrocarbon and solar powered aircrafts is that the weight of the consumable energy (hydrocarbon fuel) changes during the flight for hydrocarbon powered aircrafts but there is no change in the weight for solar powered aircrafts.

Landis et al.[2] examined the feasibility of an atmospheric flight on Venus with a solar powered aircraft. They investigated the critical design parameters of aircraft which are based on power requirement and aero-shell. Mass estimation and brief information about some sub-systems like propeller and electric motor are given., efficiency of the aircraft and effect of aspect ratio on solar powered aircrafts were examined.

The goal for another NASA funded study [14] is to confirm the availability of solar utilization in the propulsion system of an aircraft. It is planned to sustain a one hour flight in a "figure eight" flight path at an altitude of 50 meters. The initial altitude of the flight is obtained with a launching catapult system. Configuration of the solar powered aircraft is defined as "a non-conventional, high-wing aircraft with two carbon fiber composite supports…" in the paper. The design properties of the power system and fuselage, general dimensions and parameters of the aircraft and quantitative properties of control surfaces

are indicated. Aircraft sizing and weight estimation is done by stating the mass of all components. Airfoils of wing and tails, planform type and optimum operational points are chosen according to aerodynamic design and analysis. Structural design details are explained by mainly giving the details about material selection. Nickel cadmium batteries are selected to serve as a secondary power source supplement the power from solar cells in critical maneuvers. Several motor-propeller combinations were tested in wind tunnels and the most suitable configuration is selected according to the test results. The construction procedure of the aircraft is explained.

1.3 Objective

The objective of this thesis is to estimate the energy-optimal path of a small scale unmanned solar powered aircraft which is flying at a constant altitude. Similar energy optimal route planning studies in the literature ([4], [7], [8]) aim to plan the path for very limited timelines for which the location of the sun can be approximated as being fixed. The objective of this thesis differs from these previous studies by aiming to make path planning for a long timeline, which requires the motion of the sun to be included in the optimization routine. One of the most important objectives of this study is a novel optimization model to obtain the energy optimal path for long endurance flights. This new model is to be used to perform parametric studies for several important parameters and values related to the flight. Simulations are to be performed for different positions of the sun for representative days of the year and the results critically assessed and compared to evaluate the performance of the optimization algorithm.

1.4 Scope of the Thesis

The mission altitude of the aircraft is considered to be constant so the aircraft is free of any change in the pitch angle. The altitude of the mission is high enough to avoid the effects of clouds on solar resources. Also the air density and gravitational acceleration is accepted to be constant since the altitude of the aircraft does not change.

Design parameters and aerodynamic coefficients of the aircraft are taken directly from a similar aircraft which is assumed to be capable of achieving a similar mission so structural or performance criteria of the aircraft do not be examined in this thesis study.

Efficiencies of the step-down converter, battery charge, motor controller, battery discharge and maximum power point tracker are assumed to be perfect although their actual values are given in the introduction of the selected aircraft design. These parameters do not affect the idea of the optimization and their actual efficiencies are close to perfect.

Although the coefficient of the lift is indicated by the designer of the aircraft as 0.8, it depends on the angle of the attack. This value is assumed to be average of a level flight and can differ in the calculations of optimization.

The roll motion capability of the aircraft is limited and is defined in the thesis. But the resulting yaw motion can have extreme values in some critical nodes in this thesis study in spite of having some certain limits similar to roll angle in reality. Since the objective of the thesis is making a global energy optimization, local extreme values of the yaw angles do not have a significant effect on the result and can be tolerated.

The aircraft is assumed to make steady state turning flight or level flight between nodes. For level flight the aircraft flies with zero roll angles. The velocity of the aircraft is also assumed to be constant between nodes.

Mission constraints such as initial and final points of the travel are the inputs of the optimization process and are user defined. The date and beginning time of the travel should also be identified by the user similar to the grid structure of the optimization.

1.5 Thesis Overview

In Chapter 1, history of the solar powered flights, summary of the related literature and basic information about the main subjects which this thesis study includes are given. In Chapter 2, detailed information about the theory of the optimization is given. In Chapter 3, the mathematical model behind the optimization idea is indicated. Significant results are presented in Chapter 4. In the final chapter, suggestions for future studies are summarized.

CHAPTER 2

BASIC CONCEPTS

Solar based energy optimal path planning is a multidisciplinary subject that concerns mainly solar energy utilization, flight mechanics and optimal control theory. Each of these subjects is examined in this chapter as they are the main fields that form this thesis study. Solar energy utilization is basically related with the geometric relation of the sun and earth, structure of the sun light and the technology for the solar energy conversion. Flight mechanics deals with the motion and performance of the aircraft for the different flight scenarios. Optimal control theory is used directly to find an appropriate solution for different kinds of optimization problems.

Solar energy utilization mainly quantifies the potential and availability of solar energy. Additionally, technologic developments are directly related with the research area of solar energy utilization. Indicating basic definitions and concepts are required to evaluate the potential of the solar energy. Geometric relations of earth and sun affect the availability of the solar energy directly similar to atmospheric effects. Technologic properties of the solar cells are also essential for the conversion of solar energy to the electricity.

The theory of the flight mechanics is based on Newton's Second Law ($F = m.a$) and studies the motion of the aircraft by focusing on forces and controls. It is available to examine the motion of the aircraft for various kinds of flight scenarios but in the present research steady state straight flight and level turn are specifically going to be studied.

Optimal control theory contains various optimization techniques which are available for different kinds of optimization problems. But specifically, the dynamic programming technique is going to be examined since it is the most convenient optimization methodology for the problem given in this thesis study.

In this chapter, basic information about the solar energy conversion is given. Moreover, the information about the flight mechanics that is focusing on the motion and forces of steady state flight are indicated. Additionally, general information about the optimal control theory is stated in addition to the detailed information about dynamic programming and Bellman's principle of optimality.

2.1 Solar Energy Utilization

The basic concepts of the solar energy utilization will be described in this section. Since, solar powered air vehicle utilizes solar energy directly, this section is essential in understanding the incoming energy for this type of aircrafts.

Several basic definitions should be given clearly in order to understand the idea behind solar energy utilization. Some of these basic definitions will be used directly in this thesis study, but the others should also be indicated since they are connected to the solar energy conversion subject.

Since this thesis study aims to make an energy optimization between an energy balance and time, the main angles that are related with the direction of the beam radiation incident on a tilted surface are important.

2.1.1 Basic Definitions

The solar constant (G_{sc}) is one of the most important parameters for analyzing solar energy resources and it is a function of the distance between the sun and earth. Duffie and Beckman [15] define the solar constant as "the energy coming from the sun, per unit time, received on a unit area of surface perpendicular to the direction of propagation of the radiation, at mean earth – sun distance, outside of the atmosphere". Although, many different measurements have been made to determine the solar constant, The World Radiation Center adopted the value $1367 W/m^2$. Maximum irradiance (I_{max}) is used in the calculations of this study rather than the solar constant as recommended by Noth [3].

The atmosphere of the earth has an important effect on the solar radiation. The solar radiation which is not scattered by the atmosphere is known as beam radiation. The direction of solar radiation can be changed due to scattering by the atmosphere of the earth and this scattered solar radiation is known as diffuse radiation. Total solar radiation is the sum of the beam radiation and diffuse radiation [15].

Solar irradiance (G) is the rate of the radiant energy incident on a surface per unit area. Solar irradiance can be classified as beam (G_b), diffuse (G_d) by adding the appropriate subscripts to the symbol [15].

Irradiation is the incident energy that effects on a unit area and found by integrating the irradiance over a specified time. Solar energy irradiation is indicated by the term of insolation specifically [15].

In the relations of sun and angles, solar time is used rather than local clock time. Duffie and Beckman [15] define solar time as "time based on the apparent angular motion of the sun across the sky, with solar noon the time the sun crosses the meridian of the observer".

2.1.2 Solar Angles

The geometric relation between the sun and some surface of arbitrary orientation can be defined with a group of useful angles. The incoming energy of a solar powered aircraft is directly related with the solar incidence angle (θ) which is derived by using the solar angles. The most general form of the equation that defines the solar incidence angle is given in the Equation (2.1). Definitions of the most important solar angles are indicated in the Table 2.1. Also, these useful angles are represented in the Figure 2.5.

Declination angle, which is also defined with the other important angles in the Table 2.1, can be calculated with the Equation (2.2). Day of the year is symbolized with the (n) has its maximum value (23.45°) for the summer solstice.

$$\begin{aligned}\cos(\theta) = {} & \sin(\delta).\sin(\phi).\cos(\beta) - \sin(\delta).\cos(\phi).\sin(\beta).\cos(\gamma) \\ & + \cos(\delta).\cos(\phi).\cos(\beta).\cos(\omega) \\ & + \cos(\delta).\sin(\phi).\sin(\beta).\cos(\gamma).\cos(\omega) \\ & + \cos(\delta).\sin(\beta).\sin(\gamma).\sin(\omega)\end{aligned} \tag{2.1}$$

$$\delta = 23.45°\sin(360\frac{284+n}{365}) \tag{2.2}$$

Table 2.1 Solar angles **[15]**

Angle	**Definition**
Latitude (ϕ)	The angular location north or south of the equator, north positive.
Declination (δ)	The angular position of the sun at solar noon.
Slope (β)	The angle between the plane of the surface in question and the horizontal.
Surface azimuth angle (γ)	The deviation of the projection on a horizontal plane of the normal to the surface from local meridian, with zero due south, east negative, and west positive.
Hour angle (ω)	The angular displacement of the sun east or west of the local meridian due to rotation of the earth on its axis at 15° per hour, morning negative, afternoon positive.
Angle of incidence (θ)	The angle between the beam radiation on a surface and the normal to that surface.
Zenith angle (θ_z)	The angle between the vertical and the line to the sun.
Solar altitude angle (α_s)	The angle between the horizontal and the line to the sun.
Solar azimuth angle (γ_s)	The angular displacement from south of the projection of beam radiation on the horizontal plane.

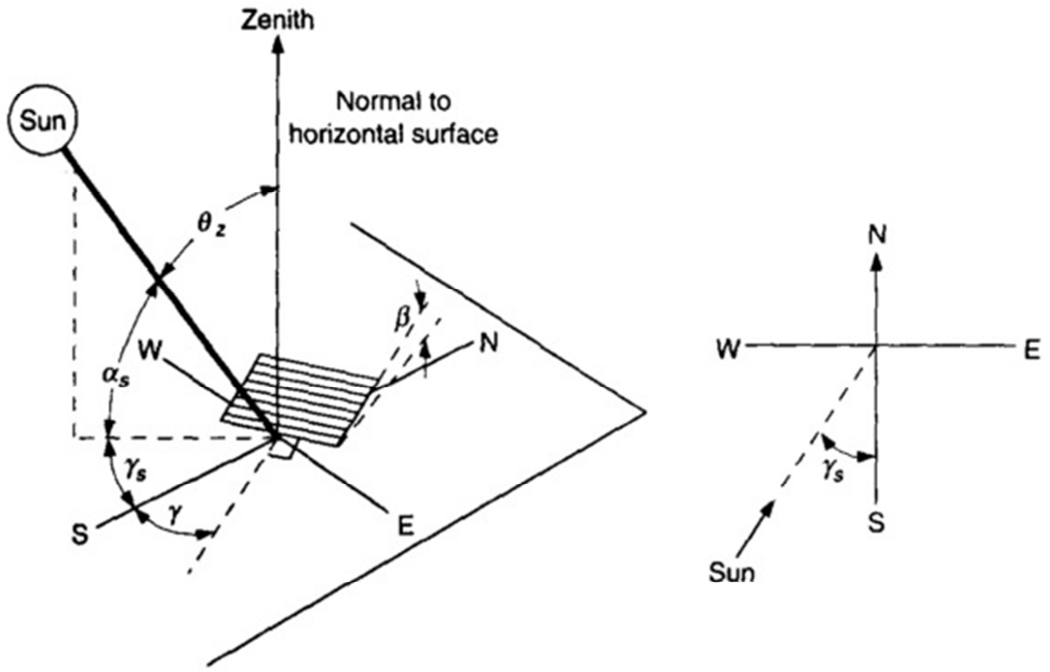

Figure 2.5 Solar angles **[15]**

2.1.3 Solar Cells

Solar cells (photovoltaic or PV cells) convert the solar energy directly into the electrical energy that is needed to sustain the flight. Photovoltaic effect causes this solar energy conversion. Different kinds of semi-conductors compose the solar cells. Silicon is one of the most preferred materials in the production of solar cells since it is widespread in nature and consequently it is cheap [3].

The working principle of a solar cell is shown in Figure 2.6. Noth explains the working principle of the solar cell as [3], "When the sun light strikes the solar cell surface the cell creates charge carriers as electrons and holes. The internal field produced by junction separates some of the positive charges (holes) from the negative charges (electrons). The holes are swept into the positive or p-layer and the electrons are swept into the negative or n-layer. When a circuit is made, the free electrons have to pass through the load to recombine with the positive holes; current can be produced from the cells under illumination."

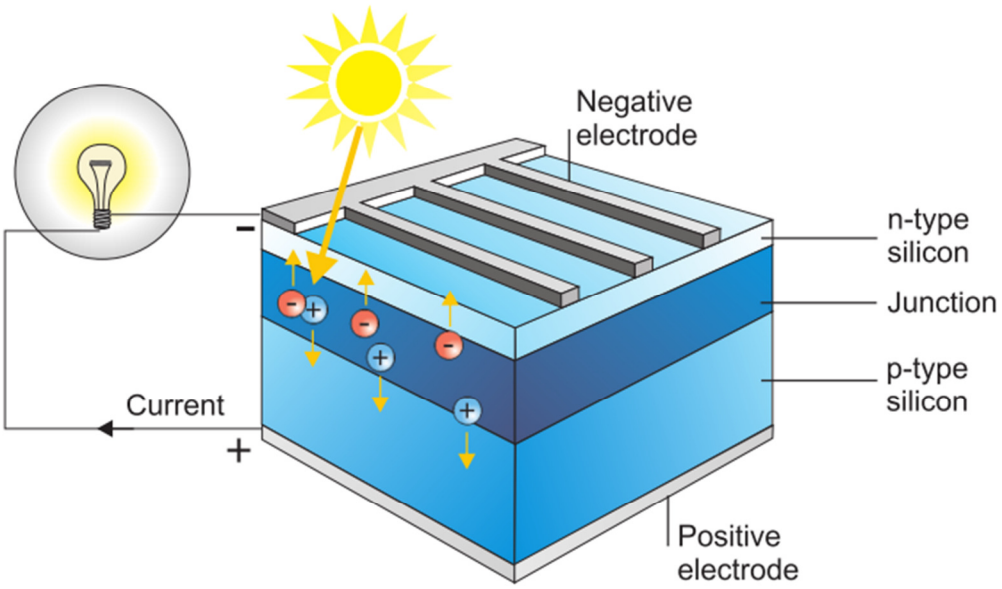

Figure 2.6 Working principle of a solar cell **[3]**

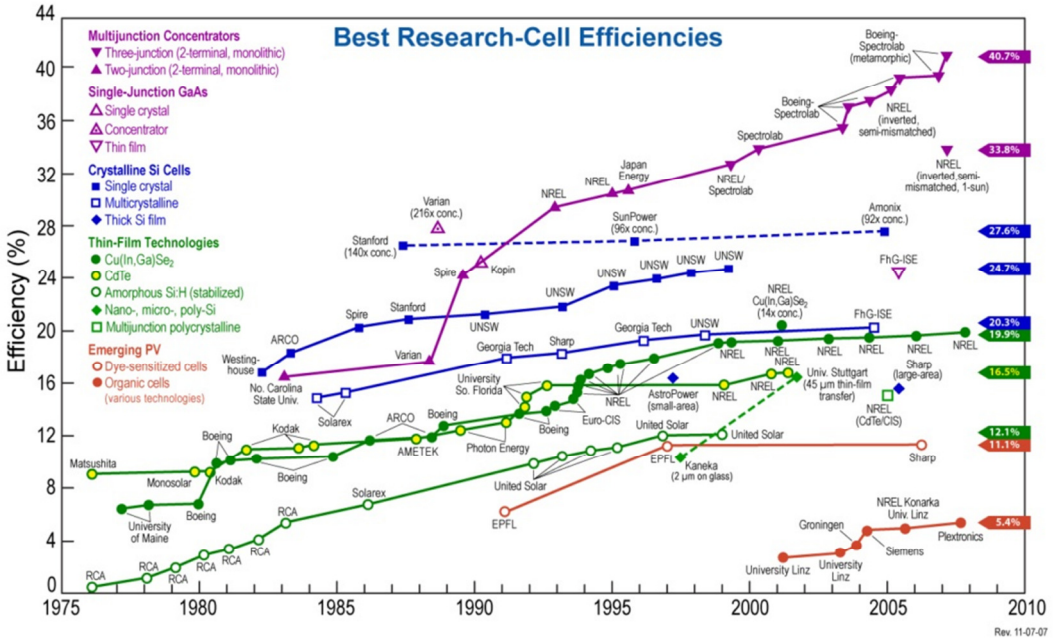

Figure 2.7 Best research-cell efficiencies **[3]**

There are different kinds of solar cells which can be varied according to the materials, manufacturing processes, etc. Silicon solar cells can be divided to three sub-groups according to the crystal type. The monocrystalline type of silicon solar cells has high efficiency because of their pure semiconducting material but their cost is also high.

Polycrystalline solar cells are more economical than monocrystalline silicon cells but they are less efficient. This type of solar cells is made from different sizes of crystal structures. The final group of solar cells is thin-layer solar cells (amorphous solar cells). This type of solar cells are thinner than $1\mu m$ and they are very flexible. Both the efficiency and cost of amorphous cells are low [3].

Higher efficiencies can be obtained from solar cells by using different kinds of materials instead of silicone. Gallium arsenide, copper indium diselenide and cadmium telluride are some examples of these materials. Manufacturing costs increases with the increment of efficiency for these kinds of solar cells [3].

There are also studies on new technologies which have low manufacturing costs. Polymer solar cells and dye sensitized solar cells are examples of these promising technologies. On the other hand, these new technologies still have some problems that need to be solved before becoming widespread in the markets [3].

The change in the efficiencies for different kinds of solar cells over 35 years is indicated in the Figure 2.7.

2.2 Flight Mechanics

Newton's Second Law constitutes the fundamentals of the flight mechanics. Trajectory analysis of an air vehicle is a study area under the subject of flight mechanics. According to the Hull [16], "Airplane flight mechanics can be divided into five broad areas: trajectory analysis (performance), stability and control, aircraft sizing, simulation and flight testing". Trajectory analysis is the key sub-group of flight mechanics for this thesis study.

2.2.1 Motions of an Aircraft and Control Surfaces

An axis system should be developed in order to define the motion of an aircraft in a systematic notation. An earth axis system is defined with respect to the direction of gravitational force, horizontal line and altitude as shown in Figure 2.8 [17]. The earth axis system is used as a reference axis system and the aircraft axis system is derived to define the angular and translation motion of the aircraft. In the body axis system of the aircraft (aircraft axis system) the origin is the plane's center of gravity. From the origin, axis X_B passes through the nose of the aircraft; axis Z_B is perpendicular to axis X_B and in the vertical plane for level flight, and axis Y_B is perpendicular to X_B and Z_B and in the starboard direction as shown in Figure 2.8. Roll, yaw and pitch motions and related moments of an aircraft are defined about the body axes and they are shown in Figure 2.9.

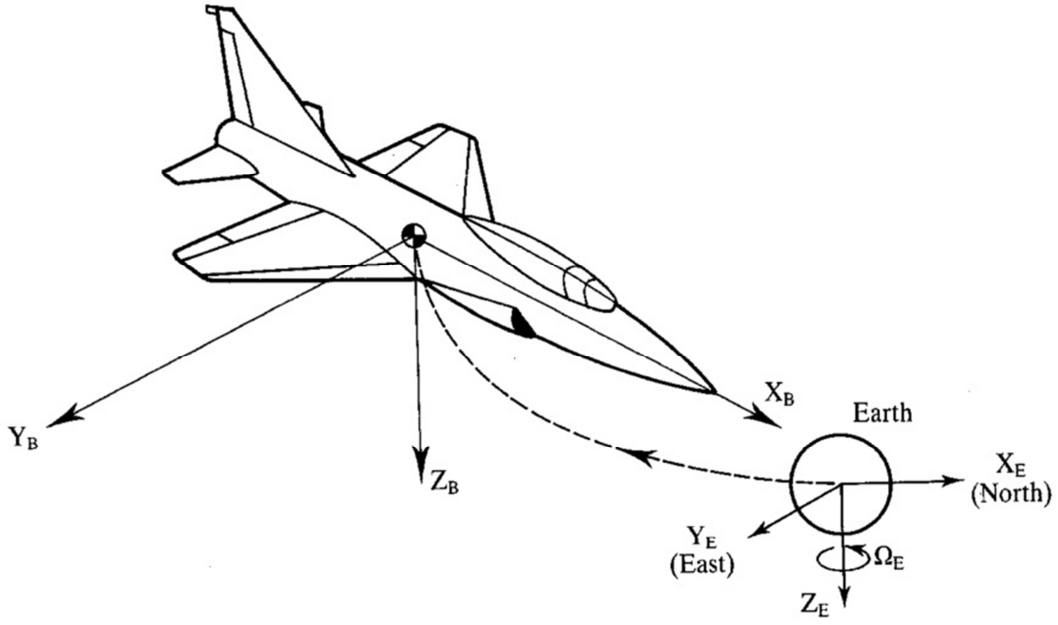

Figure 2.8 Body axes and earth axes **[17]**

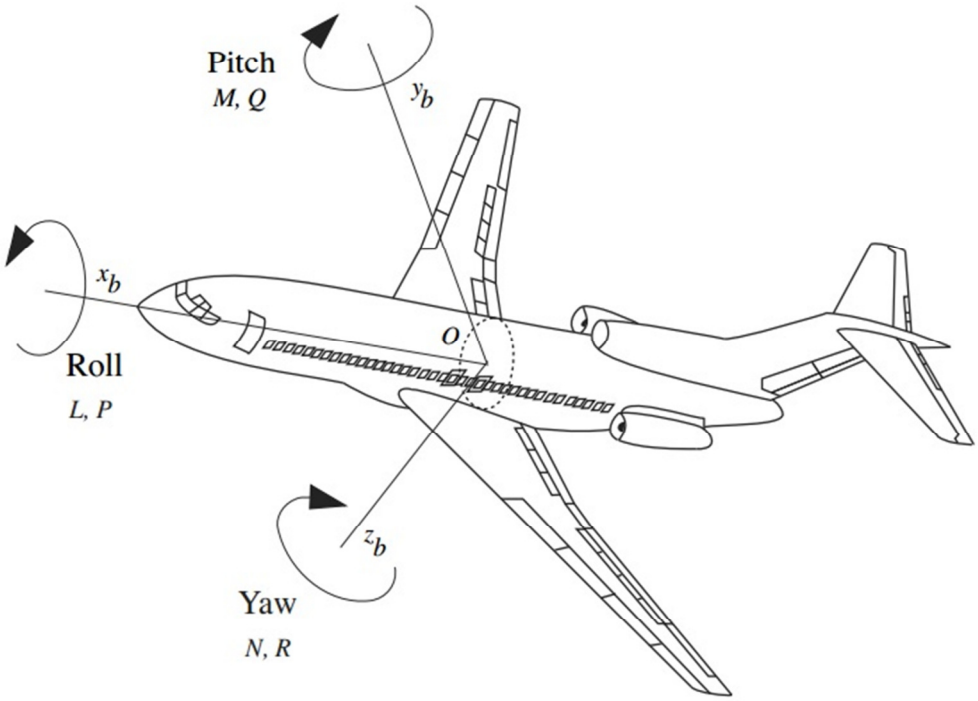

Figure 2.9 Body axes, moments, rates and controls **[16]**

An aircraft has six degrees of freedom that can be divided into two sub-groups; three of them are its angular motion about the center of gravity. Three translation motions of the center of gravity constitute the other sub-group. Control vectors affect the maneuvers of the aircraft and define the velocity and the position of the aircraft in space.

An external force or moment must affect to a body in order to obtain any change in the state of that body. The control surfaces of an aircraft create these external forces and moments. Elevator, ailerons and rudder are the traditional control surfaces of an aircraft as shown in Figure 2.10. Engines of an aircraft also provide the thrust which is the fourth traditional control of an aircraft. Extra control surfaces have been developed for modern aircrafts to enable sophisticated motion. Horizontal and vertical canards, reaction jets, variable cambered fins, and spoilers are some examples of these non-traditional controls and are shown in Figure 2.11 [17].

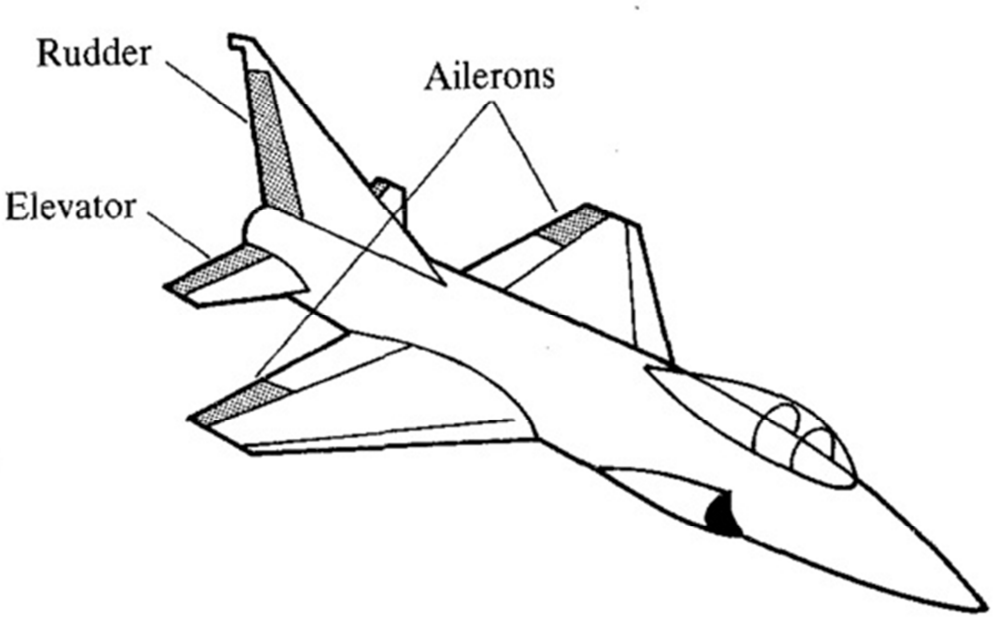

Figure 2.10 Conventional control surfaces of an aircraft **[17]**

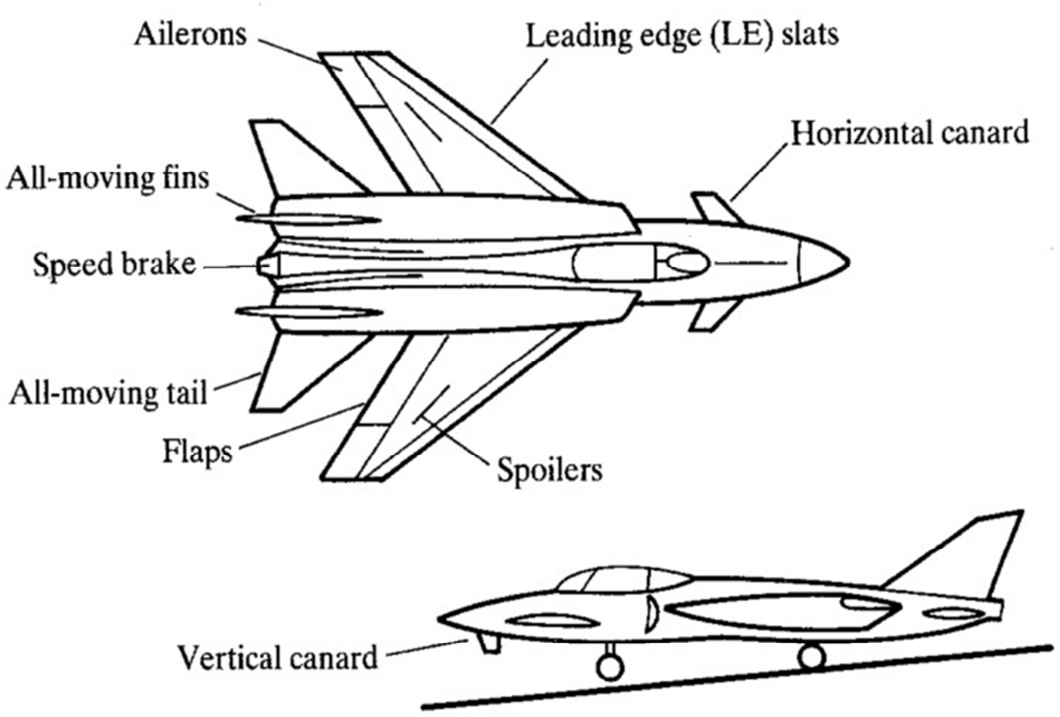

Figure 2.11 Non-traditional control surfaces of an aircraft **[17]**

2.2.2 Forces Acting on an Aircraft

Four main force components act on an aircraft during level flight and these are shown in Figure 2.12. Thrust is supplied by the engines and the lift force is provided by the wings. Drag occurs during the flight and gravitational acceleration leads to the weight force.

Lift and drag forces (L, D) are directly related with the coefficients of lift (C_L) and drag (C_D) as given in the Equations (2.3) and (2.4). Consequently airfoil of the wings is an essential parameter for the lift and drag forces since these coefficients are mainly depended on the airfoil. Moreover, air density (ρ), area of the wings (S) and velocity of the aircraft (V_∞) changes the magnitude of these forces.

$$L = C_L.\frac{\rho}{2}.S.V_\infty^2 \tag{2.3}$$

$$D = C_D.\frac{\rho}{2}.S.V_\infty^2 \tag{2.4}$$

Lift and drag forces are directly related with the coefficients of lift (C_L) and drag (C_D). The airfoil of the wings is an essential parameter for the lift and drag forces. The angle of attack is a key parameter which affects the change of drag and lift coefficients. Figure 2.13 shows the change of these coefficients with the angle of attack. Steady flow results in high lift and low drag force which sustains the conditions necessary for flight. Separation of the flow

starts after a definite point of angle of attack which is very close to the maximum ratio of coefficient of lift to coefficient of drag. Separation of the flow causes the turbulent flow that leads to a sudden loss of lift force.

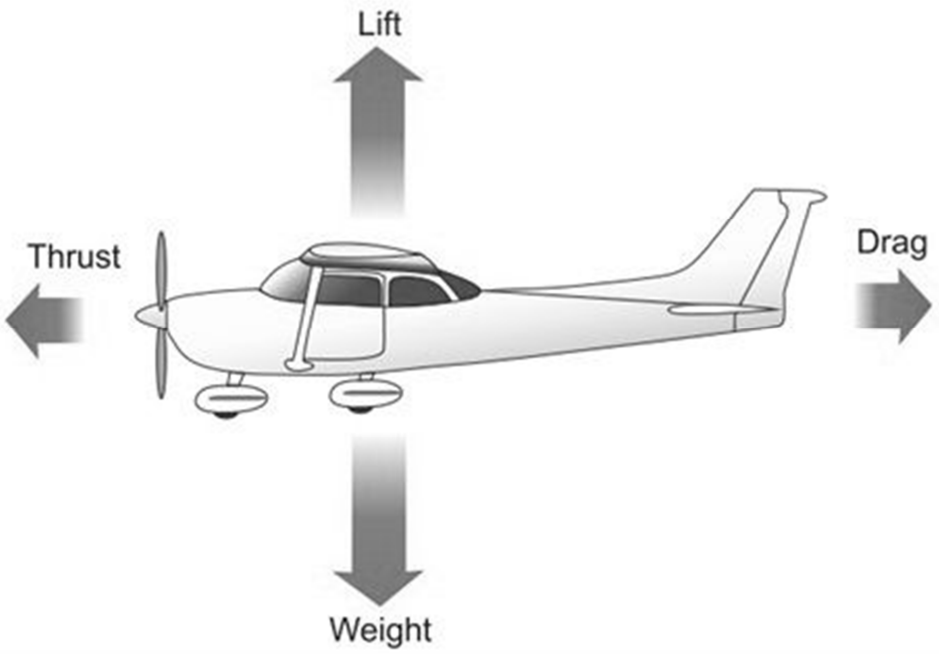

Figure 2.12 Forces acting on an aircraft **[3]**

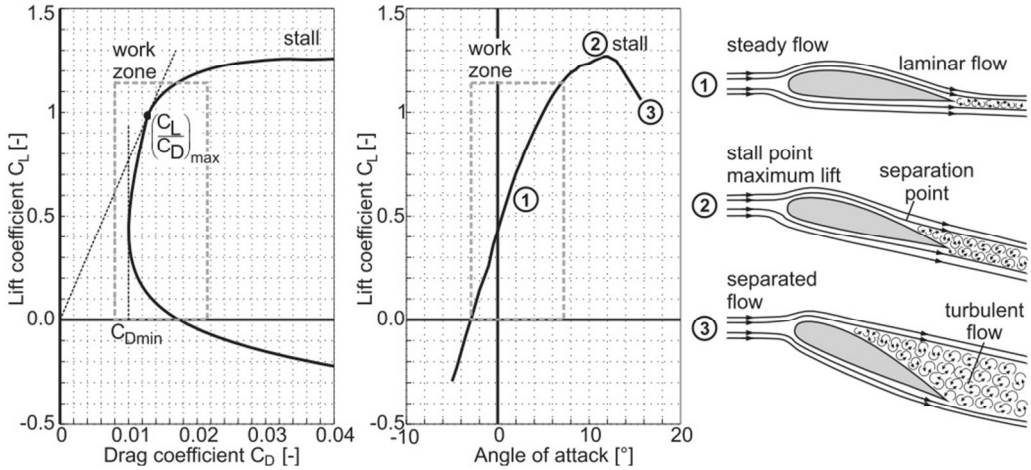

Figure 2.13 Coefficients of lift and drag depending on the angle of attack **[3]**

The lift coefficient-drag coefficient curve which is given in the Figure 2.13 shows the relation between these two coefficients.

Wings of an aircraft are the main suppliers of the lift force. On the other hand they cause a drag force. Airfoil drag coefficient ($C_{D_{afl}}$) is added into the main drag coefficient term and shows the effect of the wings on drag force.

There is an additional drag force that is induced by vortices at the wing tips [3]. This extra drag force is called the induced drag and it is represented by Equation (3.14).

Non-lifting parts of the aircraft like the fuselage and tail cause an additional drag force which is called the parasitic drag and symbolized by ($C_{D_{par}}$). Parasitic drag is added into the total drag coefficient as given in the Equation (3.14).

2.2.3 Steady State Flight

Steady state flight is a special type of flights in which there is no acceleration for the aircraft. Static performance of the aircraft examines this unaccelerated type of flight.

The simplest case of steady state flights is the steady state level flight. For level flight the pitch angle (Θ) and roll angle (Φ) of the aircraft are equal to zero. Additionally, for steady state flight, the aircraft is free of any acceleration. Moreover, for a conventional aircraft, the engine thrust line can be assumed to be aligned with the flight direction. The resulting equations of motion for the steady state level flight are reduced to Equations (2.5) and (2.6). According to these equations, the thrust (T) is equal to the drag (D) and the lift (L) is equal to the weight of the aircraft (W) for steady state level flight [18].

$$T = D \tag{2.5}$$

$$L = W \tag{2.6}$$

A level turn has a curved flight path which is shown in Figure 2.14. This curved flight path for a level turn is on a horizontal plane so that altitude for the level turn is constant. As a result, the pitch angle (Θ) of the aircraft equals to zero. The assumption of the parallel thrust vector to the free stream direction is also valid for turning flight.

The lift force that is effecting on a level turning aircraft has two components one in the vertical and one in the horizontal plane as shown in the front view of Figure 2.14. The roll angle determines the magnitudes of these two components. The vertical component of the lift force is balanced with the weight of the aircraft. Equation (2.7) gives the relation of the lift force with the weight force.

$$L.\cos(\Phi) = W \tag{2.7}$$

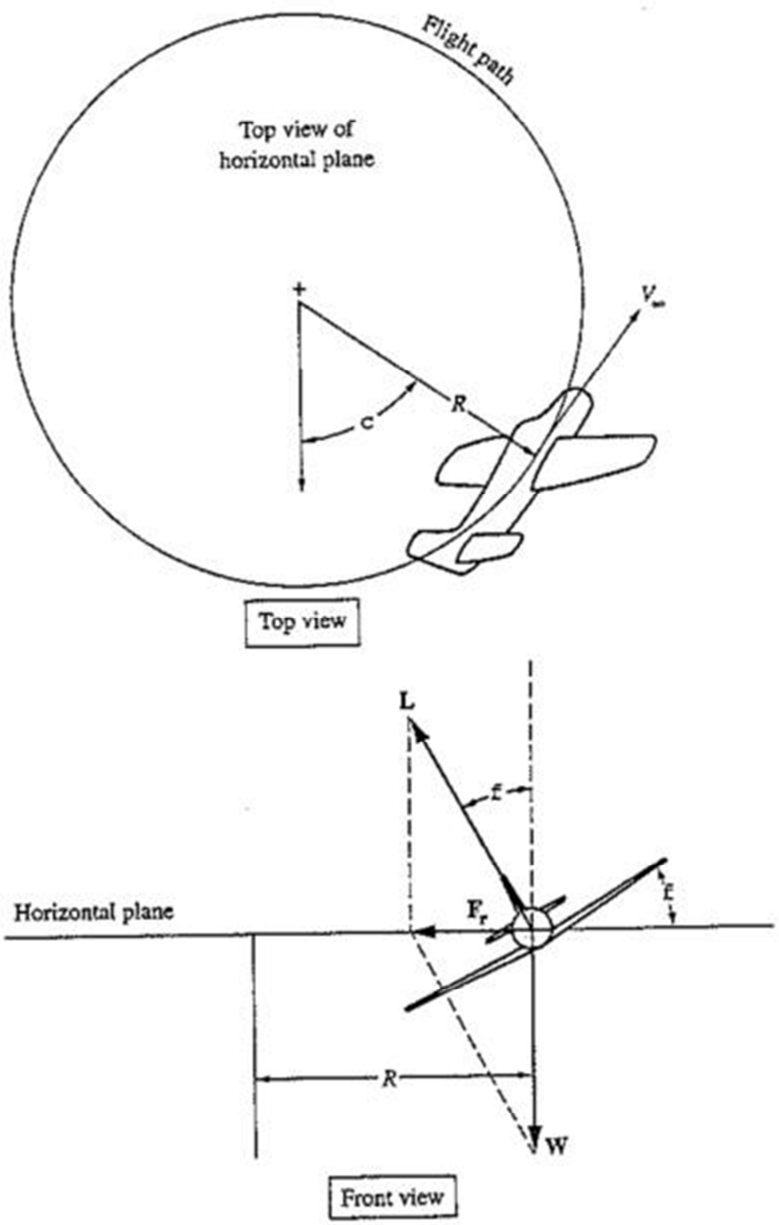

Figure 2.14 Level turn flight **[18]**

The horizontal component of the lift force (radial force) is balanced with the centrifugal force (F_r) . The second equation of the motion is presented in Equation (2.8) where (V_∞) is the velocity of the aircraft.

$$m\frac{V_\infty^2}{R} = Lsin(\Phi) \tag{2.8}$$

Combining Equations (2.7) and (2.8), the turning radius of the aircraft (R) for a steady state level turn can be derived yielding Equation (2.9).

$$R = \frac{V^2}{g.tan(\Phi)} \tag{2.9}$$

2.3 Optimal Control Theory

Optimal control theory aims to find the most available control signals that maximize or minimize the selected performance criterion by satisfying the required physical constraints of the system. The physical constraints, performance criterion and mathematical model should be described in order to formulate the optimal control problem. The state and control vectors of the optimal control problem are obtained in the definition process of the mathematical model. Admissible control, state and target sets are also defined in order to specify the acceptable values.

A performance measure (performance index) is a quantitative criterion that represents the performance of the system. Performance measures can be subjective according to the type of the problem. The standard representation of a performance measure is given in Equation (2.10) [19].

$$J = h\big(x\big(t_f\big), t_f\big) + \int_{t_0}^{t_f} g(x(t), u(t), t)dt \tag{2.10}$$

In Equation (2.10), $h(x(t_f), t_f)$ indicates the terminal cost function. The initial and final times are specified by t_0 and t_f. The user defined scalar functions of the performance measure equation are h and g.

Optimal control problems can be classified according to the type of the performance measure. Minimum-time problem, terminal control problem, minimum control effort problem, tracking problem and regulator problem are the five main groups of optimal control problems according to the performance measure.

The minimum-time problem objects to transfer a system from an initial state to the defined target set in the minimum time. The performance measure for this type of problem is simplified and becomes as shown in Equation (2.11) [19].

$$J = \int_{t_0}^{t_f} 1.dt = t_f - t_0 \tag{2.11}$$

Minimum control effort problem aims to transfer a system to the specified target area with minimum control effort expenditure (or maximum control effort depending on the case). The control effort can be varied according to the type of physical application. The rate of fuel consumption for a conventional aircraft or storage of solar energy for a solar powered aircraft can be control efforts.

The tracking type of optimal control problem tries to keep the state as close as possible to the desired state for a specified time period [19]. The equation of the performance measure is derived yielding Equation (2.12) in which, $r(t)$ designates the desired state and $Q(t)$ indicates the positive weighting matrix.

$$J = \int_{t_0}^{t_f} \|x(t) - r(t)\|_{Q_t}^2 dt \tag{2.12}$$

The regulator problem objects to hold the system at equilibrium. The regulator problem can be considered as a special type of a tracking problem. This type of problem results when the desired state values yield zero for the entire time period [19].

The last sub-group of optimal control problems is the terminal control problem. Aim of the terminal control problem is to have the final state of the system approach a desired final state [19].

2.3.1 **Dynamic Programming**

Dynamic programming is an optimal control technique that is used for solving multistage problems. The dynamic programming technique can be used to minimize (or maximize) the performance measure. According to Hull; "dynamic programming leads to a functional equation that is amenable to solution by use of a digital computer" [19].

The solution methodology for dynamic programming consists of four main steps. First, the structure of an optimal solution is characterized. Second, the value of the optimal solution is defined recursively. Third, the value of an optimal solution is computed in a bottom-up way. And fourth, the optimal solution is computed from the stored information.

In dynamic programming, the main problem is divided into smaller sub-problems and then the main solution is found by combining the solutions of these sub-problems. Independent sub-problems are solved just once; solutions of sub-problems are recorded in a table and then they are used in the solution of higher levels of problems. In this manner, the single stage problem becomes a multistage problem.

The scheme of a single stage problem is shown in Figure 2.15. In this type of problem, the control (u_0) has an effect on the input state (x_0) by bringing it to the final state (x_1). The cost of this single stage decision problem is symbolized by (J_{01}) [20].

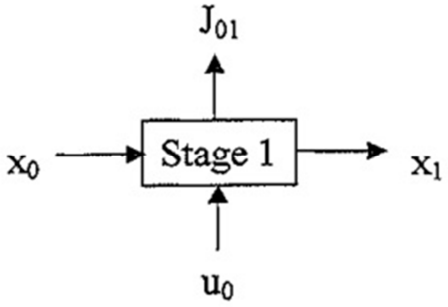

Figure 2.15 Single stage system **[20]**

The multistage decision problem can be considered as a combination of single stage problems in which the input of each stage is the output of the former stage [20]. The objective of the multistage problem is minimizing the total cost which is a function of the costs of each stage.

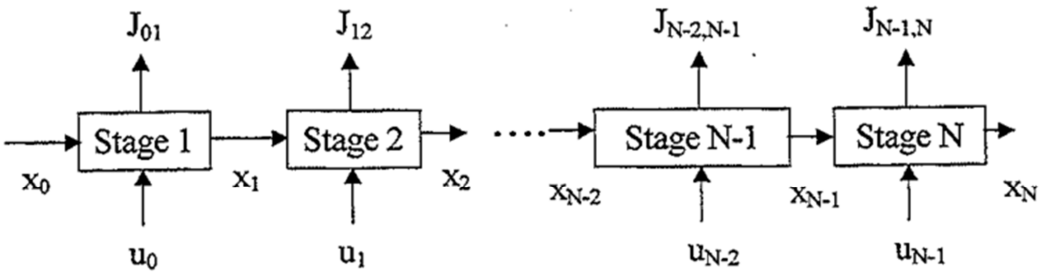

Figure 2.16 Multistage system **[20]**

The main idea behind dynamic programming is indicated by Bellman as "The Principle of Optimality". Bellman states that "An optimal policy has the property that whatever the initial state and initial decision are, the remaining decisions must constitute an optimal policy with regard to the state resulting from the first decision" [21].

A sample of a multistage decision problem is given in Figure 2.17. In Figure 2.17 (a), the optimal path for this problem is shown. The optimal solution of the segment a-b is known and it has a cost of (J_{ab}). There are two different alternatives for the remaining decisions of the segment b-e. Suppose that the optimal path of the segment b-e has a cost of (J_{be*}). Then, the optimal cost for the route a-e (J_{ae}^{*}) can be found with (2.13).

$$J_{ae}^{*} = J_{ab} + J_{be*} \tag{2.13}$$

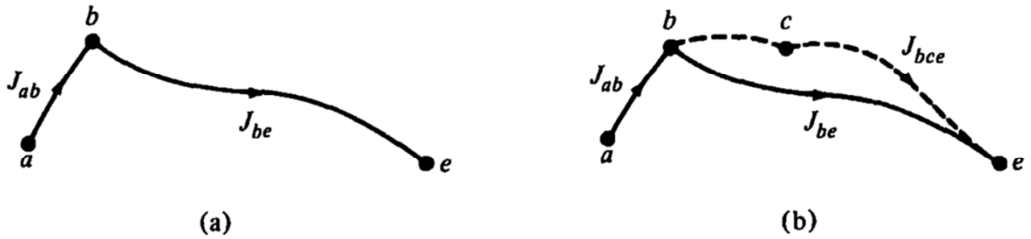

Figure 2.17 (a) Optimal Path from "a" to "e" (b) Two possible optimal paths from "b" to "e" **[19]**

According to the principle of optimality, the optimal path from “a” to “e” is free of the choices that have been made in the segment a-b since it is the initial decision. So that the optimal path is only related with the remaining decisions which are the choices of segment b-e.

CHAPTER 3

THEORY OF THE OPTIMIZATION & MATHEMATICAL MODEL

Design of a solar powered aircraft can be divided into various sub-groups which are aircraft structural design, power-system design, propulsion system design, electrical system design and control system design. In this aspect of view, solar powered aircraft design can be considered as a system engineering issue. Since, the configuration details of different aero vehicles should differ according to specific applications, an optimum design should be developed for a successful aircraft. Each of these sub-systems can be evaluated and designed according to the mission requirements and harmony with other sub-systems. Although some basic design criteria are the same for all solar powered aircrafts like light-weight, some design criteria are only valid over definite periods of design history and are related to technological limitations, such as the requirement that all solar powered aircrafts up to the present have large aspect-ratio wings.

By evaluating a solar powered aircraft, which is a system consisting of several sub-systems, it is expected that an improvement of any sub-system affects the general performance of the aircraft positively. Obtaining higher efficiency in the solar cells of any aircraft would improve the general efficiency of aircraft directly. A higher efficiency propeller would also yield more efficient airplane as would choosing a more suitable aerofoil for a definite aircraft. A long endurance flight can be achieved by improving battery technology dramatically, as well as improving all sub-systems on a small scale.

Since solar powered aircraft use solar energy to sustain flight and charge a battery, it is directly affected by changes in the grade of sunlight. Parameters such as the day of the year, panel slope, atmospheric conditions, etc. affect the total solar energy per unit area incident on the panels directly. The orientation of the solar aircraft relative to the sun becomes very critical in utilizing solar energy. The major angles of the solar aircraft on a definite path determine this crucial position. Also the flight path of this solar aircraft is directly related with major angles, such as the banking angle of a constant altitude aircraft defining the turning radius of the same airplane. Additionally, other parameters like sky cloudiness, dust concentration, pollutants and altitude significantly impact the performance of a solar powered aircraft which flies inside the atmosphere [9]. To sum up, other parameters outside the design parameters of solar aircraft and its sub-systems like atmospheric conditions and position of the aircraft have a significant role on the plane's overall performance.

All of the aircrafts are designed and used for different mission requirements and scenarios. These mission requirements have a direct effect on the paths of flight, altitudes and

velocities of aero vehicles. As an example, while loitering would be crucial for intelligence aimed unmanned small aircraft, level flight occupies the most significant part of the flight period for a commercial plane. Consequently it is very important to make an optimization between the parameters which affect solar utilization (atmospheric condition, position of the aircraft) and mission requirements which govern flight paths and characteristics in order to obtain long endurance and high efficiency. It can be useful to emphasize that the design of the aircraft does not have a direct role on this optimization process. On the other hand mission requirements affect the design process of the solar powered aircraft so the design of the aircraft is indirectly related with that optimization.

In order to make a realistic and useful energy optimization that gives the optimal path of solar aircraft for a given mission, the general dimensions and properties of aircraft should be given. Since the mission and design of an unmanned aero vehicle is very different from a passenger aircraft, the results of an optimization should differ. The design parameters of a solar aircraft and the mission requirements are the inputs of energy optimization and they need to be indicated clearly to obtain the accurate route. The mission requirements should basically involve the initial point of flight, final point of flight and allowed duration for energy optimal path planning. Aircraft design is a more detailed process which specifies the location of the solar panels on the aircraft, and the general dimensions of an aircraft such as aspect ratio, chord length, etc.

As mentioned, the position of the solar panel of a solar powered aircraft relative to the sun is very important for solar energy utilization. The position of the sun in the sky and the sun's motion over the given period should be inputs to the optimization process because this position is crucial to determine the major angles of the aircraft on a path. Atmospheric conditions are also important factors which affect solar energy utilization. Air density changes with altitude and clouds have shading effects on solar panels.

Energy optimization for optimal path-planning of a solar powered aircraft features the interaction between aircraft kinematics, energy collection and energy loss [8]. Aircraft kinematics is related with energy loss, because drag is directly connected with energy loss. Also, the design of the aircraft directly determines the drag force and is one of the main factors effecting solar energy utilization and consequently energy gain.

The remaining parts of this chapter are structured as follows: First, the design parameters of the selected aircraft "Sky-Sailor" are given. The design parameters of the aircraft are the main inputs to the optimization algorithm. The necessary equations for energy gain of the solar powered aircraft are indicated in the second sub-section of this chapter. Then the energy consumption equations of the aircraft are stated in the next sub-section. Finally, the theory behind the optimization is summarized in the last sub-section. This last section of the chapter is the most critical part since it represents a novel method for making an energy optimal path planning for solar powered aircrafts for long endurance.

3.1 Design Parameters

The design parameters of the unmanned air vehicle Sky-Sailor which is shown in Figure 1.4 are assumed to perform the optimization algorithm. Noth [3] declares the mission of the aircraft as achieving surveillance at low altitude or serving as a high altitude communication platform. Sky-Sailor is designed to sustain a continuous flight at constant

altitude [3]. In this view, the mission scenario and resulting design parameters of the Sky Sailor are consistent with the mission requirements of the aircraft which is needed for this thesis study.

The parameters of the aircraft model can be divided into three main classes: the first group of these parameters is directly connected with the technology of the components and these parameters are assumed to be constant for a specifically optimized application [3]. This class of parameters is indicated in the Table 3.1.

Table 3.1 Constant parameters of the Sky-Sailor design **[3]**

Parameter	Value	Unit	Description
C_L	0.8	-	Airfoil lift coefficient
$C_{D_{afl}}$	0.013	-	Airfoil drag coefficient
$C_{D_{par}}$	0.006	-	Parasitic drag coefficient
e	0.9	-	Oswald's efficiency factor
I_{max}	950	$[W/m^2]$	Maximum irradiance
k_{bat}	190.3600	$[J/kg]$	Energy density of lithium-ion
k_{sc}	0.32	$[kg/m^2]$	Mass density of solar cells
k_{enc}	0.26	$[kg/m^2]$	Mass density of encapsulation
k_{mppt}	0.00042	$[kg/W]$	Mass to power ratio of MPPT
k_{prop}	0.008	$[kg/W]$	Mass to power ratio of prop. group
k_{af}	0.44/9.782	$[kg/m^3]$	Structural mass constant
m_{av}	0.15	$[kg]$	Mass of autopilot system
η_{bec}	0.65	-	Efficiency of step-down converter
η_{sc}	0.169	-	Efficiency of solar cells
η_{cbr}	0.90	-	Efficiency of the curved solar panels
η_{chrg}	0.95	-	Efficiency of battery charge
η_{ctrl}	0.95	-	Efficiency of motor controller
η_{dchrg}	0.95	-	Efficiency of battery discharge
η_{grb}	0.97	-	Efficiency of gearbox
η_{mot}	0.85	-	Efficiency of motor
η_{mppt}	0.97	-	Efficiency of MPPT
η_{pr}	0.85	-	Efficiency of propeller
P_{av}	1.5	$[W]$	Power of autopilot system

Mission parameters constitute the second group. This group is mainly connected with the environmental conditions of the selected mission altitude. Air density, duration of the day and night, and time and location of the flight are typical examples for this group. Moreover, parameters related with payload can be included in this class [3]. This group of parameters is given in Table 3.2.

Table 3.2 Mission Parameters **[3]**

Parameter	Value	Unit	Description
m_{pld}	0.05	[kg]	Payload mass
η_{wthr}	0.7	-	Irradiance margin factor
P_{pld}	0.5	[W]	Payload power consumption
ρ	0.47	$[kg/m^3]$	Air density (9000m,-46°C)
g	9.782	$[m/s^2]$	Gravitational acceleration (9000 m)

Wingspan and the aspect ratio comprise the final group of parameters which are stated in the Table 3.3. These two parameters are obtained by Noth [3] at the end of an optimization process which is aimed to determine the optimum layout of the aircraft.

Table 3.3 Parameters connected with the shape of the aircraft **[3]**

Parameter	Value	Unit	Description
m	2.6	[kg]	Total mass
AR	12.9	-	Aspect ratio
b	3.2	$[m]$	Wing span
Γ	0.122	$[rad]$	Dihedral angle

Some of these parameters (from all three different classes of parameters) are used directly in the energy optimal path planning model, while the parameters are indicated to give a general description of solar powered aircraft.

The solar cells used in the design of the Sky-Sailor are RWE-S-32 type silicon cells of RWE Space. The technical specifications of the solar cells are given in Table 3.4. This type of solar cells has some mechanical flexibility which makes it possible to apply to airfoils. On the other hand, their fragile structure requires great care during integration [3].

Table 3.4 Technical properties of the RWE-S-32 solar cells **[3]**

Description	Value	Unit
Thickness	130	$[\mu m]$
Efficiency	16.9%	-
Weight	320	$[g/m^2]$

In total 216 cells cover an area of $0.58\,m^2$ on the upper surface of the wings and give a voltage of 19 V and a maximum current of 1.6 A. The solar cells are divided into 3 equivalent groups as shown in Figure A.1. The solar cells are integrated by covering with a fiber glass reinforced coating that provides a non-reflective surface [3].

Although optimization algorithm is developed according to the design properties of the "Sky-Sailor" aircraft, the methodology includes all of the solar powered aircrafts which are designed according to the classical approach. Aircrafts with constant aspect ratio wings which has a limited structural flexibility are convenient to be optimized with the algorithm developed in this thesis by changing the value of the design parameters. Since dihedral angle of the aircraft is defined in the energy collection model, the optimization algorithm allows performing the optimization process both for the aircrafts that have horizontal wings or dihedral angle. On the other hand, aircrafts that have revolutionary design similar to the "Helios" aircraft of NASA are not convenient to be optimized with the algorithm. Since there can be some extra conditions which should be considered for the different types of design properties, the algorithm should be revised for these types of solar powered aircrafts.

3.2 Energy Collection Model

Energy collection of the solar powered aircraft is a function of the angle of incidence (θ) between the sun and solar cells of the aircraft, area and efficiency of the solar cells (a_{sc}, η_{sc}), efficiency of the curved solar panels (η_{cbr}), maximum irradiance (I_{max}) and time of the travel (t_{tr}) as given in the Equations (3.1) and (3.2). In this manner, energy gain of a solar powered aircraft can be studied under the subject of solar energy utilization.

$$if\ 0^\circ < \theta < 90^\circ, \qquad E_{in} = \eta_{cbr}.\eta_{sc}.I_{max}.a_{sc}.\cos(\theta).t_{tr} \tag{3.1}$$

$$if\ \theta \leq 0^\circ\ or\ \theta > 90^\circ, \qquad E_{in} = 0 \tag{3.2}$$

The angle of incidence is one of the most critical angles in the optimization of solar energy and it can be calculated by Equation (2.1). Angle of incidence should vary between 0 and 90 degrees for solar energy utilization. There is no solar energy income (E_{in}) for the other values of the solar incidence angle.

As can be seen on the technical drawing of the "Sky-Sailor" in the Figure A.1, the wing of the aircraft is divided into three main parts as central, left and right wings. The central wing is horizontal to the y-axis of the aircraft that can be considered horizontal to the ground for an unrolled flight. The left and right wings have a definite dihedral angle (Γ) according to the y-axis that represents the horizontal line. There are three main series of solar panels which are placed on the central, left and right wings. Consequently it is required to define three different solar incidence angles ($\theta_c, \theta_l, \theta_r$) for the three different groups of solar panels as given in Equations (3.3), (3.4) and (3.5) which defer only in terms of their tilts β (central), β + Γ (left) and β - Γ (right).

$$\begin{aligned}\cos(\theta_c) = {} & \sin(\delta).\sin(\phi).\cos(\beta) - \sin(\delta).\cos(\phi).\sin(\beta).\cos(\gamma) \\ & + \cos(\delta).\cos(\phi).\cos(\beta).\cos(\omega) \\ & + \cos(\delta).\sin(\phi).\sin(\beta).\cos(\gamma).\cos(\omega) \\ & + \cos(\delta).\sin(\beta).\sin(\gamma).\sin(\omega)\end{aligned} \tag{3.3}$$

$$\begin{aligned}\cos(\theta_l) = {} & \sin(\delta).\sin(\phi).\cos(\beta+\Gamma) - \sin(\delta).\cos(\phi).\sin(\beta+\Gamma).\cos(\gamma) \\ & + \cos(\delta).\cos(\phi).\cos(\beta+\Gamma).\cos(\omega) \\ & + \cos(\delta).\sin(\phi).\sin(\beta+\Gamma).\cos(\gamma).\cos(\omega) \\ & + \cos(\delta).\sin(\beta+\Gamma).\sin(\gamma).\sin(\omega)\end{aligned} \tag{3.4}$$

$$\begin{aligned}\cos(\theta_r) = {} & \sin(\delta).\sin(\phi).\cos(\beta-\Gamma) - \sin(\delta).\cos(\phi).\sin(\beta-\Gamma).\cos(\gamma) \\ & + \cos(\delta).\cos(\phi).\cos(\beta-\Gamma).\cos(\omega) \\ & + \cos(\delta).\sin(\phi).\sin(\beta-\Gamma).\cos(\gamma).\cos(\omega) \\ & + \cos(\delta).\sin(\beta-\Gamma).\sin(\gamma).\sin(\omega)\end{aligned} \tag{3.5}$$

There is a direct connection between the solar angles and flight angles of the solar aircraft. Surface slope (β) and surface azimuth (γ) can be defined in terms of yaw and roll angle as given in the Equations (3.6) and (3.7).

$$\beta = roll\ angle \tag{3.6}$$

$$\gamma = -yaw\ angle \tag{3.7}$$

Since three different solar incidence angles are defined specifically for the solar panel series of "Sky-Sailor", the energy collection model which is given by Equation (3.1) is needed to be extended. Equation (3.8) gives the extended energy income model for incidence angles between 0 and 90 degrees which is used in the optimization model. Since there is no energy income for negative and higher than 90 degrees of solar incidence angles, it is not required to update the Equation (3.2).

$$E_{in} = \frac{1}{3}.\eta_{cbr}.\eta_{sc}.I_{max}.a_{sc}.t_{tr}.[\cos(\theta_c) + \cos(\theta_r) + \cos(\theta_l)] \tag{3.8}$$

The efficiency of the solar cell and maximum irradiance are indicated in the Table 3.1. Additionally area of the solar cells is given in the same chapter. In the manner of the grid structure of optimization, energy income is calculated for each grid point one by one. As a result, the time of the travel varies according to the different optimization parameters such as length between two grid points and average velocity of the aircraft.

$$t_{tr} = \frac{Grid\ Length\ [m]}{Average\ Velocity\ of\ the\ Aircraft\ [\ m/s\ ]} \tag{3.9}$$

Since the solar powered aircraft is assumed to fly at a constant altitude above the clouds, there is no atmospheric effect on the solar cell that causes a reduction in the normal irradiance below I_{max}.

3.3 Energy Consumption Model

The energy consumption of the solar powered aircraft is estimated by Equation (3.10) and it is directly connected with the thrust (T) of the aircraft. Like for other solar powered aircrafts, the thrust of the Sky-Sailor is provided by a propeller. Efficiencies of the propeller (η_{pr}), gearbox (η_{grb}) and motor (η_{mot}) have effects on the thrust; consequently they change the level of the energy consumption. Moreover, energy loss increases with the increasing velocity. The velocity of the aircraft is assumed to be constant, in the mission

scenario of the flights which are optimized in this thesis study. Similar to the energy collection equation, the energy loss of the aircraft depends on the time of the travel (t_{tr}) which is indicated by Equation (3.9). Unsurprisingly, energy consumption becomes higher for larger timelines.

$$E_{out} = \frac{V_{aver}.T}{\eta_{pr}.\eta_{mot}.\eta_{grb}}.t_{tr} \tag{3.10}$$

The velocity of the aircraft is assumed to be constant for steady state flight. There is no acceleration component for a constant speed vehicle. Consequently the thrust and the drag of the aircraft are equals as given in Equation (2.5). The drag force on the aircraft is calculated by Equation (3.11). Air density (ρ) is calculated for a constant flying altitude and is given in Table 3.2.

$$D = \frac{1}{2}.\rho.V_{aver}^2.S.C_d \tag{3.11}$$

The surface area of the wings (S) is a key parameter in calculating the drag force that acts on an aircraft. The wing span (b) and aspect ratio (AR) of the wings form Equation (3.12) that yields the required surface area of the wings, where the aspect ratio is the ratio of wingspan to the chord length.

$$S = \frac{b^2}{AR} \tag{3.12}$$

The coefficient of drag (C_D) can be calculated with Equation (3.13) in where ($C_{D_{afl}}$) , is the airfoil drag coefficient, ($C_{D_{par}}$) is the parasitic drag coefficient and ($C_{D_{ind}}$) is the induced drag coefficient.

$$C_D = C_{D_{afl}} + C_{D_{par}} + C_{D_{ind}} \tag{3.13}$$

The induced drag is defined by Equation (3.14). The aerodynamic ratio (k) is a key variable in calculating the induced drag which is a function of Oswald's efficiency factor (e) and aspect ratio.

$$C_{D_{ind}} = C_L^2.k \tag{3.14}$$

$$k = \frac{1}{e.\pi.AR} \tag{3.15}$$

The Oswald efficiency factor (e) represents the load distribution on the wing in Equation (3.15). The value of the Oswald efficiency factor varies between 0 and 1. In the ideal case the Oswald efficiency factor is 1 and there is an elliptical load distribution on the wing.

The coefficient of lift is calculated using Equation (3.16). Since there is a balance between the weight and lift forces of the aircraft for constant altitude flight as given with Equation (2.7), the coefficient of lift can be defined in the terms of the weight force.

$$C_L = \frac{2W}{\rho . v_{aver}^2 . S . \cos(\Phi)} \tag{3.16}$$

The thrust requirement for an aircraft which sustains a steady state flight is directly related with the roll angle. The minimum thrust requirement of an aircraft occurs for horizontal flight which means zero roll angles. Equation (3.16) summarizes the relation between roll angle, weight and thrust requirement clearly. The coefficient of lift must increase with increasing roll angle which causes an increment on the drag force as given in Equation (3.16). The requirement of the thrust increases with a rise in drag force, and consequently the energy consumption of the aircraft to sustain the flight become higher.

3.4 Optimization Algorithm

The aim of the optimization algorithm is making the energy optimal path planning of a solar powered aircraft by calculating the energy balance recursively and considering time-mission constraints. The principle behind the optimization algorithm is dynamic programming and Bellman's Principle of Optimality [21]. Yaw and roll angles of the aircraft are the variables which are required to be chosen at any node in the grid structure, consequently there variables are the control inputs. The position of the aircraft on x-axes and y-axes are the state variables which are needed to be given to make the correct decision.

The optimal control problem of energy optimal path planning is very convenient to solve using dynamic programming since it is easy to divide the problem to smaller sub-problems as shown in Figure 3.1, solve each sub-problem separately, and find the main optimal solution by evaluating the solutions of sub-problems recursively.
A grid structure is defined between the initial and final points of the travel. Energy gain and loss equations are calculated between each grid point. Several solution matrixes are generated in order to make the calculations in a systematic way. Calculated energy balance values are read from the solution matrix and used in the performance measure (cost function) where the user defined time constraint is also added to the calculation. The cost matrix has the essential role of making an energy optimization and generating the results.

In this sub-section, matrix of the grid points for the optimization is represented using a small scale model containing 4 columns and rows of resulting in a square solution matrix of 16 elements. On the other hand, a much larger grid system and solution matrixes are used to obtain the results that will be presented in the final section. Similarly, the represented system in this sub-section includes only 3 different roll angle alternatives between any two grid points as shown in Figure 3.2 (1 negative, 1 positive and 1 neutral roll angles). On the other hand seven different roll angle alternatives are used to get optimal results in the final chapter of the thesis (3 negative, 3 positive and 1 neutral roll angles) with the roll angle steps being user defined.

For neutral roll angles, the central wing is horizontal to the ground. If the yaw angle of the aircraft is zero (which means the aircraft flies due east) the central solar cell group faces due south. Whereas a negative roll angle results in the central solar cell group facing to the north for an aircraft heading due east.

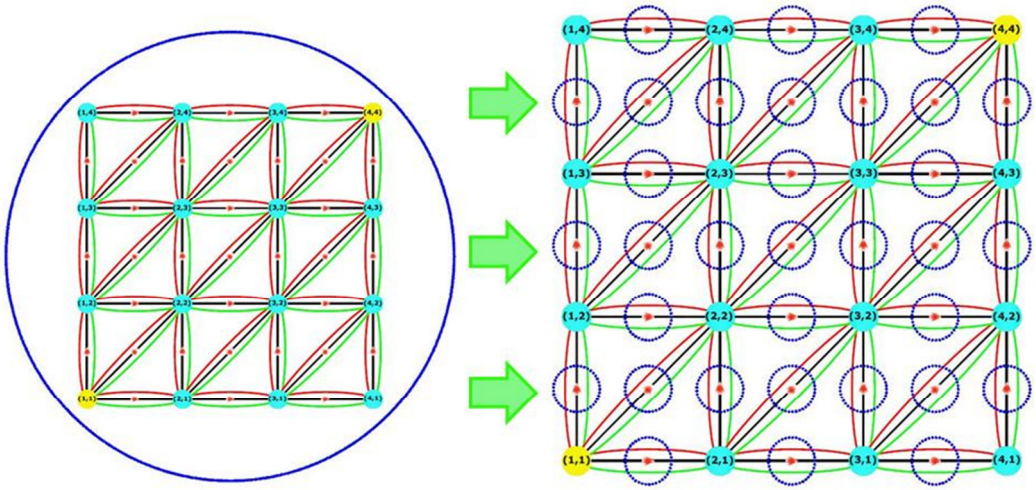

Figure 3.1 Dividing the main problem to the smaller sub-problems

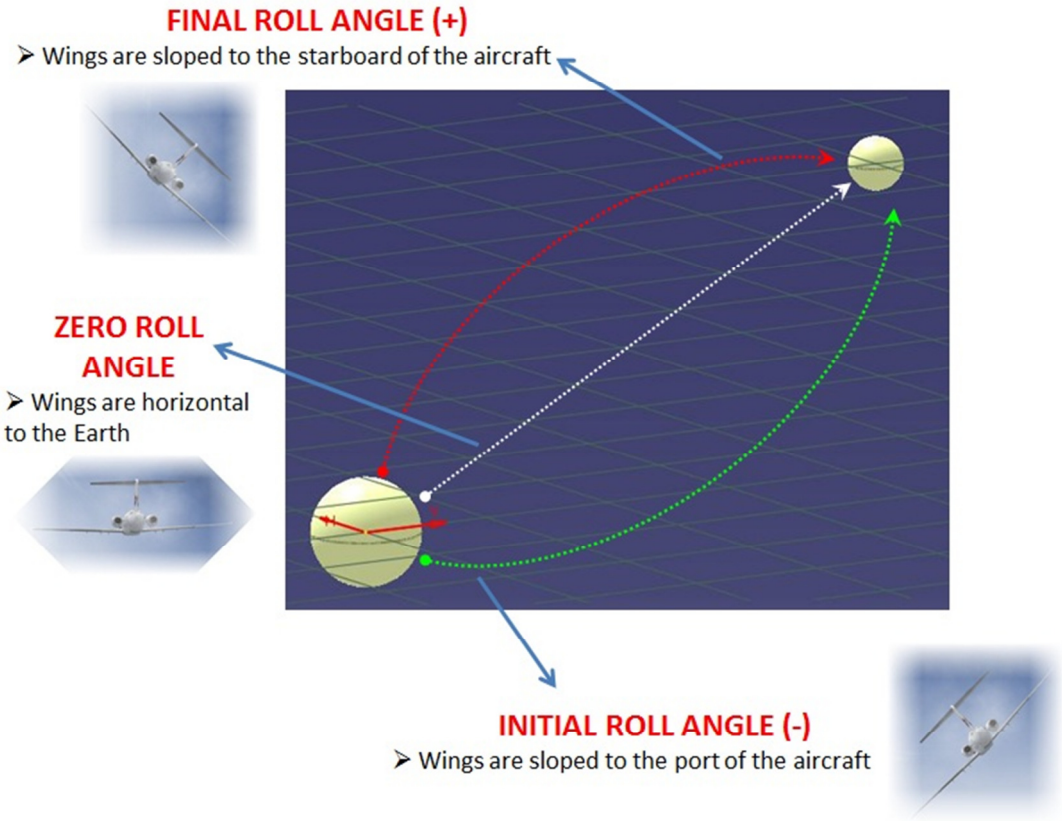

Figure 3.2 Roll angle alternatives between two nodes

For an aircraft making a steady state turning flight rather than level flight between two nodes, there are two main cases which are needed to be described clearly. The relation between speed, roll angle and turning radius of the aircraft is described by Equation (2.9) in Chapter 2. According to the Equation (2.9), the turning radius (R) of the aircraft depends on the velocity, gravitational acceleration and roll angle. For fixed values of these parameters, the turning radius has a constant value.

If the length between two grid points (x_g) is less than turning diameter $(2R)$, the distance that aircraft travels (x_t) can be calculated by Equations (3.17) and (3.18). Equation (3.17) gives the angle that the aircraft travels between the grid points (ε). The parameters required for calculating Equations (3.17) and (3.18) are demonstrated in the Figure 3.3.

$$if\ x_g < 2R\ , \qquad \varepsilon = 2.\arcsin(\frac{x_g}{2R}) \tag{3.17}$$

$$if\ x_g < 2R\ , \qquad x_t = 2\pi R\varepsilon \tag{3.18}$$

The second case for a steady state turning aircraft occurs if the length between two grid points (x_g) is larger than the turning diameter $(2R)$. The traveling angle between the grid points (ε) equals to 2π as given in the Equation (3.19) for this case. The aircraft is assumed to repeat half a full steady state turn and then makes a new steady state turn to arrive at the final grid point. Repeating times of the half of a full tour (K) are calculated by Equation (3.20). The total distance traveled by the aircraft for the second case is calculated by Equation (3.21). The aircraft is assumed to be capable of making the extreme maneuver of starting a rolling flight after finishing the half of a full turn on a straight line between two nodes as shown in the Figure 3.4.

$$if\ x_g \geq 2R\ , \qquad \varepsilon = 2\pi \tag{3.19}$$

$$\mathrm{K} = \frac{x_t}{2R} \tag{3.20}$$

$$if\ x_g \geq 2R\ , \qquad x_t = 4\pi^2 R\mathrm{K} \tag{3.21}$$

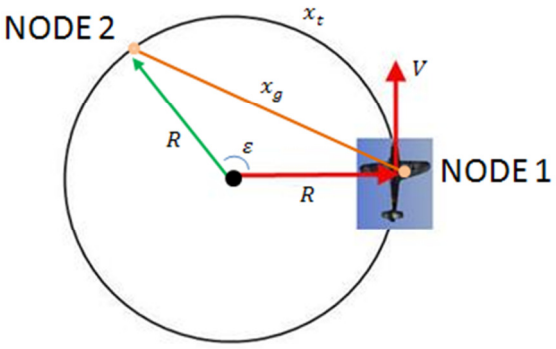

Figure 3.3 Single steady state turn between two nodes

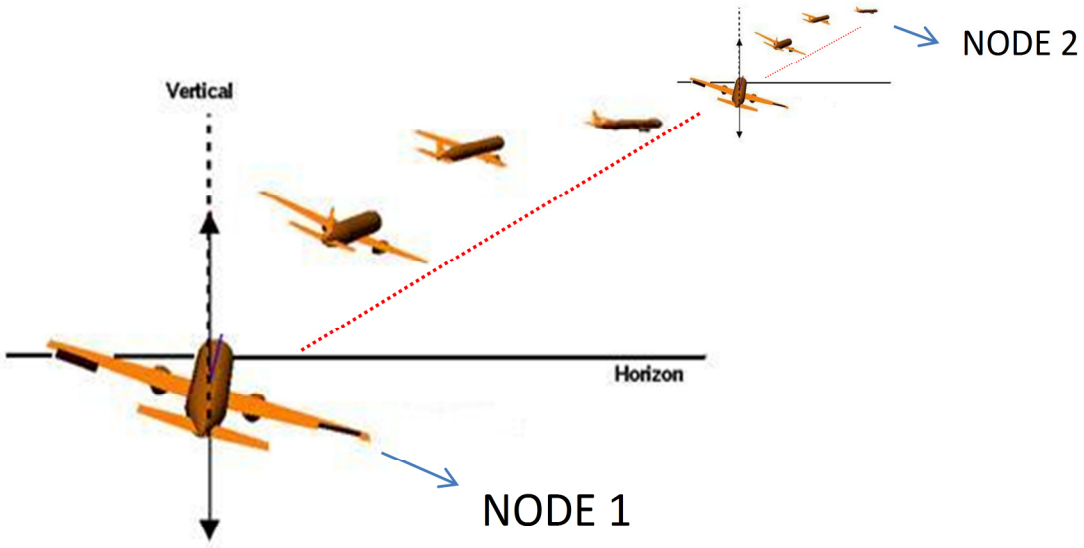

Figure 3.4 Repeated steady state turn between two nodes

The initial and final points of the aircraft on the x-axes and y- axes are defined by the user. These coordinates can be identified as the mission constraints of the aircraft. Other mission constraints, such as the latitude of the aircraft and the time of the day at the initial point of the travel also must be defined to make a connection between the solution coordinate system and real world directions. The number of the day in the year must be defined since it is directly used to calculate the declination of the sun.

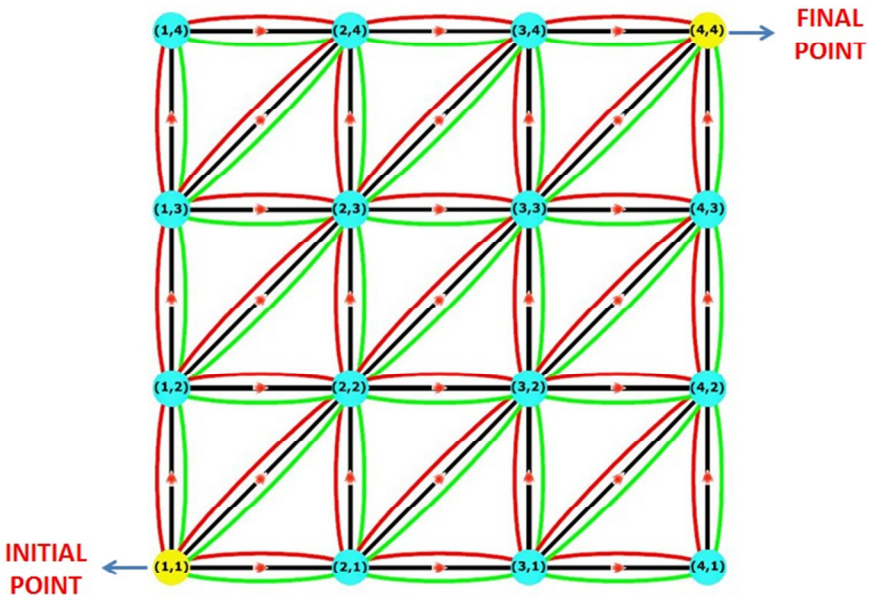

Figure 3.5 Definition of the initial and final points in the grid structure

After identifying the initial and final mission constraints, the structure of the grid is constructed by defining the length between grid points in each of the x- axes and y- axes. Although length between grid points does not have a massive effect on the character of the energy optimal path, an optimal grid length is advantageous to define. A finer grid structure results in more accurate results. On the other hand, the calculation load of the optimization increases rapidly by making the grid structure finer as can be seen clearly in the "Appendix F" which presents the change of calculation load by increasing number of nodes quantitatively. By considering these effects and recollecting the experience on the different optimization studies, it is convenient to indicate that value of the grid length of 200 meters both in x-axes and y-axes gives the optimal results in case of accuracy and time.

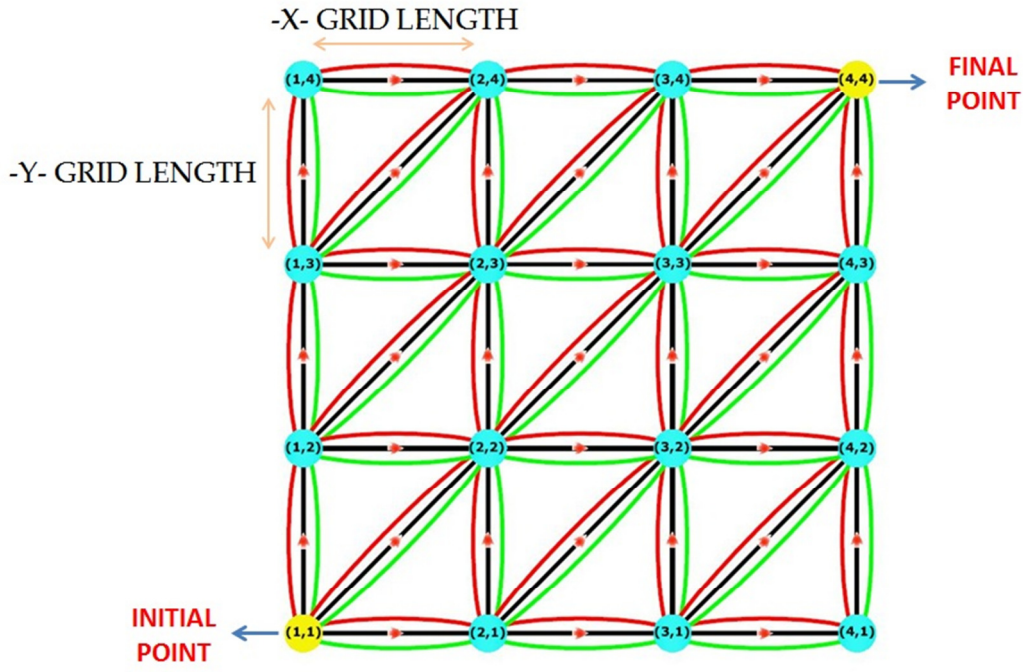

Figure 3.6 Definition of the length between grid points in the –x- and –y- axes

The inner grid points shown in Figure 3.7 are generated automatically after defining the mission constraints (initial point, final point and initial latitude) and length between grid points. The grid is a triangular mesh structure which allows 3 different yaw angles (0°, $\pm 45^{\circ}$, $\pm 90^{\circ}$). Negative yaw angles result in flights in the South, West and South-West directions, whereas positive yaw angles result in flights in the North, East and North-East directions.

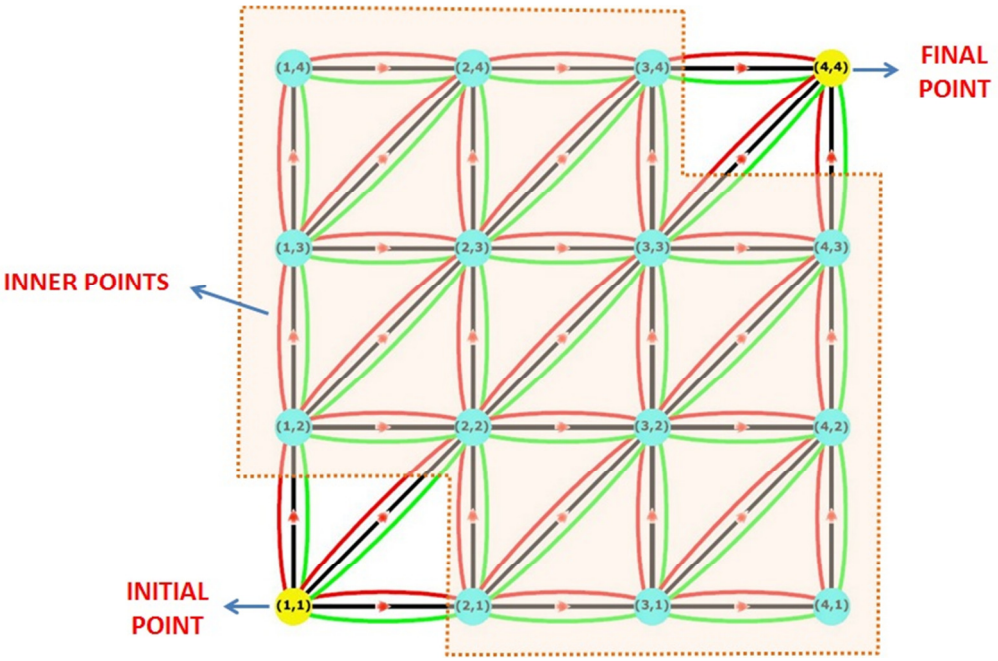

Figure 3.7 Inner points of the grid structure

Motion of the aircraft is only allowed in the directions toward the final point as shown in Figure 3.8. Specifically, if the destination of the travel is in the direction of North-East, then it is not allowed to travel in the South, West or South-West directions. It is required to add a constraint on the motion of the aircraft to avoid a loop and reduce the calculation load.

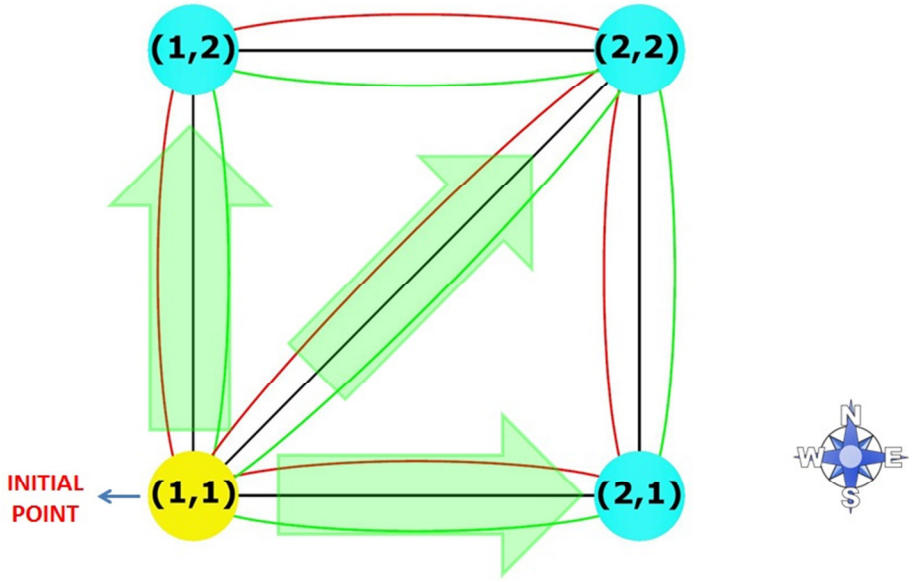

Figure 3.8 Allowed directions for the motion of the aircraft traveling to North-East

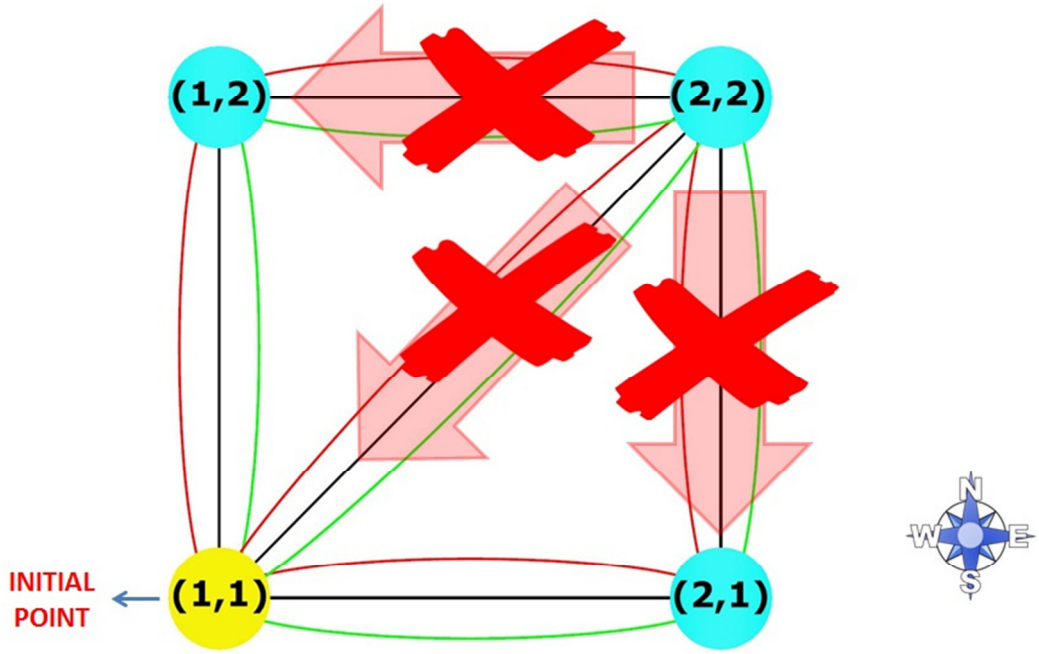

Figure 3.9 Prohibited directions for the motion of the aircraft traveling to North-East

The solar powered aircraft tends to follow the longest path during the day light under the allowed limitations since larger travel time means higher energy income and balance. A term that represents time consumption should be added in the cost function to supply the energy-time optimization and avoid having the aircraft travel along the borders of the grid system to travel over the longest distance and gain higher energy. Time penalty sectors are defined as given in Figure 3.10. Minimum cost for time is assigned to the "Time Penalty Sector 1" which means traveling from the initial point to the final point directly. The cost for the other time penalty sectors increase regularly and symmetrically around the first one. Bigger costs are assigned for the higher levels of time penalty sectors which reduce the chance the aircraft from traveling over the borders of the grid.

Time penalty sectors are visualized in three dimensions as shown in Figure 3.11. White lines show the grid structure from the initial point to the destination. The transparent areas in red color represent the imaginary penalty sectors. As can be understood from the figure, the minimum level of time penalty is defined for the direct flight from the initial point to the final one. On the other hand, the degree of the penalty for time increases exponentially toward the outer parts of the grid structure. The yellow line represents the degree of the time penalty increment. The minimum value of the time penalty and the degree of the increment are user defined. Consequently the user can arrange the optimal path of the aircraft systematically by arranging these parameters in the algorithm.

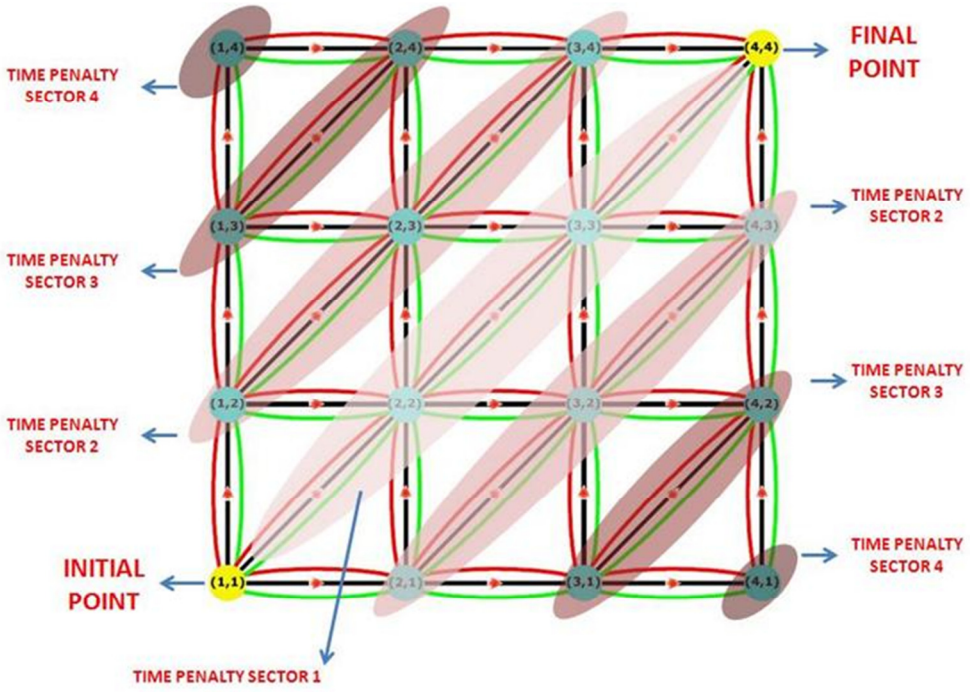

Figure 3.10 Time penalty sectors in the grid structure

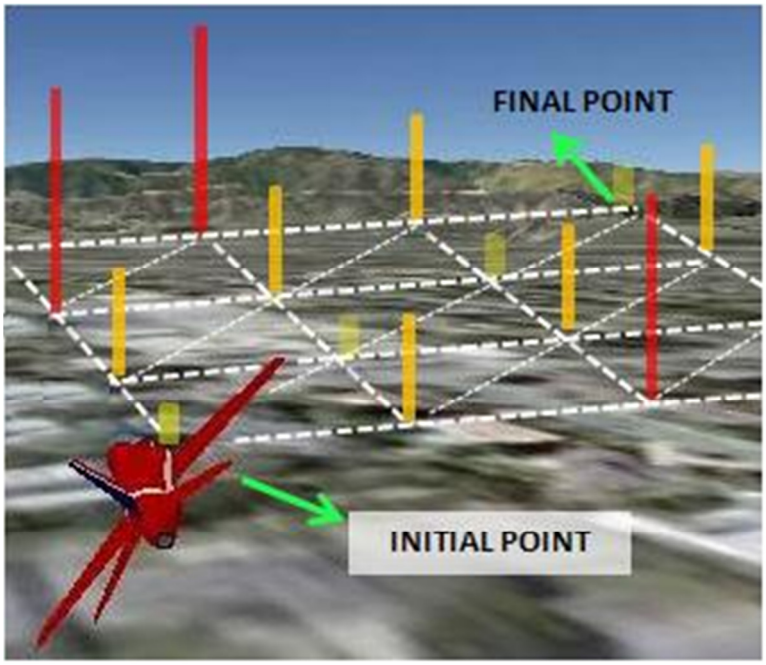

Figure 3.11 Three dimensional view of time penalty sectors

The equation of performance measure (cost function) is given by Equation (3.22) which is derived from Equation (2.10) and is a more specific case of the most general form. The energy balance term inside the formula $\left(E_{in_i} - E_{out_i}\right)$ is found by the energy gain and consumption equations. The time cost ($Time\ Penalty_i$) is user defined. The level of the cost for time is adjusted by setting the time penalty parameters inside the solution algorithm. For higher degree costs for time, the aircraft tends to make a direct flight from the initial point to the final point. On the other hand if the time cost is low then the aircraft tends to travel over the longest path during day light hours.

$$J = \int_{i=1}^{m} \left[\left(E_{in_i} - E_{out_i}\right) + Time\ Penalty_i\right].dt \tag{3.22}$$

Since the energy optimization of the aircraft is made for a long timeline, a dynamic solar model is developed to simulate the motion of the sun during the travel of the aircraft. According to this dynamic solar model, user defined solar time at the beginning of the travel is assigned to the initial point (1, 1). Energy income and consumption of solar aircraft when traveling from initial point to its neighboring grid points (1, 2), (2, 1) and (2, 2) are calculated separately by assuming that the hour angle is constant during the travel between two grid points and it is equivalent to the hour angle of the initial grid point (1, 1). Performance measure (cost function) is evaluated for each traveling line and for each roll angle alternative. Traveling time of the line and specific roll angle alternative that has maximum performance measure is kept in the manner of the dynamic programming. This traveling time which is added to the solar time at the initial point and solar time for the neighboring grid points are obtained by that way. Solar times and corresponding hour angles for the other points in the grid are calculated by repeating the same technique again and again for each point in the grid.

Grid structure of the algorithm is divided into three main parts in order to obtain the dynamic solar time model as can be seen in the Figure 3.12. "Zone 1" and "Zone 2" are the boundaries of the grid structure and solar time is calculated by Equation (3.23) and Equation (3.24) in these areas. The assigned solar time for the initial point (1, 1) is required in calculating the following solar times for these first two time zones. Solar time in the "Zone 3" is calculated by using the calculated solar times in the "Zone 1" and "Zone 2" as formulated in Equation (3.25). In Equations (3.23), (3.24) and (3.25) solar time in the grid points is symbolized by (ST) and the time spent by the aircraft between two nodes by obtaining the maximum performance measure is symbolized by (IT). To sum up, using the former solar time in calculating the (IT) to obtain the latter solar time by using the dynamic programming is the main idea in forming dynamic solar time model of the optimization algorithm.

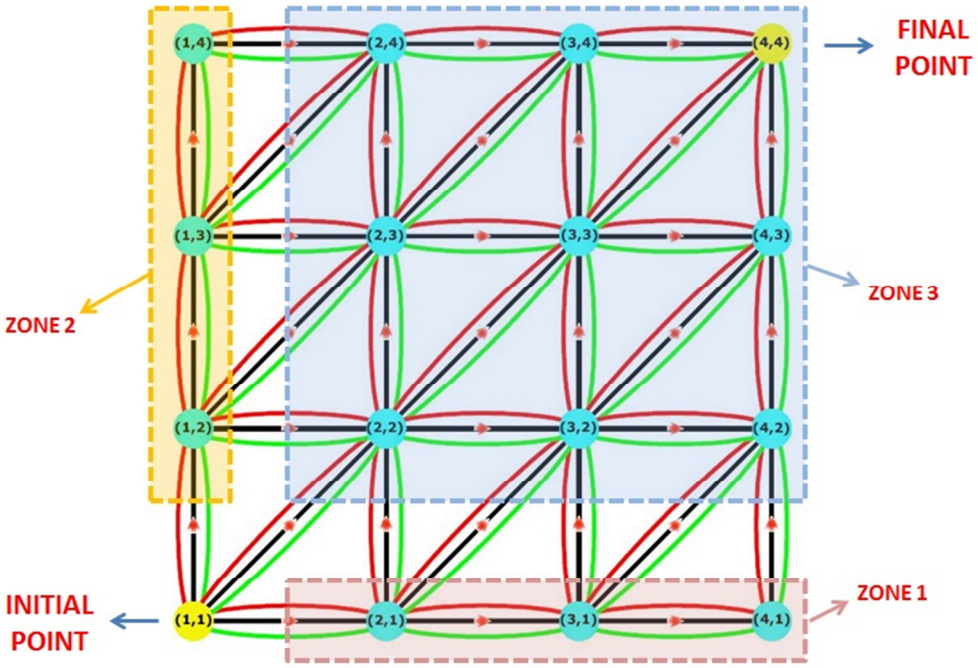

Figure 3.12 Time zones in the grid structure

$$ST\ (i+1,j) = ST(i,j) + max_{\phi}[IT(i,j,\Phi_1), IT(i,j,\Phi_2), IT(i,j,\Phi_3)] \tag{3.23}$$

$$ST(i,j+1) = ST(i,j) + max_{\phi}[IT(i,j\ ,\Phi_1\ ), IT(i,j,\Phi_2), IT(i,j,\Phi_3)] \tag{3.24}$$

$$\begin{aligned} &ST(i+1,j+1) = \\ &max\{[ST(i,j) + max_{\Phi}[IT(i,j,\Phi_1), IT(i,j,\Phi_2), IT(i,j,\Phi_3)\ ], \\ &[ST(i,j+1) + max_{\Phi}[IT(i,j+1,\Phi_1), IT(i,j+1,\Phi_2), IT(i,j+1,\Phi_3)], \\ &[ST(i+1,j) + max_{\phi}[IT(i+1,j,\Phi_1), IT(i+1,j,\Phi_2), IT(i+1,j,\Phi_3)]\} \end{aligned} \tag{3.25}$$

Inner costs (IC) and nodal costs (NC) are calculated while defining the dynamic solar time model and time penalty sectors by Equations (3.26) and (3.27). Inner costs are found by selecting the optimum roll angle that maximizes the cost between two grid points. The energy gain and loss equations between the grid points should be calculated and the cost of time needs to be assigned to find the optimal inner cost as defined in Equation (3.22). The optimal inner cost and corresponding roll angles are kept in an inner cost matrix while the others are thrown away in the manner of dynamic programming. Nodal costs are obtained by applying the formula given in Equation (3.27) to the system shown in Figure 3.13. Equation (3.27) is derived by applying the Bellman's Principle of Optimality for this optimal control problem specifically. After selecting the optimal nodal cost and inner cost couple which maximizes the performance measure for the node in question, the optimal cost couple is kept in another cost matrix which is defined as a nodal cost matrix, and the non-useful values are thrown away similar to previous stage.

$$IC(i,j) = max_{\phi}\,[IC(i,j,\Phi_1), IC(i,j,\Phi_2), IC(i,j,\Phi_3)] \tag{3.26}$$

$$NC(i+1,j+1) = max\{[NC(i,j) + IC(i,j)], [NC(i,j+1) + IC(i\,,j+1\,)], [NC(i+1,j) + IC(i+1,j)]\} \tag{3.27}$$

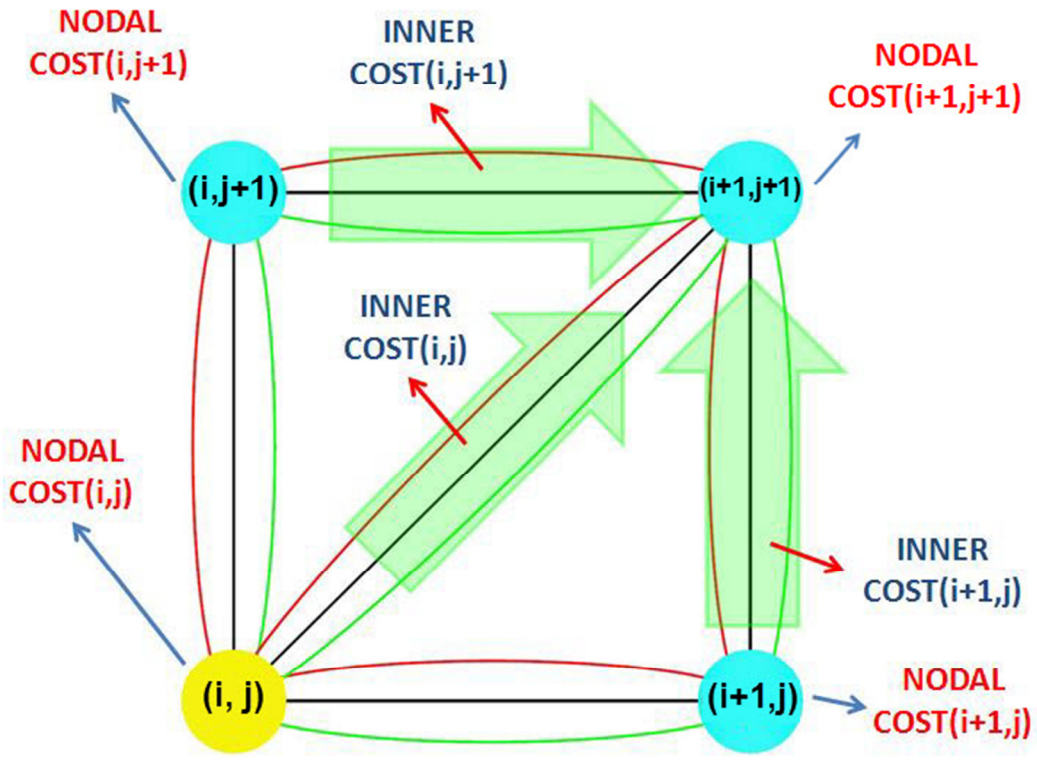

Figure 3.13 Calculation of the nodal costs

The final cost (performance measure) is found by reading the nodal cost in the final point. For the specific example given in this Chapter, the nodal cost in the node of (4, 4) gives the final cost. The optimal route from the initial point to the final point is found by reading the corresponding indices of the cost matrix values that gives optimal (highest performance measure) costs. Likewise, the optimal roll angles are obtained by reading the corresponding indices of roll angles for the best performance measure.

The results of the optimization process for the different cases will be presented in the next chapter. Comments of the results will be stated in addition to the results in the Chapter 4.

CHAPTER 4

RESULTS & DISCUSSION

An energy optimal path planning algorithm is capable of determining the optimal path of an unmanned solar powered aircraft for any date of the year and for any location on earth. Initial and final positions of the aircraft on earth are required to be defined by the user as well as the beginning time and date of the travel. Travel time of the aircraft for a user defined mission scenario is not an input for the optimization algorithm since the velocity of the aircraft is constant for the entire mission.

The optimal control technique of dynamic programming is used as the tool for optimization. A performance measure (cost function) is constituted from the terms energy income, energy consumption and time penalty in which the time penalty is user defined. Degree of time penalty is assigned by the user in the beginning of the optimization process. Four time penalty levels are defined for the results presented in this chapter. The first is zero level of time penalty which means actually there is no time penalty. The others are low, moderate and high level of time penalties in which time penalty values are 2.2, 2.6 and 3.1. These values are selected to make the concept of time penalty more comprehensible for readers. Varied combinations of these time penalty levels are chosen according to the flight profile of different cases.

The energy optimal route for the defined conditions is the main output of the algorithm. Moreover, the change of the optimal roll angle of the aircraft with time is also needed to be given since it is another flight parameter which is directly related with energy income and consumption of the aircraft. In addition to essential flight parameters of the aircraft, critical information about the energy balance of the aircraft is indicated like change in power generated, power consumption and net power of the aircraft during its travel. Solar time is given rather than flight time for these energy graphs since solar time is directly related with level of energy. Although the most of the fundamental flight information is calculated by the optimization algorithm, this information is provided in this section because of not being directly related with energy optimal route of the aircraft.

Although it is possible to make an energy optimization for a wide range of mission scenario alternatives, three main profiles are chosen in this chapter to illustrate the performance of the algorithm. The first mission is a direct flight on the East-West axis on the equator starting at 4 a.m. on the morning of the spring equinox. The second mission is a direct flight on the South-North axes starting at 4 a.m. from the equator on the summer solstice. The final and the most complicated mission is a flight starting from the equator at 4 a.m. to a destination point 250 kilometers away on the East axes and again 250 kilometers away in North axes. Four critical dates of the year are chosen to test the performance of the

algorithm for this type of flight which are the winter solstice, summer solstice, autumn equinox and spring equinox.

4.1 Case 1: Flight on East-West Axes on the Spring Equinox on the Equator

The first mission scenario case tests the optimization algorithm for a special time of the year for a special position of the earth. The equinoxes at the equator are unique as the sun rises due east, sets due west, moves across the sky in a vertical east-west plane, and for a horizontal surface as a zero angle of incidence at solar noon.

The solar powered aircraft starts its mission at 4 a.m. on the Equator and travels 600 kilometers to the east with constant velocity. The mission of the aircraft is planned to optimize the route for all the day light from sunrise to sunset. Two extreme time penalty levels are tested which are zero and high time penalty levels.

The aircraft keeps unrolled flight with zero banking angle for the entire travel for both of the extreme time penalty levels as shown in Figure 4.1 and Figure 4.3. This result is as expected since there is no sunlight during the night time so the aircraft should travel with minimum energy consumption and during the day the sun rays impact horizontal surface on an east-west vertical plan, so that maximum energy gain and minimum energy consumption can be sustained by an unrolled flight during day time. According to the energy balance situation of this case, the power generated has a regular character and power consumption is constant since there is no change in roll angle as can be seen in Figure 4.2 and Figure 4.4.

Total energy produced, consumed and net energy is given in the Table 4.1 with the total flight time for both two levels of time penalties. All of the values are same for two different types of time penalties since the flight path is same for them. Since the aircraft flies directly to the destination point without any roll maneuver, total flight time can be calculated easily by dividing the direct distance between initial and the final points to the velocity of the aircraft.

Table 4.1 Total flight time and total energy balance of the aircraft for Case 1

	Unit	**Zero Level of Time Penalty**	**High Level of Time Penalty**
Total Energy Produced	[kJ]	2293.2	2293.2
Total Energy Consumed	[kJ]	1086.4	1086.4
Total Net Energy	[kJ]	1206.8	1206.8
Total Flight Time	[s]	60000	60000

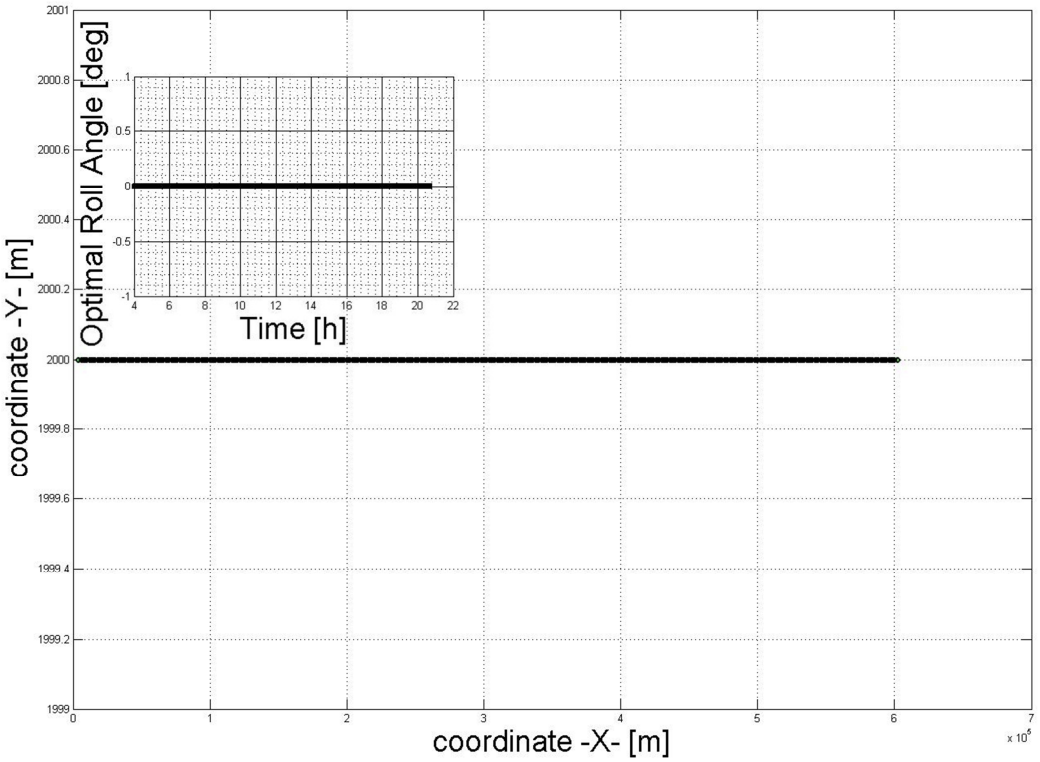

Figure 4.1 Energy optimal route and roll angle for Case 1 for zero level of time penalty.

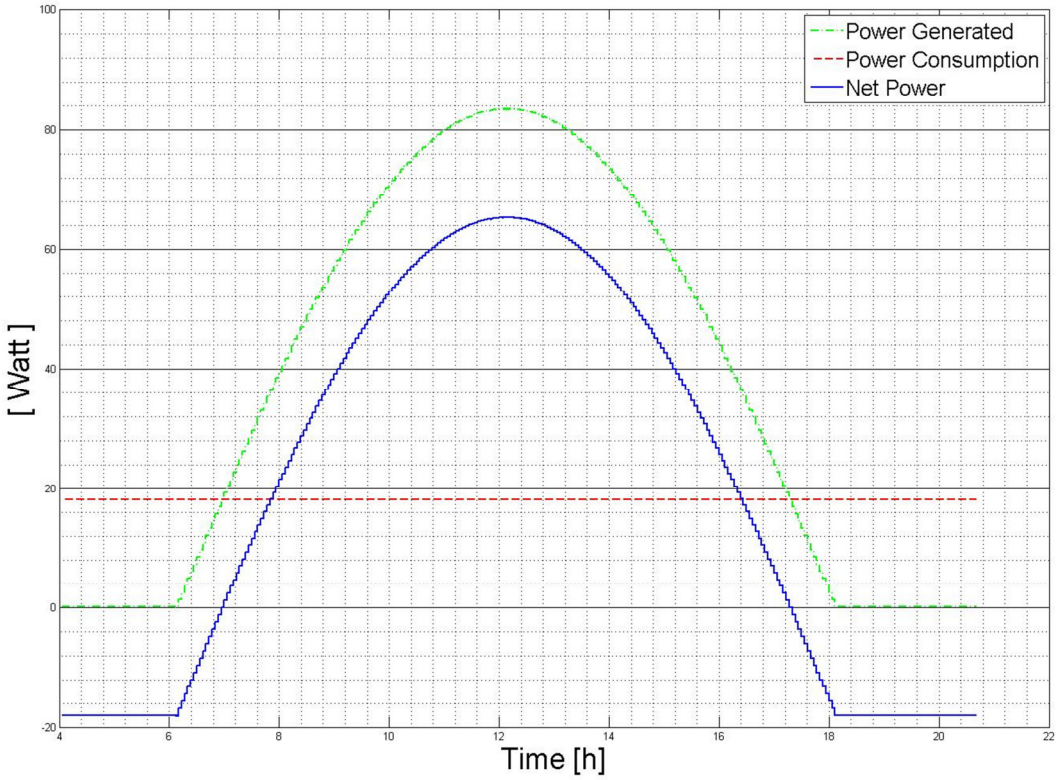

Figure 4.2 Power generated, power consumption and net power for Case 1 for zero level of time penalty.

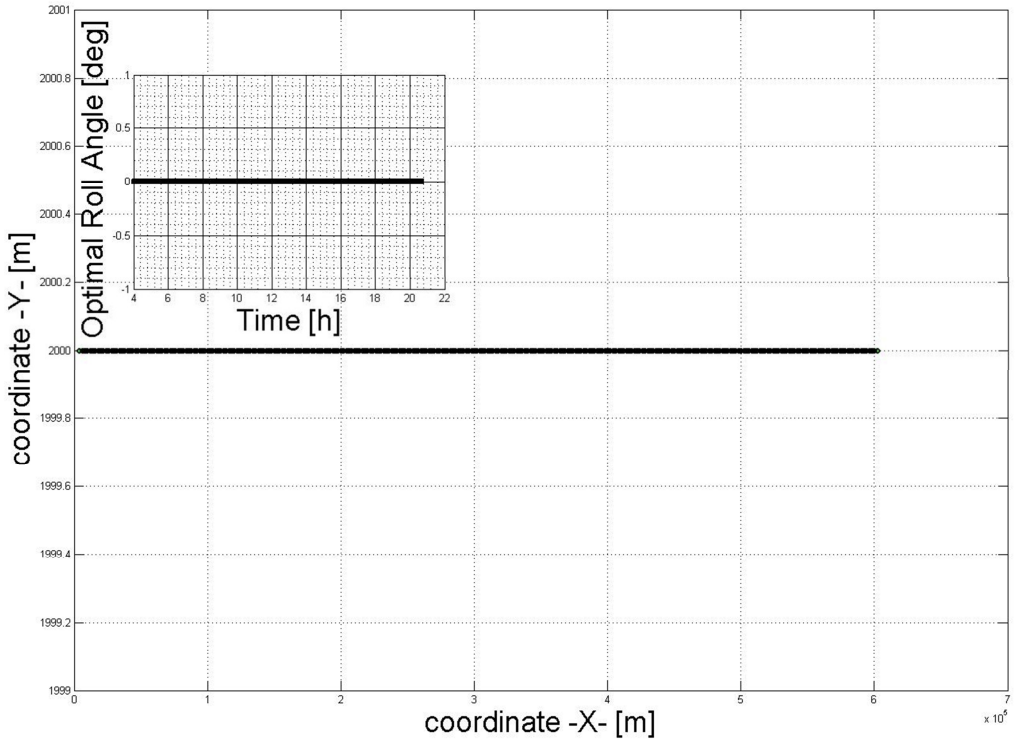

Figure 4.3 Energy optimal route and roll angle for Case 1 for high level of time penalty.

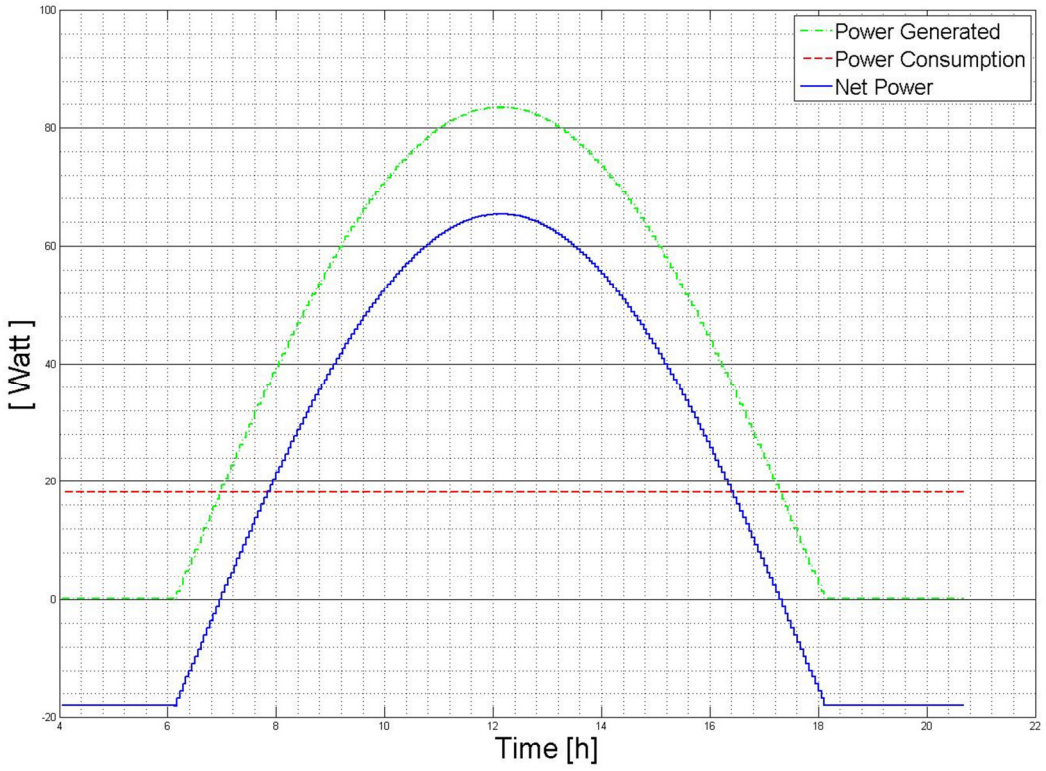

Figure 4.4 Power generated, power consumption and net power for Case 1 for high level of time penalty.

4.2 Case 2: Flight on South-North Axes on the Summer Solstice in the Northern Hemisphere

The solar powered aircraft starts its travel at 4 a.m. from the equator and travels to the north on the summer solstice of Northern Hemisphere (21st of June) for this case. The mission of the aircraft is to travel 600 kilometers to the north with constant velocity. The distance of the travel is arranged to analyze the motion of the aircraft from sunrise to sunset. This mission scenario is performed to test the roll angle attitude of the optimization algorithm with a very basic profile.

Three different time penalty levels are applied for this case as indicated before. Zero time penalty level is performed rather than low time penalty level for this case since it is more meaningful to test the zero time penalty level specifically for this type of motion.

Figure 4.5 indicate the motion of the aircraft for the zero time penalty level flight of Case 1. The roll angle of the aircraft is zero until sunrise and after sunset as expected. The aircraft starts to make a very high roll angle to the east at sunrise and keeps this roll angle over the early morning to maximize the power generated. The roll angle decreases step by step from morning to solar noon as the sun moves higher in the sky and then switches from a positive to negative in the early afternoon. In the afternoon the roll angle character of the aircraft is perfectly symmetrical with the morning with its roll angle level increasing from early afternoon to sunset.

The energy balance situation of the aircraft for the zero time penalty level flight of Case 1 can be analyzed from Figure 4.6. The power generated increases regularly from sunrise to almost 10 a.m. and has a local peak at the end of this first period. After the power generated reach its local maximum slightly before 10 a.m., the power generated decreases slightly due to the aircraft also decreasing its roll angle by a discrete amount to adjust its solar panels according to the motion of the aircraft. After decreasing its roll angle, the power generated decreases dramatically at first but starts to increase again up to the level of the first local extreme point. The power generated reaches its second local peak around 11 a.m., which actually has the same value as the first peak. This routine is repeated again before solar noon and in the afternoon. The solar aircraft first decreases its roll angle around noon and then increases it step by step to the west to minimize the solar incidence angle due to the moving sun.

Although the power generated has several peak points during the day time with the same power values, the net power has its maximum value around the solar noon as expected as follows. The solar aircraft consumes more energy to sustain a flight with higher roll angle. In the early morning and late afternoon the aircraft needs to fly with higher roll angle relative to solar noon to minimize its solar incidence angle. Consequently, the power consumption of the aircraft rises in these periods of the day.

A moderate time penalty level is applied to the same mission scenario and the results are given in Figure 4.7 and Figure 4.8. The solar powered aircraft decreases its roll angle to reduce the flight time due to the effect of increasing the time penalty value. Since the aircraft flies on a shorter arc with a smaller roll angle, it is meaningful to have smaller roll angle values with higher time penalties.

As can be seen from Figure 4.5 and Figure 4.7, in the early morning and in the late afternoon the aircraft keeps its maximum roll angle (30 degrees) for a longer time for a zero time penalty level flight than for the moderate time penalty level flight. This difference in the flight profile of the aircraft affects the power generated directly by having a lower local peak point for the early morning for the moderate time penalty level relative to the zero penalty level. Three different roll angle steps are distributed almost equally for the moderate time penalty level flight. On the other hand, flight time of the maximum roll angle step (30 degrees) is clearly higher than the others for low time penalty level flight. This situation is also easy to predict since the aircraft consumes more time for a higher roll angle flight. The roll angle distribution of the aircraft is also symmetrical according to the solar noon.

Although the maximum level of the power generated is same for low and moderate time penalty level flights, the area under the power generated curve for low level time penalty level flight is larger than the other as can be seen from Figure 4.6 and Figure 4.8. This result is clear since the aircraft lose its generated energy by reducing its flight time.

The high time penalty level is also tried for the same mission scenario and the results are shown in Figure 4.9 and Figure 4.10. The aircraft flies directly to the final destination point with a zero banking angle flight to minimize the travel time as can be seen in Figure 4.9. The solar panels on the wings act as non-tracking solar panels that face to straight up and consequently the power generated curve has a regular character which has its peak at solar noon.

Table 4.2 indicates the values of the total energy produced, total energy consumed, total net energy and total flight time for three different time penalty levels for Case 2. As can be predicted both total energy produced, consumed, total net energy and total flight time decreases with the increasing level of time penalty. Results in the Table 4.2 support the role of the time penalty defined in the Chapter 3.4.

Table 4.2 Total flight time and total energy balance of the aircraft for Case 2

	Unit	**Zero Level of Time Penalty**	**Moderate Level of Time Penalty**	**High Level of Time Penalty**
Total Energy Produced	[kJ]	2683	2454.2	2167.6
Total Energy Consumed	[kJ]	1500.2	1316.8	1086.4
Total Net Energy	[kJ]	1182.8	1137.4	1081.2
Total Flight Time	[s]	76895.6	71301.7	60000

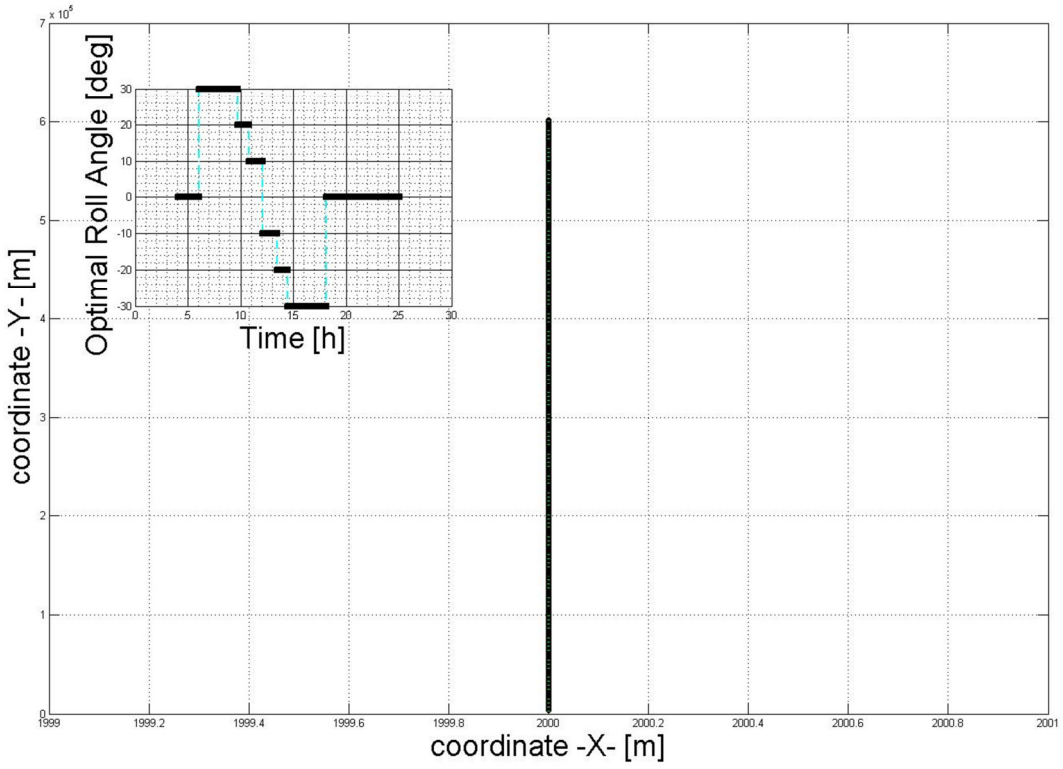

Figure 4.5 Energy optimal route and roll angle for Case 2 for zero level of time penalty.

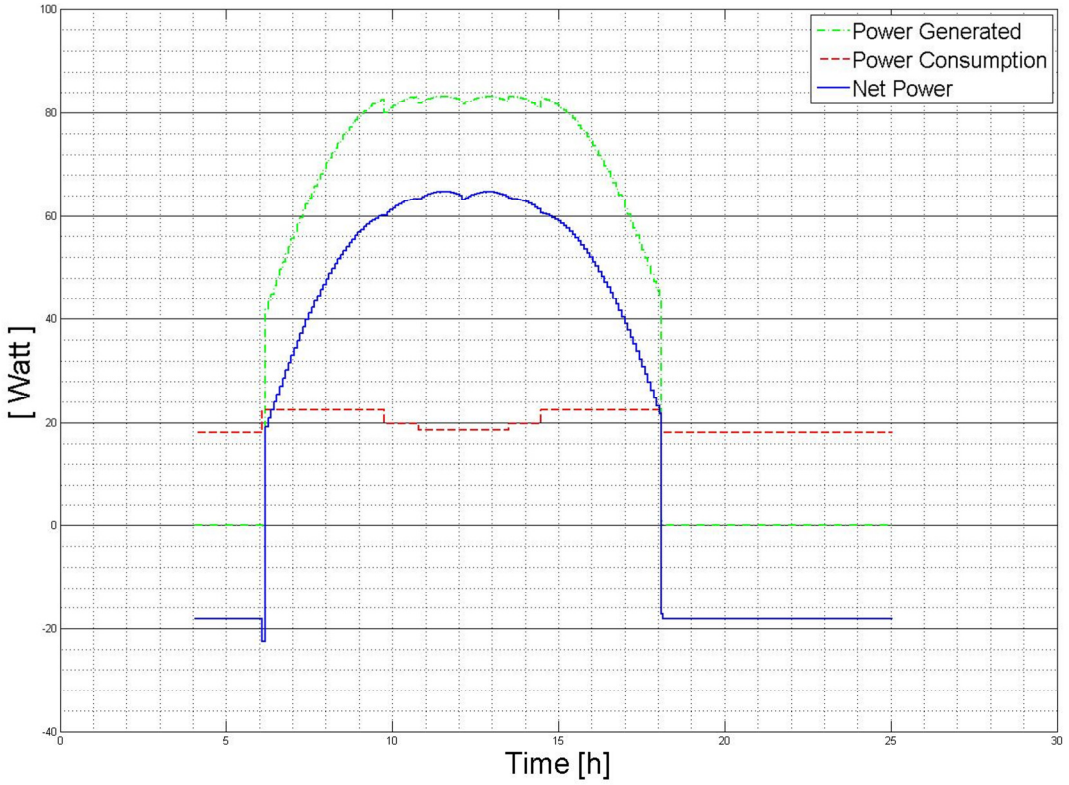

Figure 4.6 Power generated, power consumption and net power for Case 2 for zero level of time penalty.

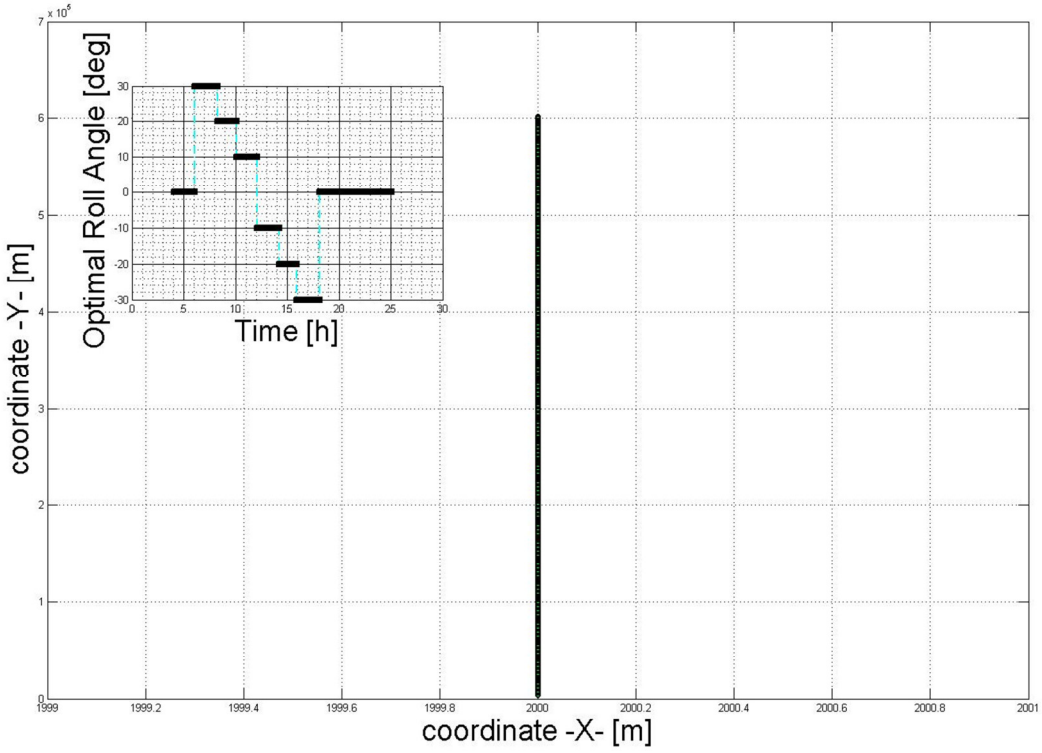

Figure 4.7 Energy optimal route and roll angle for Case 2 for moderate level of time penalty.

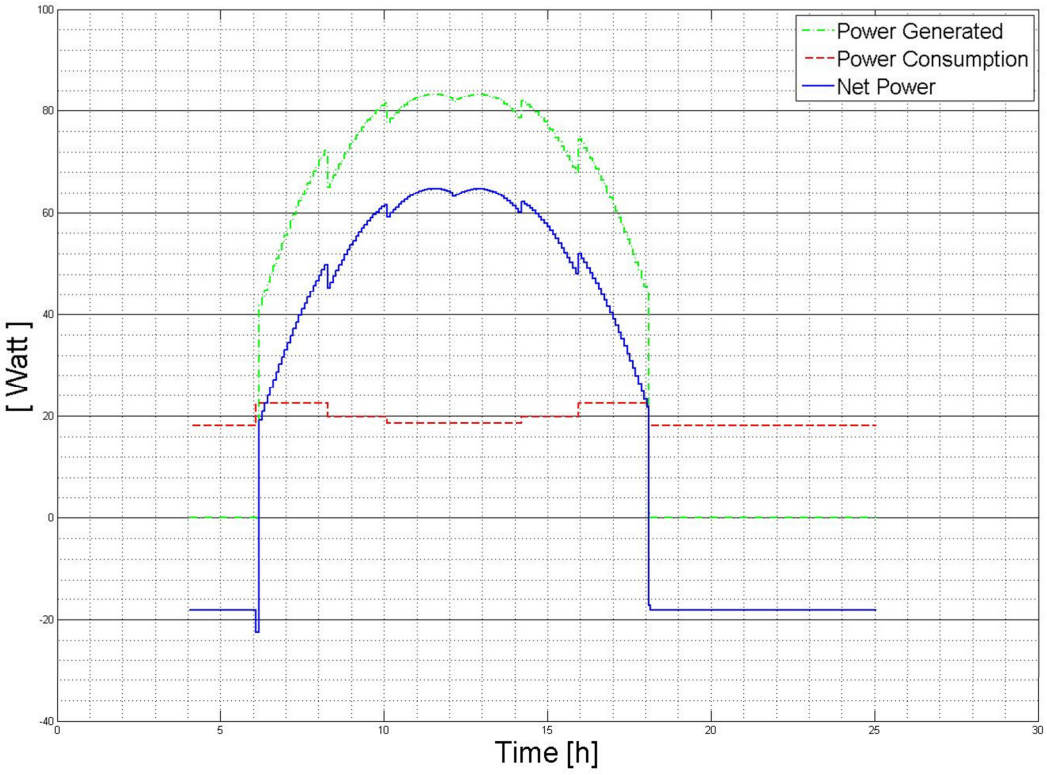

Figure 4.8 Power generated, power consumption and net power for Case 2 for moderate level of time penalty.

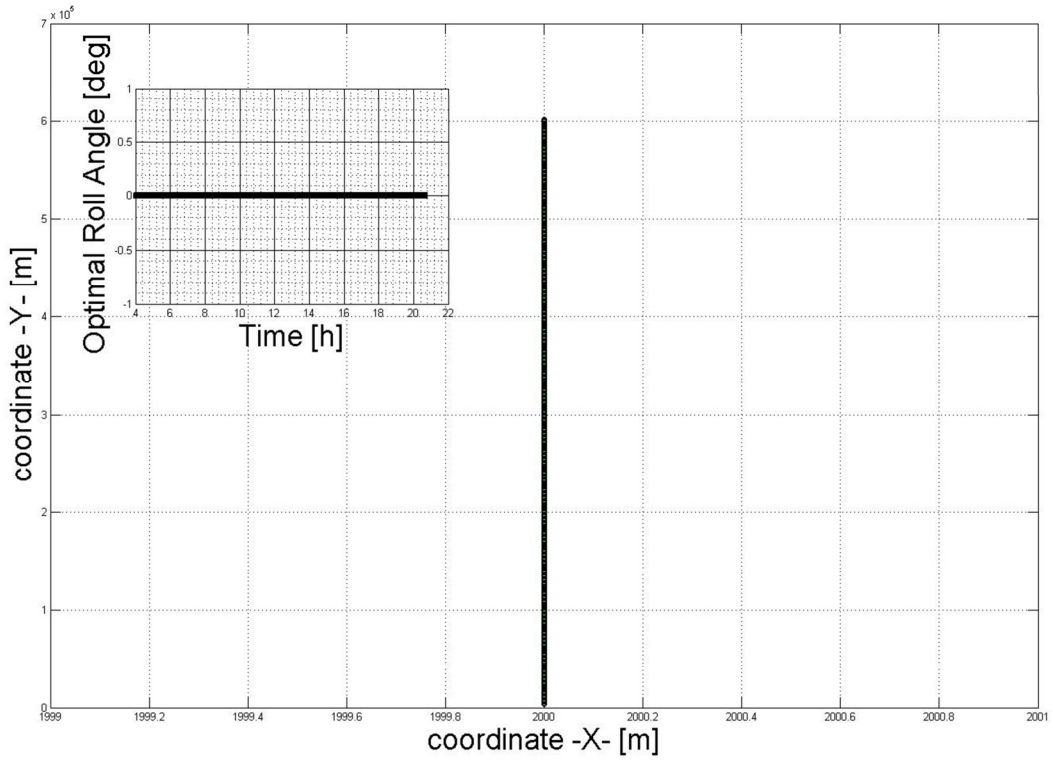

Figure 4.9 Energy optimal route and roll angle for Case 2 for high level of time penalty.

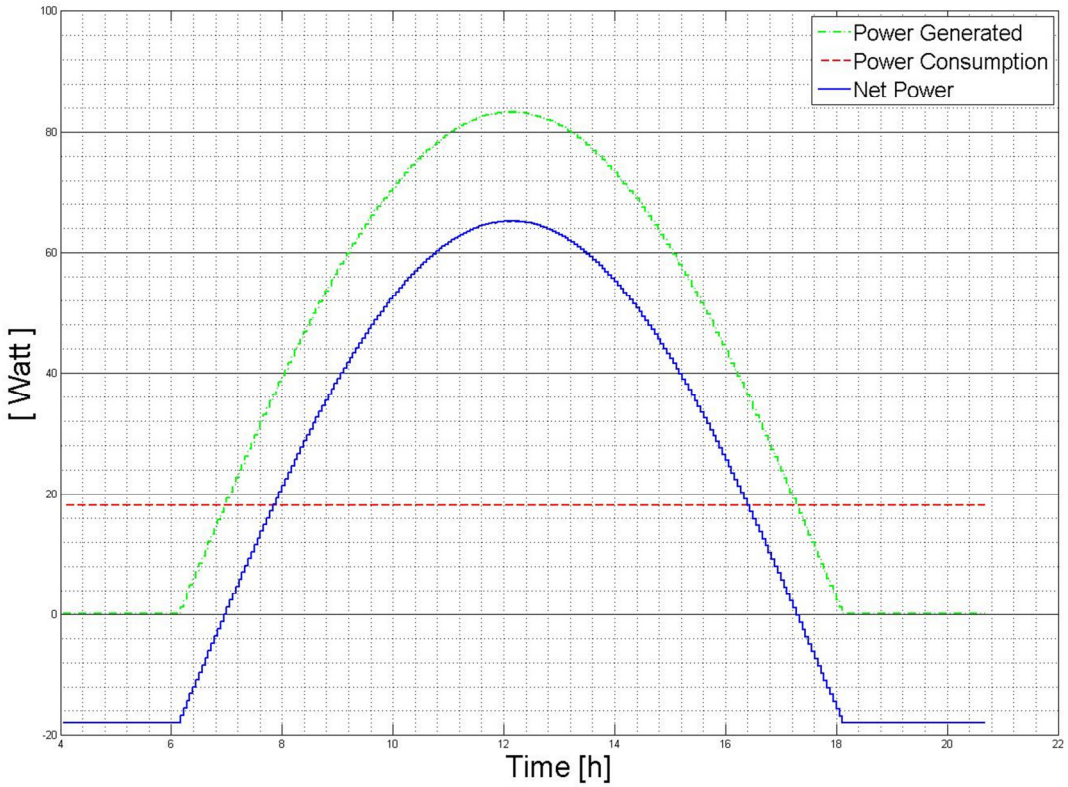

Figure 4.10 Power generated, power consumption and net power for Case 2 for high level of time penalty.

4.3 Case 3: Two Axes Flight on the Spring Equinox for the Northern Hemisphere

In the first two cases, the flights of the solar powered aircraft on south-north and east-west (single axis) paths are optimized to test the performance of the algorithm. Two axes flight where the aircraft must move in both the north and east directions is chosen for the third case since it is a more realistic type of flight scenario and it is also better to illustrate the capabilities and limitations of the optimization algorithm.

The initial point of the travel is chosen as the latitude of Ankara (39.55 degrees N). The aircraft starts its travel at 4 a.m. and flies 250 kilometers in both the east and north directions. These values are selected to optimize the route and roll angle of the aircraft for all the day light time and to make the output graphics more comprehensible. The spring equinox is chosen to perform the optimization process and take the outputs for this case. The results of the other three critical dates of the year (autumn equinox, winter solstice and summer solstice) are also given in the Appendix C.

Three main time penalty levels are tested for the case optimized in this sub-section (and for the three other similar cases in the Appendix C) which are low, moderate and high time penalty level of optimizations.

Figure 4.11 and Figure 4.12 are the main outputs of the optimization process which have a low level of time penalty level. The aircraft flies directly to the destination point before sunrise and after sunset with zero banking angle, which has minimum level of energy consumption. The flight character of the aircraft during the night time is logical and can be predicted easily. The aircraft starts to fly to the east with a high roll angle by facing its wings and solar panels to the south in the early morning. Then it heads to the north and utilizes the sun rays by facing its solar panels to the east. The effect of the time penalty can be seen in the areas which are bordered and signed with red and blue points in the Figure 4.11. The aircraft heads to the destination point with the effect of the time penalty in these areas rather than making a longer travel and collecting more solar energy. The aircraft still has a high banking angle in these time penalty affected zones. The area between the red and blue bordered zones shows the movement of the aircraft around solar noon. The aircraft makes a direct flight to the east around the solar noon by making a high roll angle and facing its solar panels to the south. The path of the aircraft after early afternoon (after 3 p.m.) is almost symmetrical with path in the early morning with its high level of roll angle in the opposite direction of the morning. The aircraft head to the north first by facing its solar panels to the west and then heads to the east in the late afternoon.

Figure 4.12 shows the energy balance situation of the aircraft during its travel. The regularly increasing area of the generated power between 6 a.m. and 10 a.m. reflects the energy income of the aircraft during its flight before the red signed zone. The aircraft keeps a constant roll angle in this area with a regular power generated character. In the red and blue bordered zones (which also correspond to the same colored zones in Figure 4.11) the aircraft change its yaw and roll angles periodically and the power generated curve has a dynamic character consequently.

Moderate and high levels of time penalties are also applied for the same mission scenario and results are indicated with Figure 4.13, Figure 4.14, Figure 4.15 and Figure 4.16. Relative to the lower time penalty zone, the aircraft tends to make a more direct flight with

increasing level of time penalty degree. On the other hand, the aircraft still keeps making banking flight which means that the flight time is reduced by flying directly to the destination rather than making a straight flight with zero bank angle.

The red and blue bordered areas in the Figures in question keep expanding with increasing level of time penalty which means that the time penalty component of the performance measure forces the aircraft to make a straighter flight. On the other hand, the route of the aircraft at solar noon keeps its straight character to the east with aircraft's sloped wings to the south. As a result, the areas in the early morning and in the late afternoon are affected directly from increasing level of time penalty by becoming straighter from the initial point to the destination point.

The roll angle of the aircraft generally varies between 20 degrees and 30 degrees (positive before the solar noon and negative after the solar noon) in the red and blue signed areas of the flight. This situation affects the power generated curves directly as can be seen in Figure 4.14 and Figure 4.16. There are two concrete curve characters for the Figures in question. A wider curve with lower peak point reflects the 30 degrees banked flight while the narrower curve with higher peak level shows the 20 degrees banked flight.

Total amount of energy produced and consumed are given in addition to the total net energy and total flight time in the Table 4.3. Solar powered aircraft tends to travel form initial point to the destination in a shorter time with decreasing energy production and consumption with increasing level of time penalty. Consequently, the results presented in the Table 4.3 support the role of the time penalty and idea of the optimization similar to the Table 4.1 and Table 4.2.

The aircraft flies directly to the destination point in night time for the cases which are represented in the Appendix C. Solar panels of the aircraft faces to the sun by daytime and the aircraft can deviate from the maximum energy balance position during the moment of the flight to obtain a higher energy collection for entire flight path. As a result, properties of the optimized flight paths of the cases which are represented in the Appendix C are consistent with the case given in this sub-section.

Table 4.3 Total flight time and total energy balance of the aircraft for Case 3

	Unit	**Zero Level of Time Penalty**	**Moderate Level of Time Penalty**	**High Level of Time Penalty**
Total Energy Produced	[kJ]	1814.9	1712.2	1618.6
Total Energy Consumed	[kJ]	907.9	859.4	811.9
Total Net Energy	[kJ]	907	852.8	806.7
Total Flight Time	[s]	61469.4	60649.3	59625.6

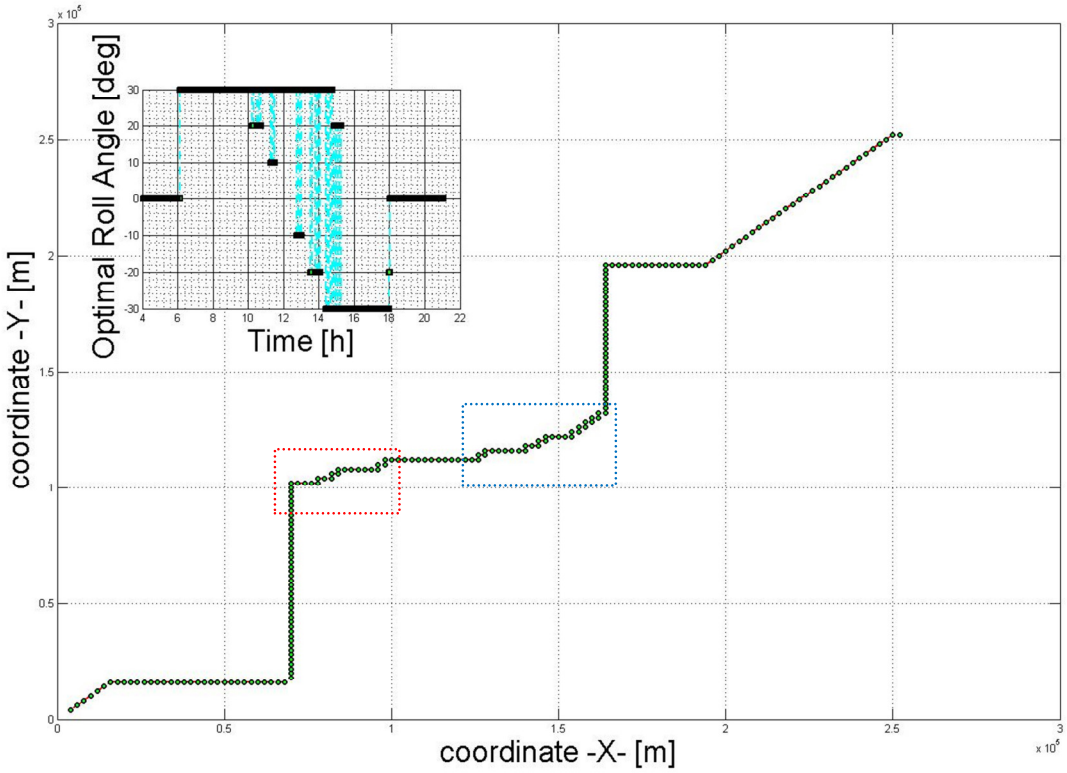

Figure 4.11 Energy optimal route and roll angle for Case 3 for low level of time penalty.

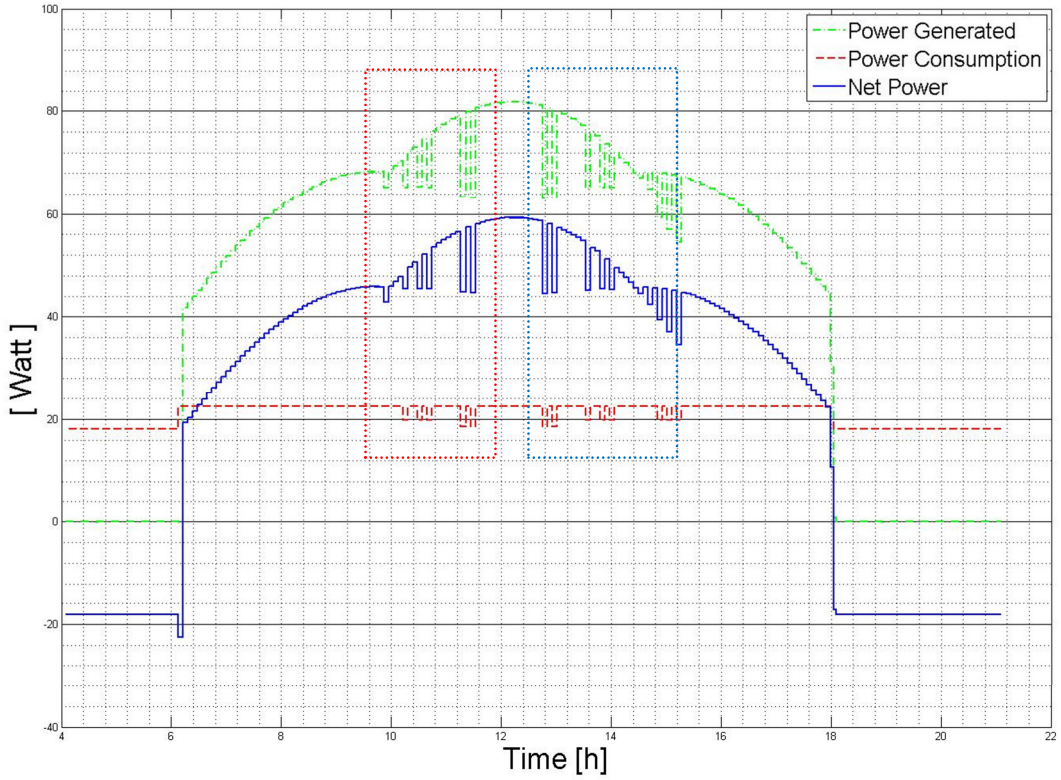

Figure 4.12 Power generated, power consumption and net power for Case 3 for low level of time penalty.

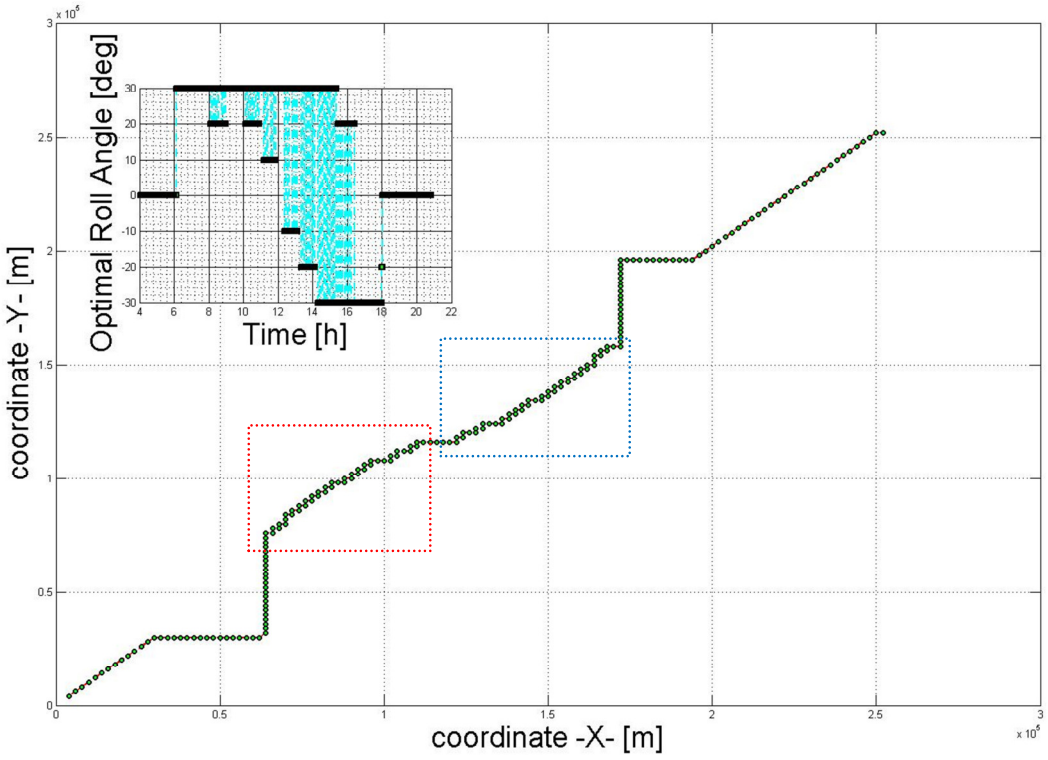

Figure 4.13 Energy optimal route and roll angle for Case 3 for moderate level of time penalty.

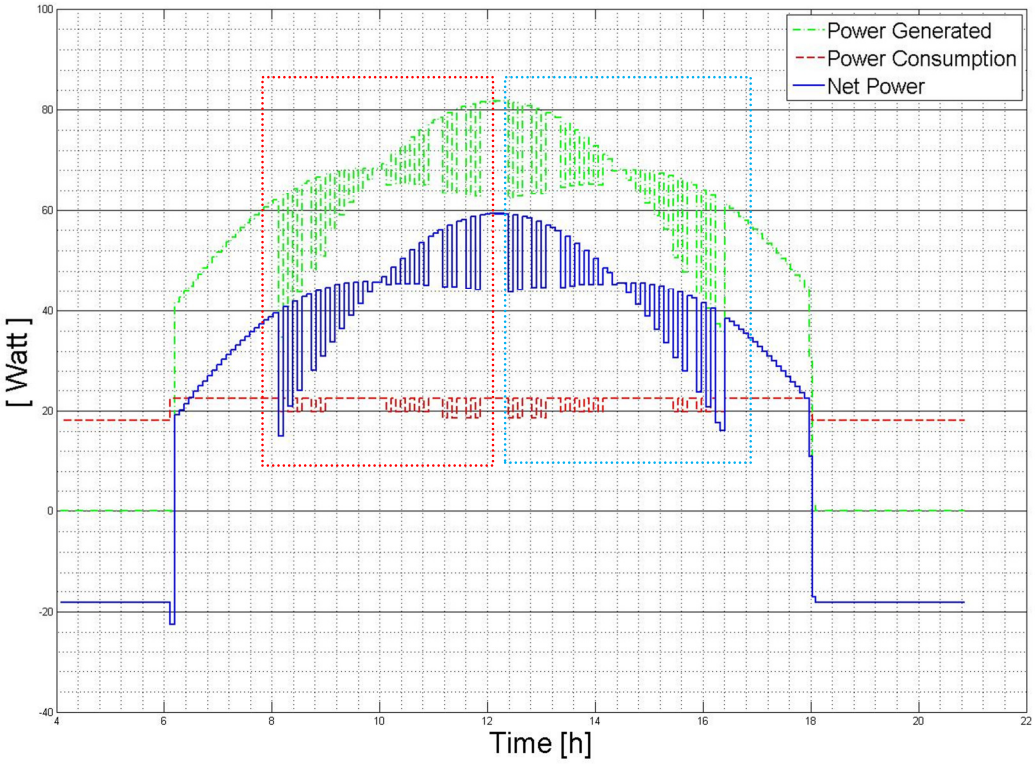

Figure 4.14 Power generated, power consumption and net power for Case 3 for moderate level of time penalty.

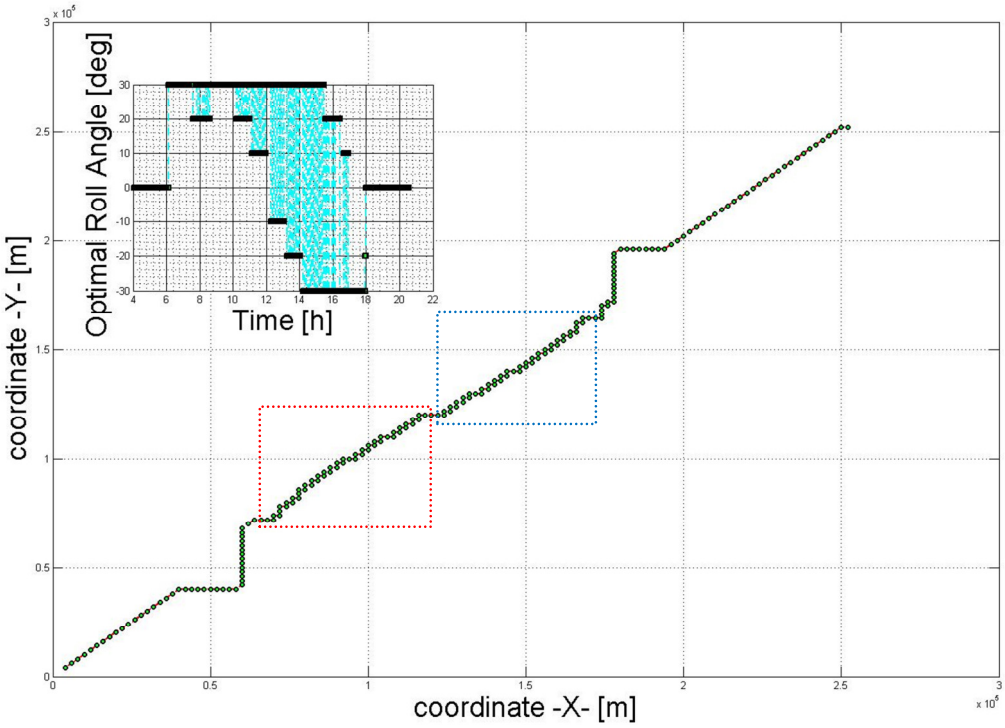

Figure 4.15 Energy optimal route and roll angle for Case 3 for high level of time penalty.

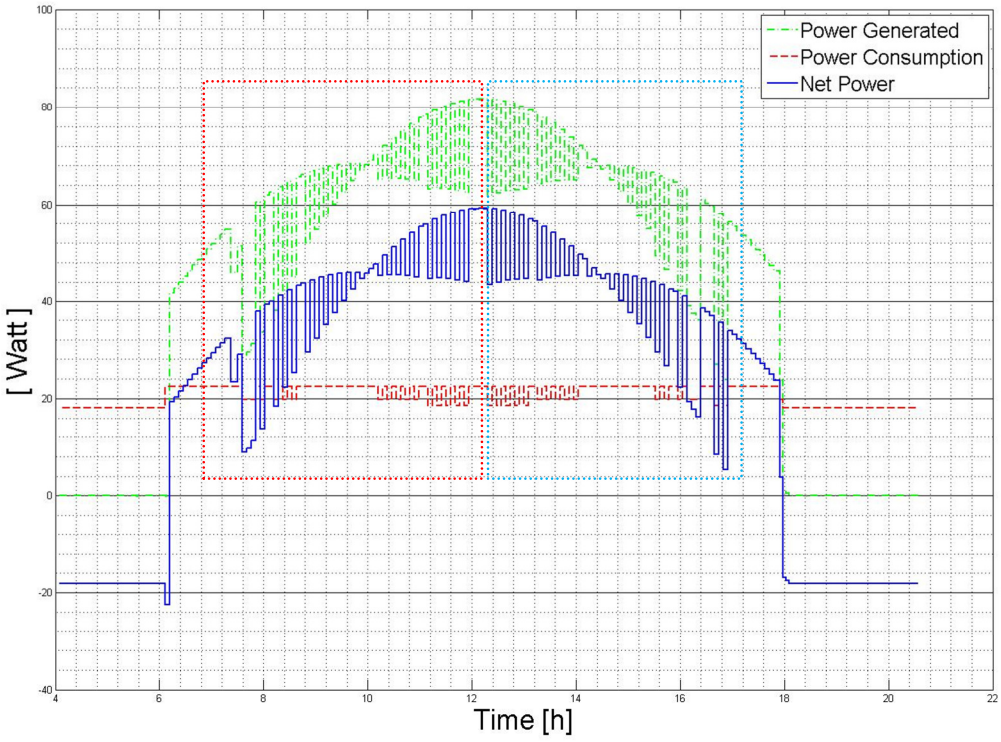

Figure 4.16 Power generated, power consumption and net power for Case 3 for high level of time penalty.

CHAPTER 5

CONCLUSIONS & FUTURE WORK

5.1 Conclusions

In this thesis, a novel method is developed to make the energy optimal path planning of an unmanned solar powered aircraft for a long timeline characterized by the sun's position changing during the flight. The literature about the related subjects is summarized in Chapter 1. General concepts about flight mechanics, solar energy conversion and optimal control techniques (especially dynamic programming) are given in the second chapter. The concepts underlying the optimization are explained in the third chapter which is the theoretical heart of the thesis study. Several important mission scenarios are tested and results are discussed in the Results and Discussion chapter.

The critical role of the roll angle for solar powered aircrafts both on energy generation and energy consumption is the most important concept behind this thesis study. The overall energy level of the batteries in a solar powered aircraft can be maximized by optimizing the roll angle during the flight. There are also several constraints on the mission and the technical capabilities of the aircraft which must be taken into account.

Flights with shorter timelines are generally discussed and optimized in the current literature of flight route optimization for solar powered air vehicles. The main reason for this situation is the very high computation loads of optimization processes for higher timelines. This thesis study differs from the current literature by focusing on the general position and roll angle of a solar aircraft in a large area and long timeline rather than analyzing the motion of the aircraft in detail in a very limited time. Analyzing long timelines also brings extra problems apart from calculation loads. The position of the sun in the sky is accepted as constant in the existing literature for optimization studies that analyze limited timelines. In the present work a novel dynamic solar model which simulates the motion of the sun for long flight times that is synchronized to the motion of the aircraft is developed by using dynamic programming.

The problem is easily divided into smaller sub problems so the dynamic programming method is also used as an optimal control technique which reduces the computation load significantly. A performance measure which is a quantitative criterion of the selection set of parameters to be maximized is defined to perform the optimization process. Control of the time penalty component is given to the user since it should be user defined.

Design parameters, technical capabilities and main dimensions of the aircraft are taken from a convenient solar powered aircraft which is explored in the thesis study and these properties are used as the inputs of the optimization process [3]. The aircraft is assumed to fly at a constant altitude over the clouds so shading effect of the clouds is not taken into account.

The velocity of the aircraft is assumed to be constant for the entire flight which turns the flight mechanics part of the thesis into a steady state flight problem. The aircraft makes a steady state turn or steady state level flight between grid points with this assumption.

5.2 Future Work

Examining the energy optimal route of a solar powered aircraft is a quite new study area and this thesis constitutes a starting point for optimization studies of longer timelines. This study can be extended in the future according to the items below to make more accurate calculations, recommend a more realistic flight path, include more complicated mission cases and develop a more user friendly interface.

The extreme maneuvers of the aircraft at some critical points such as initial and final points of the steady state turns and the changes of the heading angle in the route can be eliminated be optimizing locally. An energy loss term can be derived for these critical points and this energy loss term during extreme maneuvers can be added to the cost function. More realistic outputs can be obtained by focusing on the tolerated extreme maneuver zones.

Optimization is performed for a steady state flight which always has constant velocity in this thesis study. The velocity of the aircraft can be varied by adding some other possible velocity values for the aircraft. Change of the velocity during the flight affects the flight mechanics equations. Steady state turn and steady state level flight would not be valid anymore. Different and more complicated maneuvers of the aircraft could be added to the flight profiles for this situation.

Additional missions can be assigned by utilizing the current dynamic programming optimization fundamentals of this algorithm. The traveling salesman problem is a well-known type of optimization problem which is very convenient to solve with the dynamic programming technique. This popular problem can be combined with the energy optimal route planning of solar powered aircrafts. This type of problem can have a potential application area in the future with the possible usage of solar powered aircrafts in intelligence and surveillance operations.

A new parameter which represents the altitude of the aircraft can be added to the current optimization algorithm. Effects of the atmosphere should be considered for this case. Information about the weather conditions can be input for the optimization study by reading them from TMY data or some other database.

Finally, a graphical user interface which makes the algorithm easier to use can be developed. This kind of interface is not required for the users that examine the current code and this thesis. On the other hand, it can be advantageous for the potential professional usage of algorithm.

REFERENCES

[1] Nam T., Soban D.S., Navris D.N., 2005, "Power Based Sizing Method for Aircraft Consuming Unconvential Energy", In 43rd AIAA Aerospace Science Meeting and Exhibit, Nevada.

[2] Landis A., Colozza A., LaMarre C.M., 2002, "Atmospheric Flight on Venus", AIAA-2002-0819, NASA/TM-2002-211467.

[3] Noth A., 2008, "Design of Solar Powered Airplanes for Continuous Flight", ETH Zurich.

[4] Klesh A.T., Kabamba P.T., 2007, "Energy-Optimal Path Planning for Solar-Powered Aircraft in Level Flight", AIAA 2007-6655.

[5] Herwitz S.R., Johnson L.F., Arvesen J.C., Higgins R.G., Leung J.G., Dunagan S.E., 2002, "Precision Agriculture as a Commercial Application for Solar-Powered Unmanned Aerial Vehicles", AIAA 2002-3404.

[6] SOLAR IMPULSE, Last accessed August 22, 2012, http://solarimpulse.com/en/.

[7] Klesh A.T., Kabamba P.T., 2009, "Solar-Powered Aircraft: Energy-Optimal Path Planning and Perpetual Endurance", Journal of Guidance, Control and Dynamics Vol.32.

[8] Spangelo S.C., Gilbert E.G., Klesh A.T., Kabamba P.T., Girard A.R., 2009, "Periodic Energy-Optimal Path Planning for Solar-Powered Aircraft", AIAA 2009-6016.

[9] Rizzo E., Frediani A., 2008, "A Model for Solar Powered Aircraft Preliminary Design", The Aeronautical Journal, pp. 57-78.

[10] Colozza A.J., 1993, "Effect of Power System Technology and Mission Requirements on High Altitude Long Endurance Aircraft", Sverdup Technology Inc., NASA Lewis Group.

[11] Colozza A.J., Scheiman D.A., Brinker D.J., 1998, "GaAs/Ge Solar Powered Aircraft", NASA/TM-1998-208652.

[12] Chichka D.F., Speyer J.L., 1998, "Solar Powered, Formation Enhanced Aerial Vehicle Systems for Sustained Endurance", NCC4-97040.

[13] Ehernberger L.J., Donohue C., Teets E.H., 2004, "A Review of Solar-Powered Aircraft Flight Activity at the Pacific Missile Range Test Facility, Kauai, Hawaii", 11th Conf. on Aviation, Range and Aerospace Meteorology, Hyannis.

[14] Collaborative Writing in Industry: Solar Powered Multipurpose Remotely Powered Aircraft, n.d., Worcester Polytechnic Institute, Proceedings of the NASA/USRA Advanced Design Program 7th Summer Conference.

[15] Duffie J. A., Beckman W. A., 1991, *Solar Engineering of Thermal Process*, Wiley Interscience, New York, pp. 3-46.

[16] Hull D. G., 2007, *Fundamentals of Airplane Flight Mechanics*, Springer, New York, pp. 1-14.

[17] McLean D., 1990, *Automatic Flight Control Systems*, Prentice Hall, Cambridge, pp. 1-62.

[18] Anderson J. D., 1999, *Aircraft Performance and Design*, McGraw-Hill, Singapore, pp. 199-337.

[19] Kirk D. E., 2004, *Optimal Control Theory: an Introduction*, Dover Publications, New York, pp. 3-107.

[20] Soylu R., 2012, ME 507 Applied Optimal Control, Middle East Technical University, Lecture/Class.

[21] Bellman R.E., Dreyfus S.E., 1962, *Applied Dynamic Programming*, The Rand Corporation, Santa Monica, pp. 180-231.

APPENDIX A

TECHNICAL PROPERTIES OF THE SELECTED AIRCRAFT

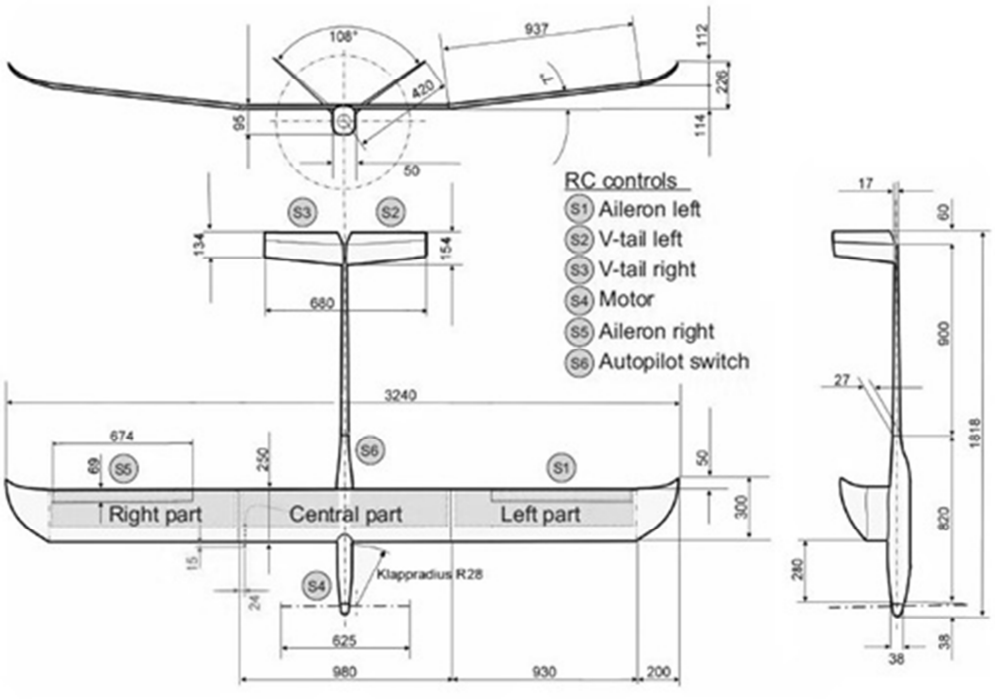

Figure A.1 Technical drawing of the selected aircraft **[3]**

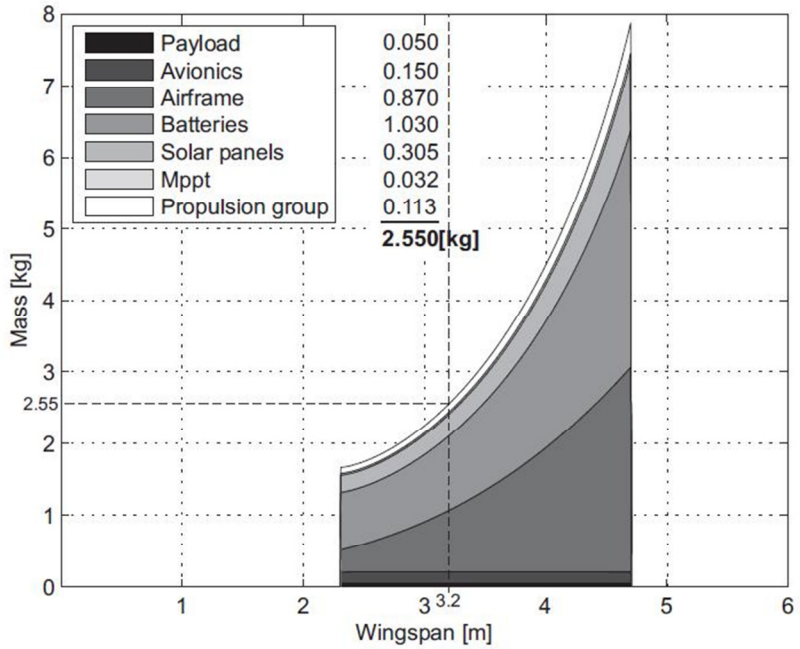

Figure A.2 Mass distribution of the Sky-Sailor for the aspect ratio of 13 **[3]**

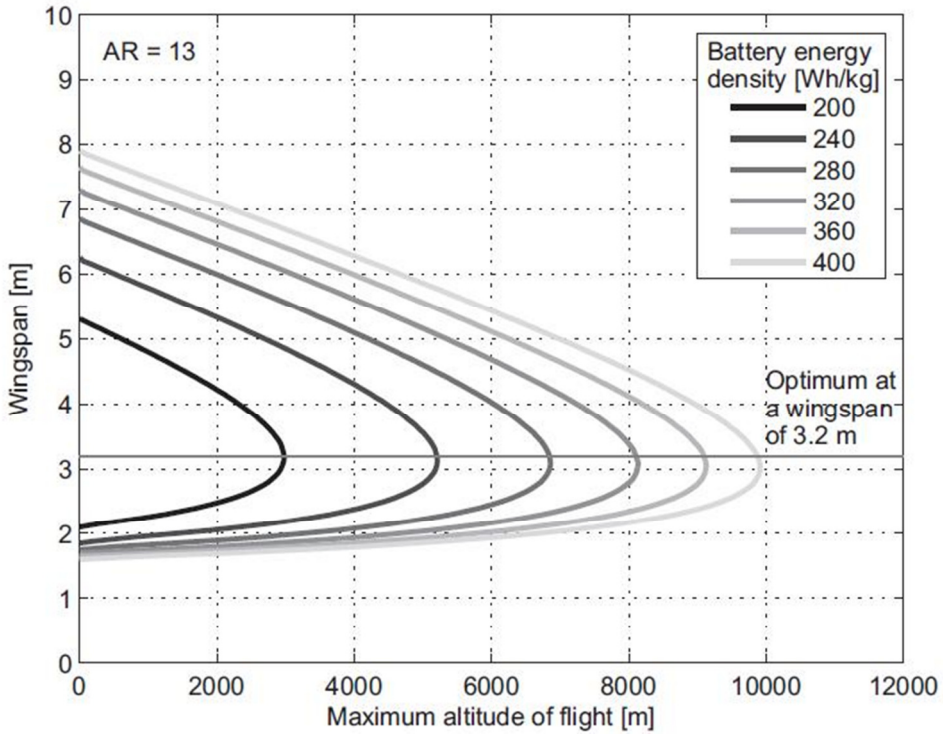

Figure A.3 Evolution of the maximum altitude of flight with the battery gravimetric energy density and wingspan **[3]**

APPENDIX B

INTEGRATION OF THE SOLAR CELLS

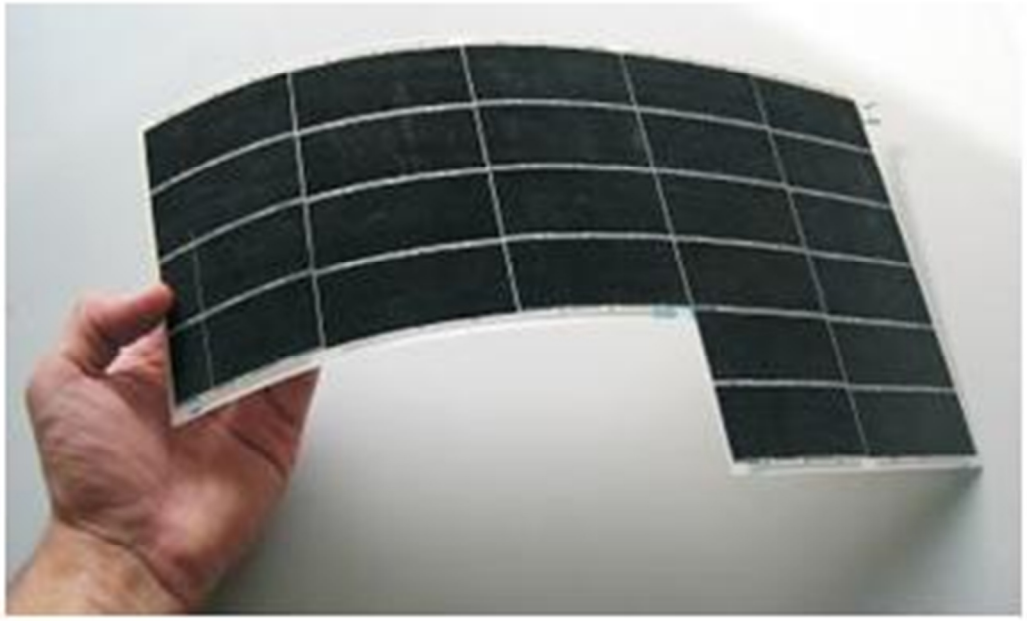

Figure B.1 Flexible solar cells **[3]**

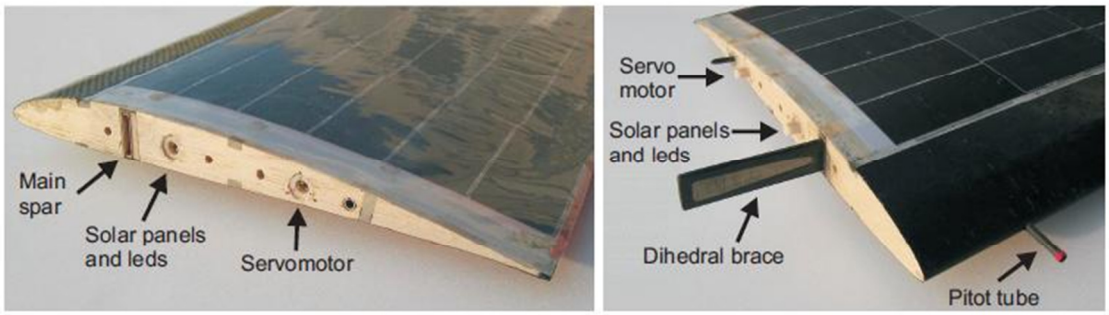

Figure B.2 Mechanical and electrical connections of the wings **[3]**

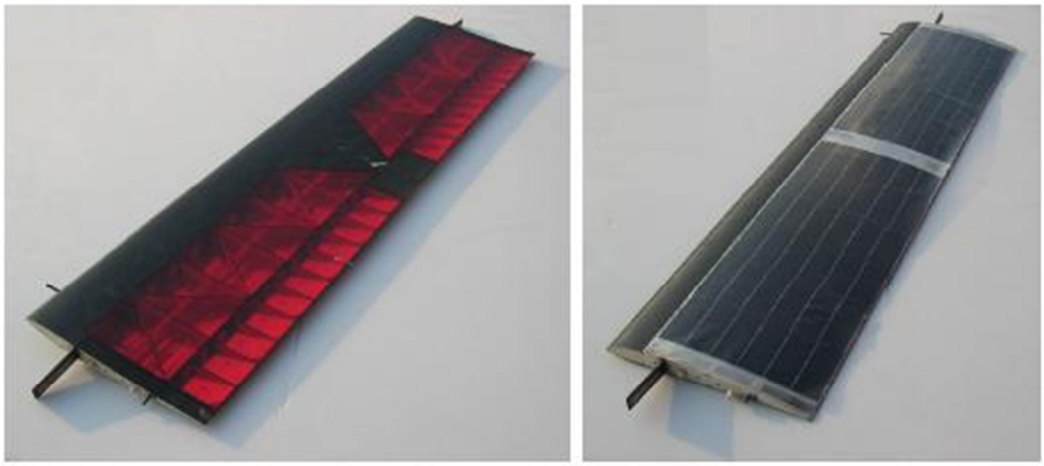

Figure B.3 Upper and lower side of the central wing **[3]**

APPENDIX C

OTHER RESULTS OBTAINED FROM TWO AXES FLIGHT

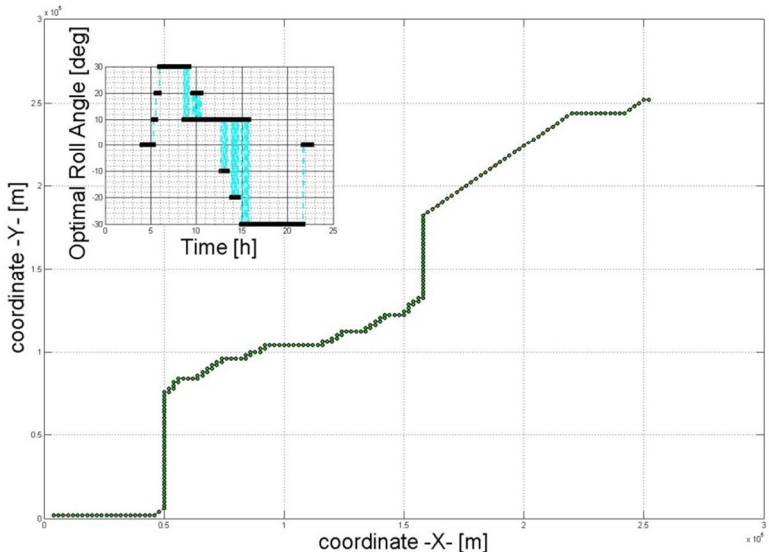

Figure C.4 Energy optimal route and roll angle for low level of time penalty at summer solstice

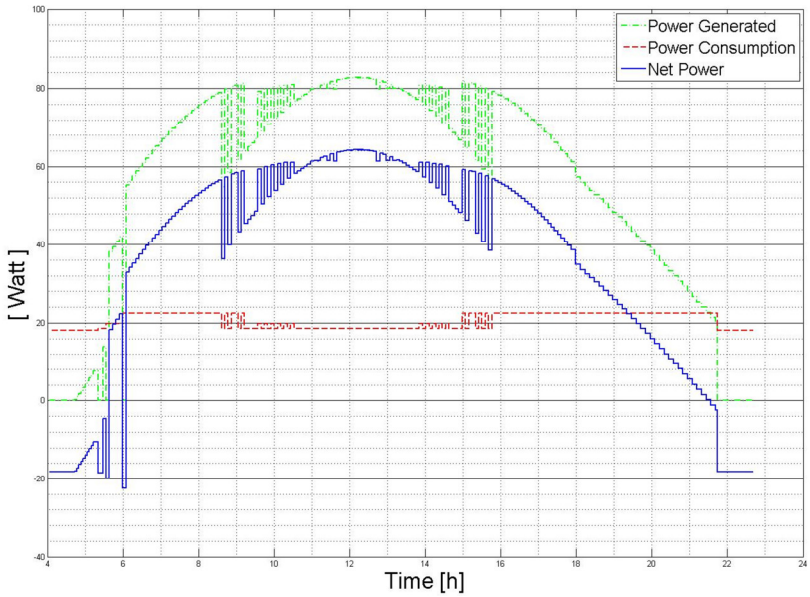

Figure C.5 Power generated, power consumption and net power for low level of time penalty at summer solstice

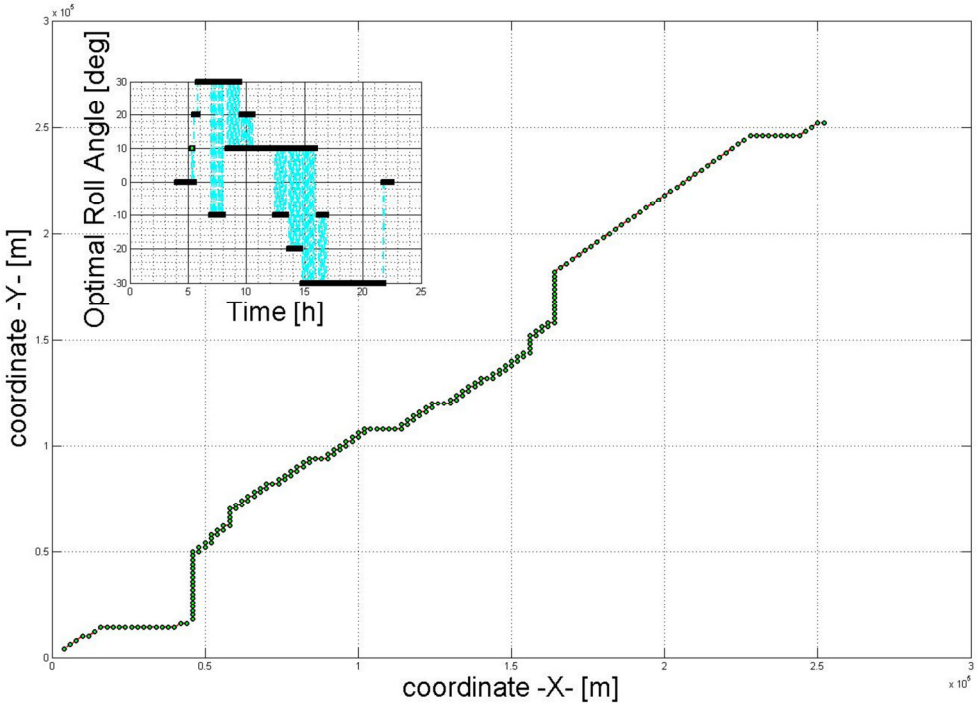

Figure C.6 Energy optimal route and roll angle for moderate level of time penalty at summer solstice

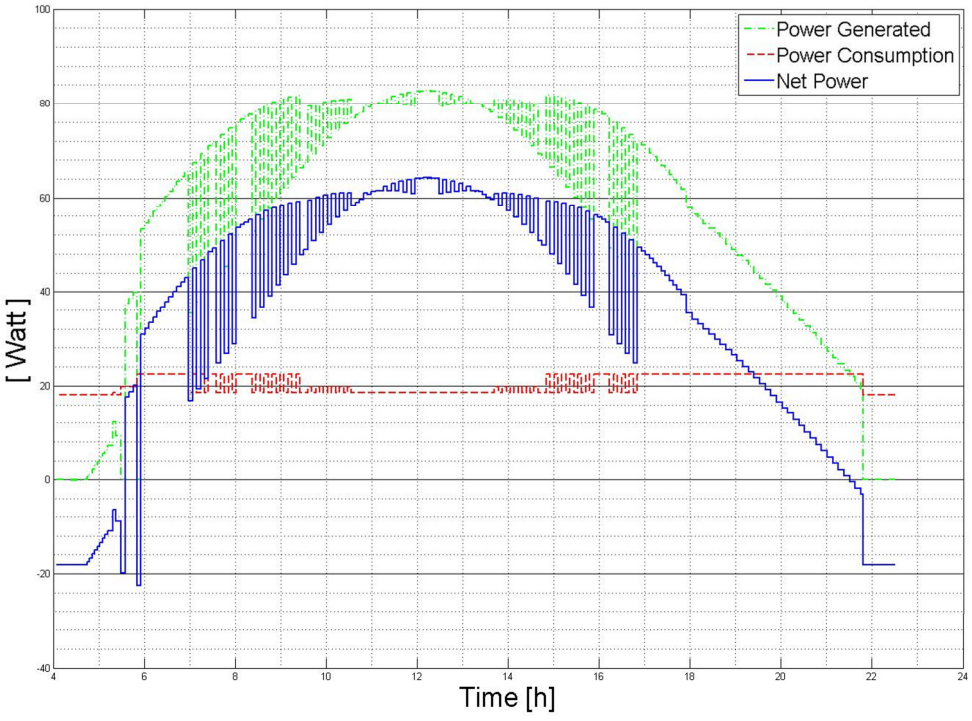

Figure C.7 Power generated, power consumption and net power for moderate level of time penalty at summer solstice

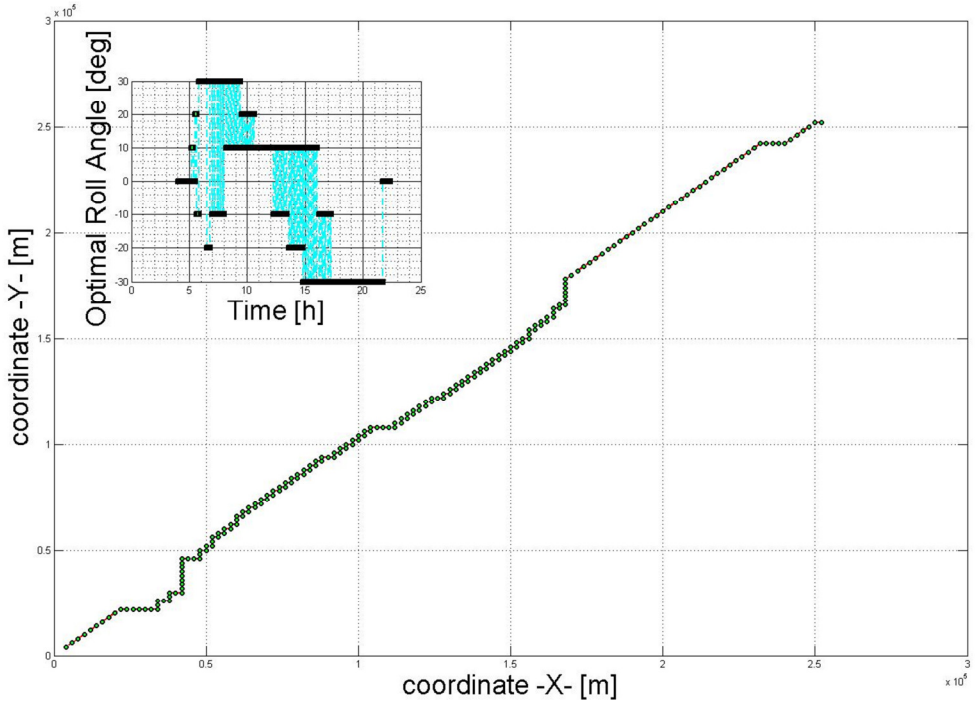

Figure C.8 Energy optimal route and roll angle for high level of time penalty at summer solstice

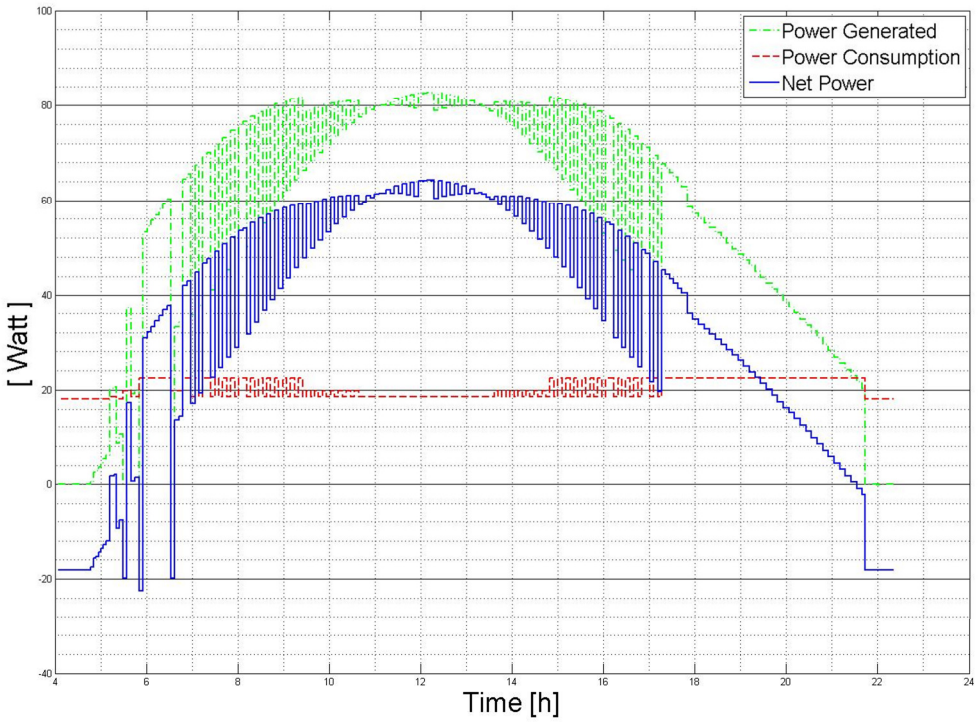

Figure C.9 Power generated, power consumption and net power for high level of time penalty at summer solstice

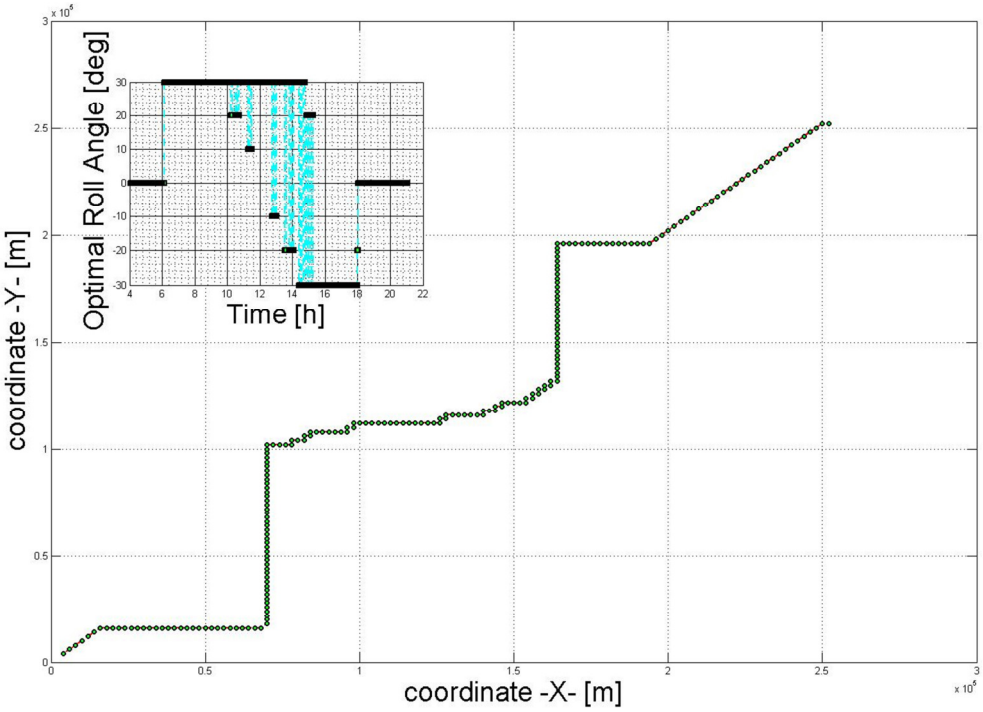

Figure C.10 Energy optimal route and roll angle for low level of time penalty at autumn equinox

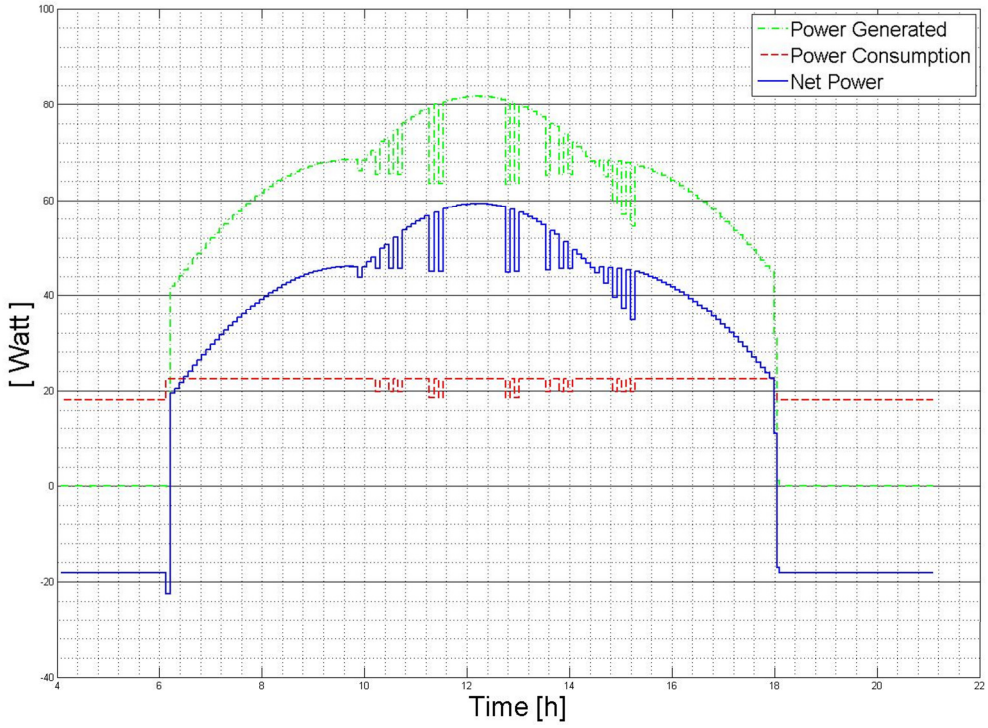

Figure C.11 Power generated, power consumption and net power for low level of time penalty at autumn equinox

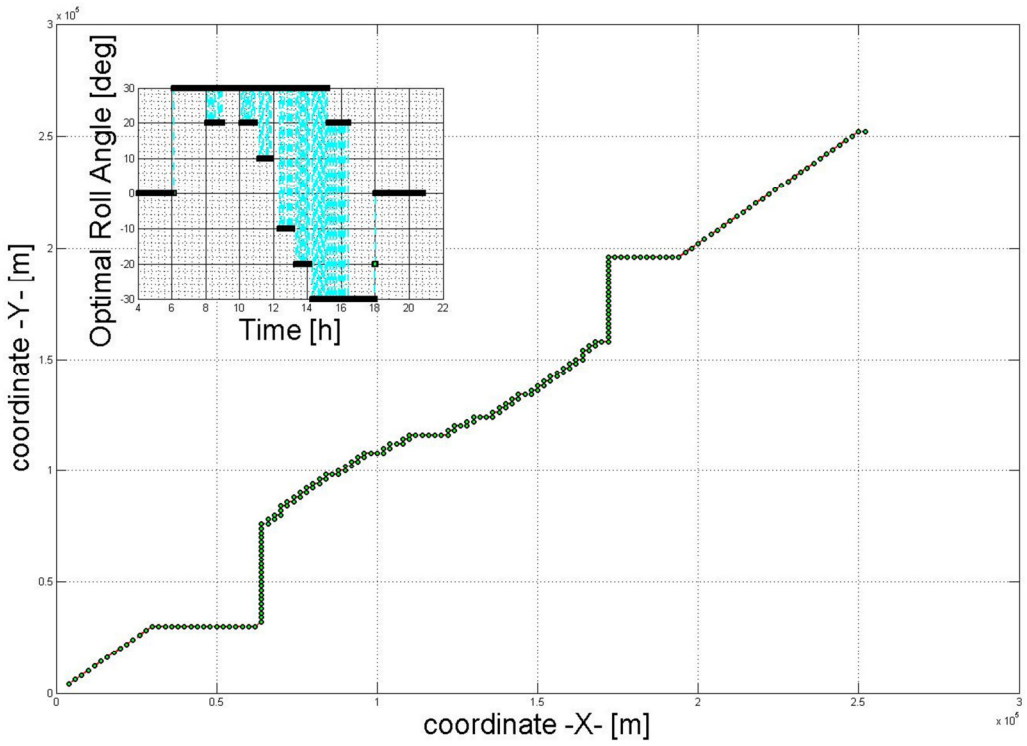

Figure C.12 Energy optimal route and roll angle for moderate level of time penalty at autumn equinox

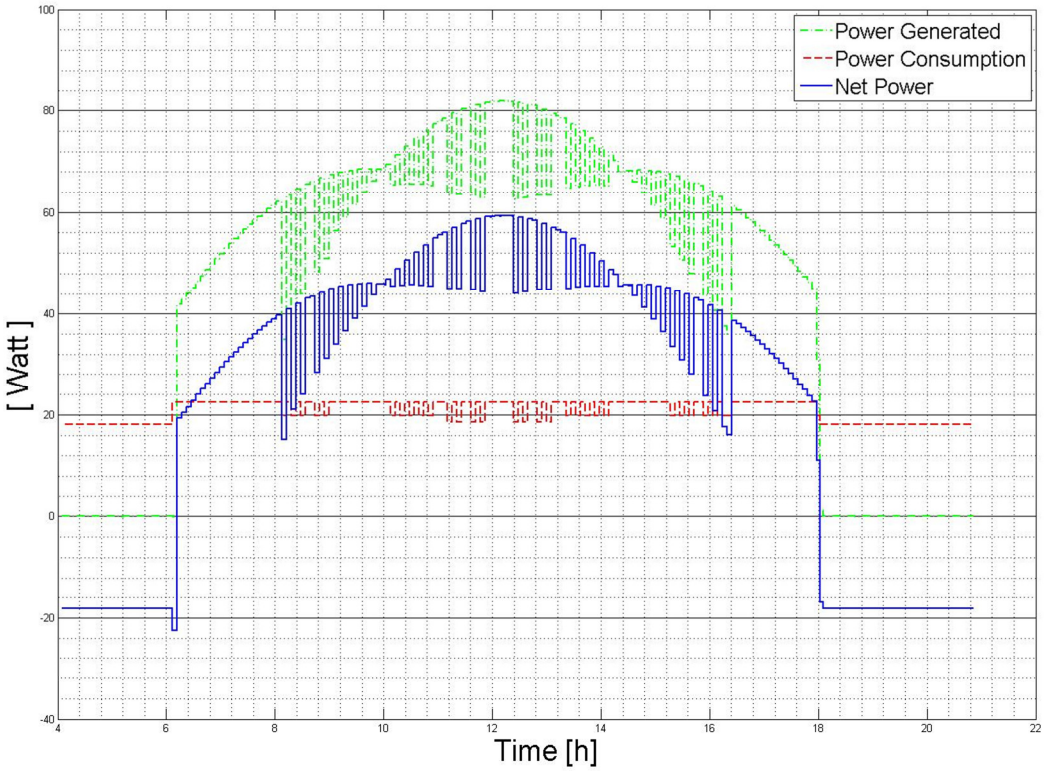

Figure C.13 Power generated, power consumption and net power for moderate level of time penalty at autumn equinox

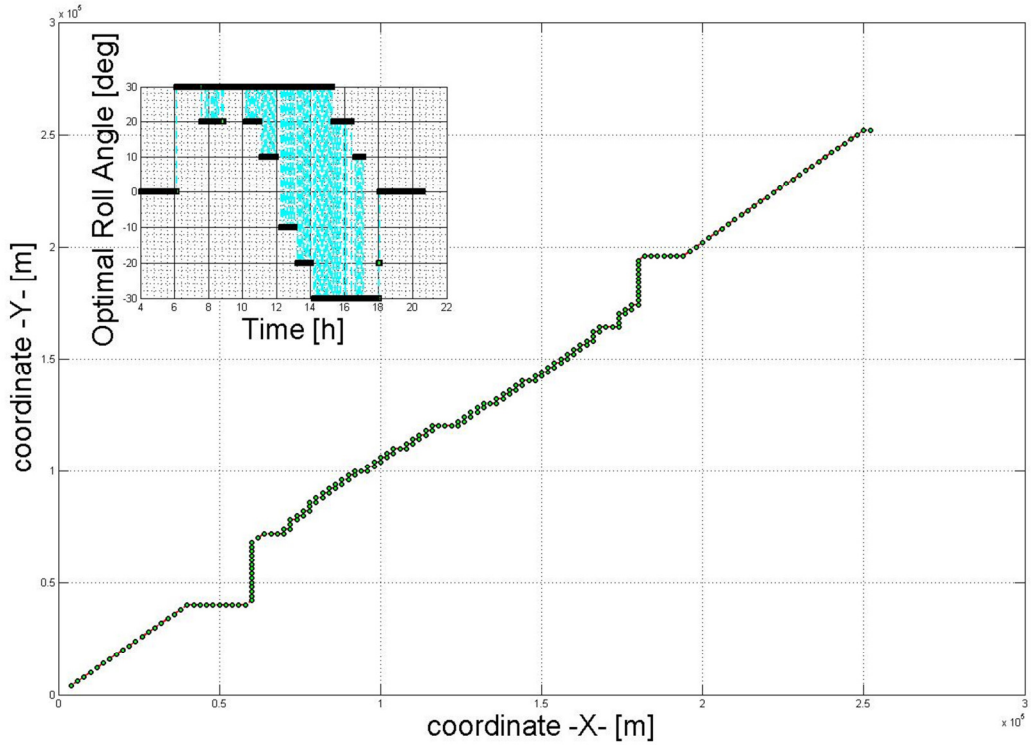

Figure C.14 Energy optimal route and roll angle for high level of time penalty at autumn equinox

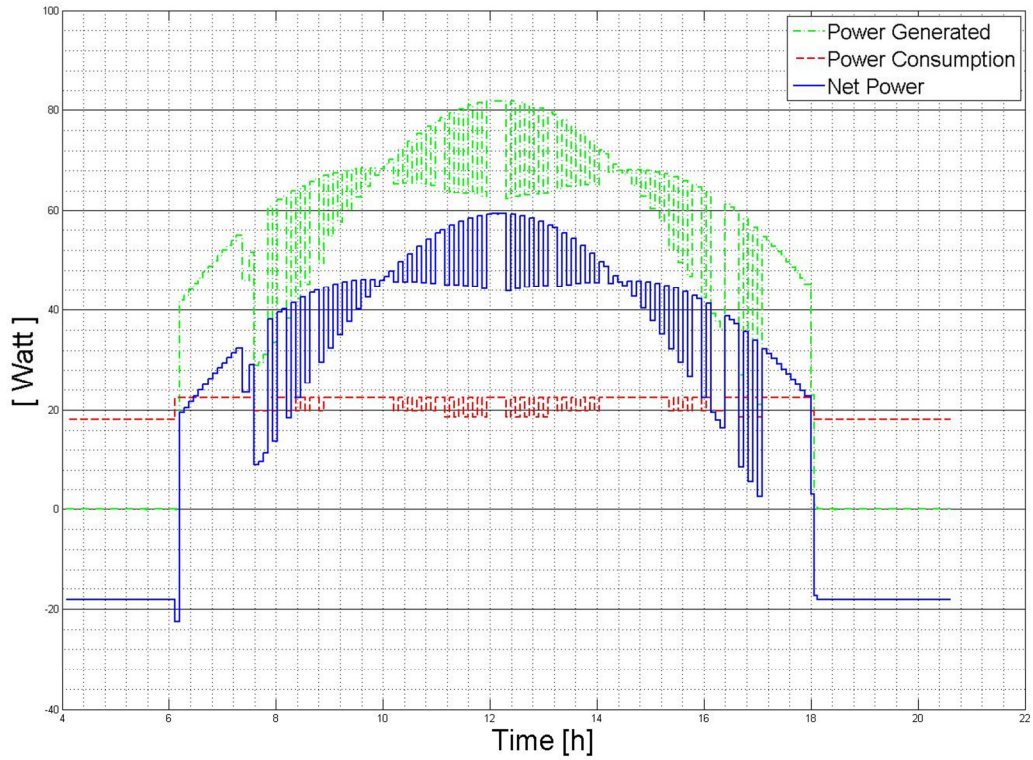

Figure C.15 Power generated, power consumption and net power for high level of time penalty at autumn equinox

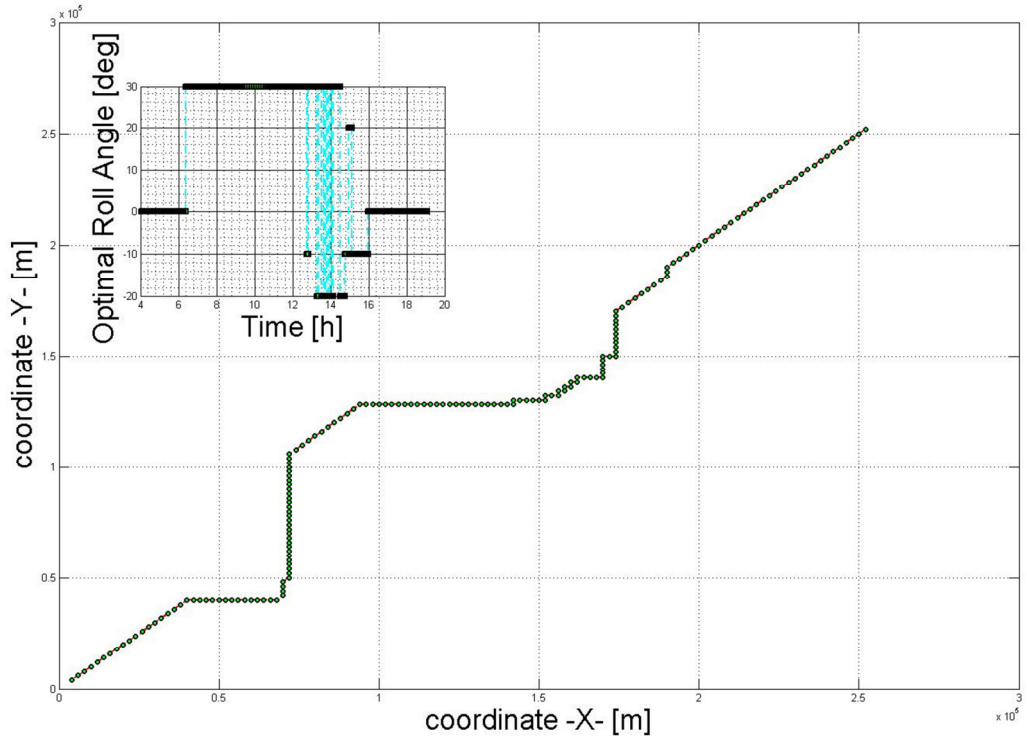

Figure C.16 Energy optimal route and roll angle for low level of time penalty at winter solstice

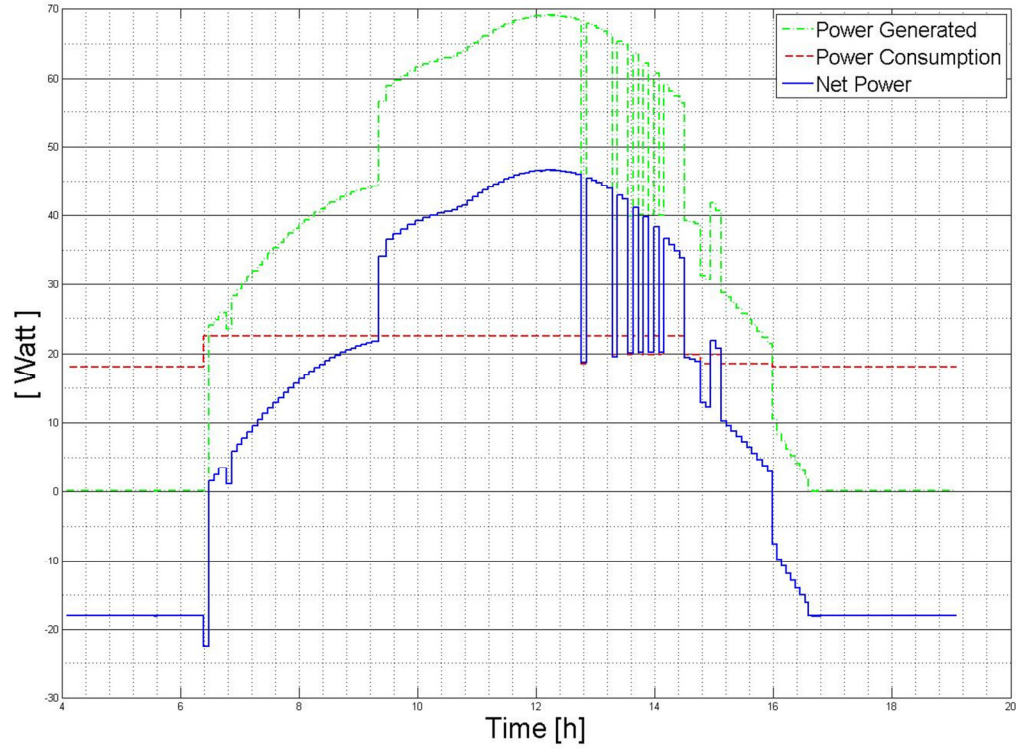

Figure C.17 Power generated, power consumption and net power for low level of time penalty at winter solstice

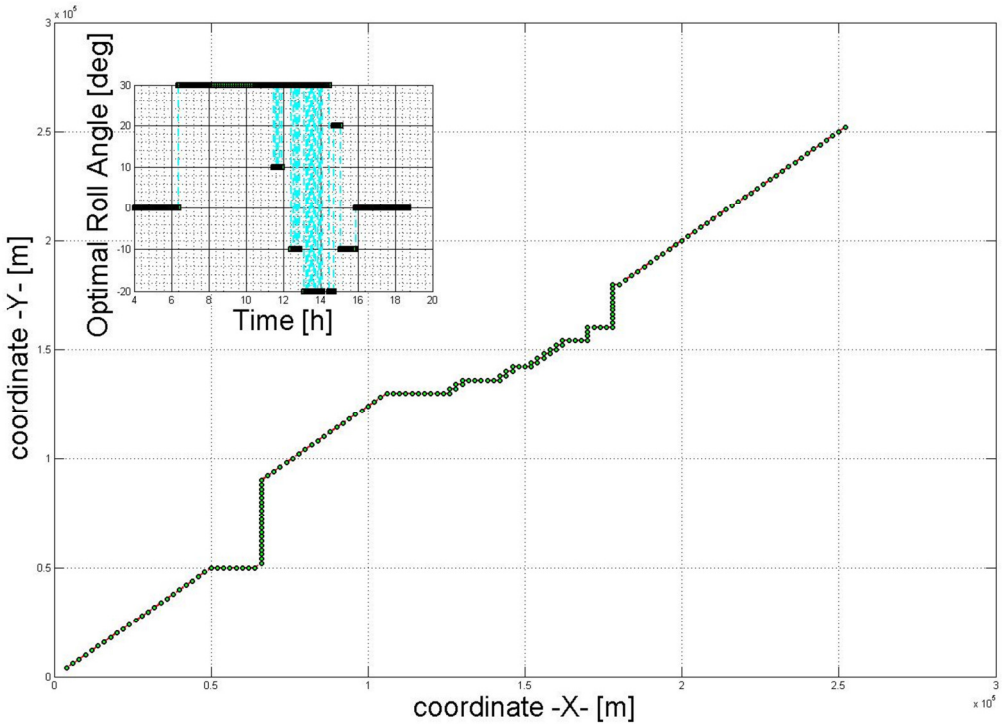

Figure C.18 Energy optimal route and roll angle for moderate level of time penalty at winter solstice

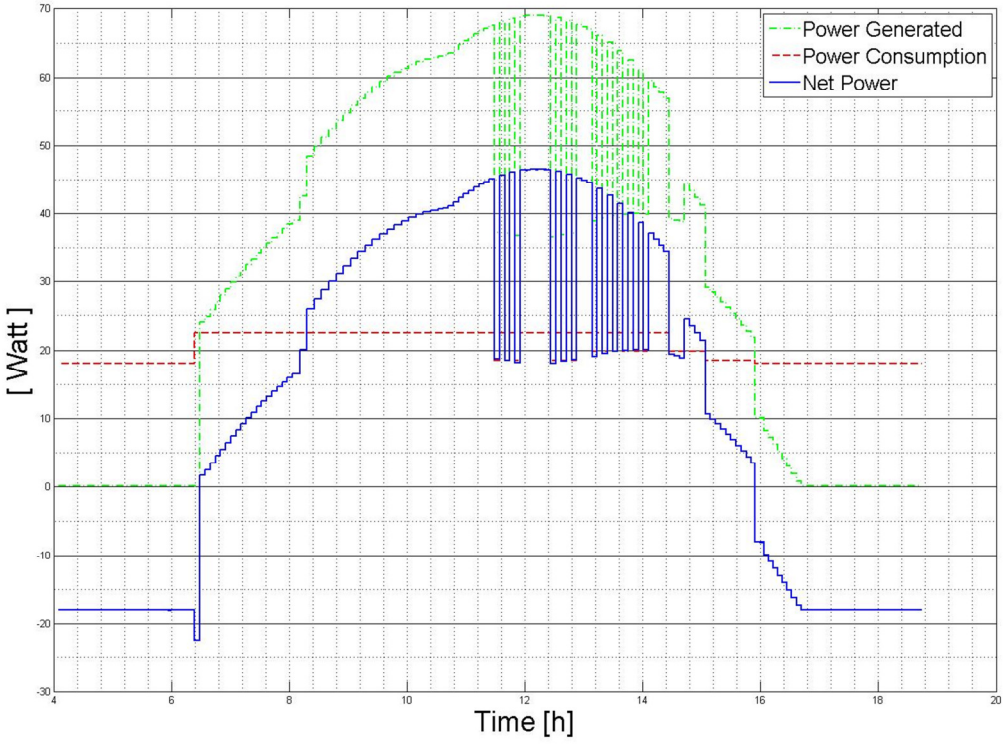

Figure C.19 Power generated, power consumption and net power for moderate level of time penalty at winter solstice

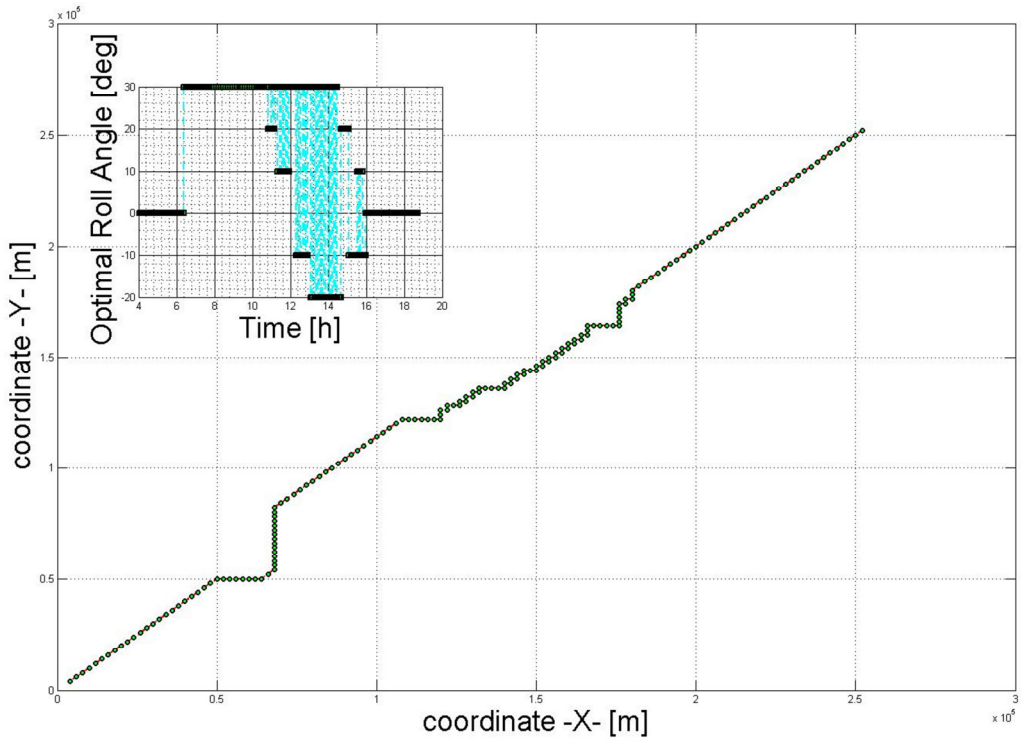

Figure C.20 Energy optimal route and roll angle for high level of time penalty at winter solstice

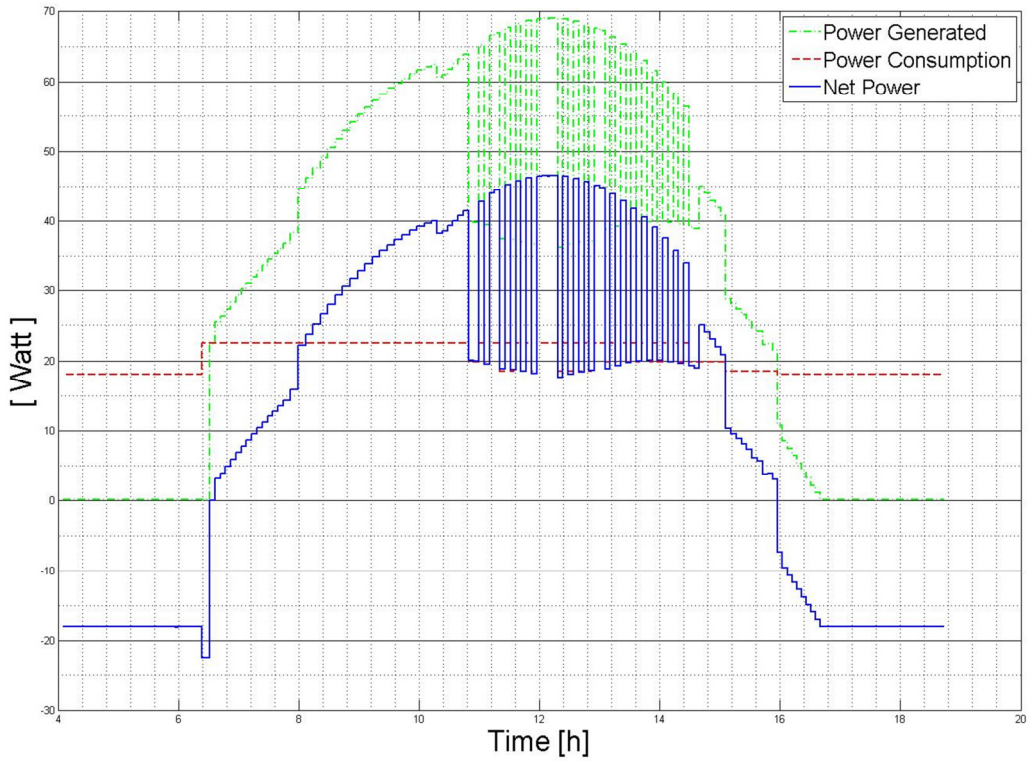

Figure C.21 Power generated, power consumption and net power for high level of time penalty at winter solstice

APPENDIX D

FLOW CHART OF THE OPTIMIZATION ALGORITHM

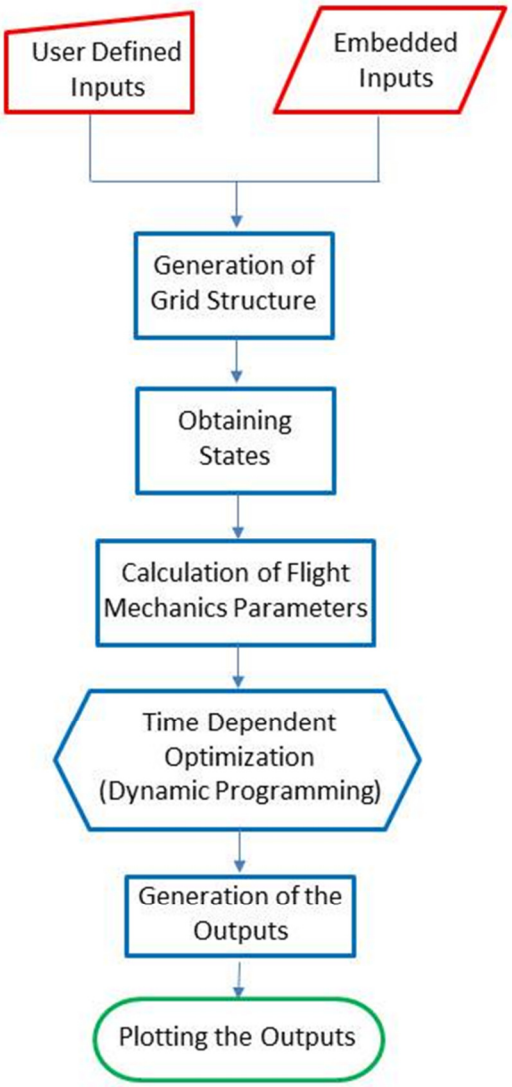

Figure D. 1 Flow chart of the optimization algorithm

APPENDIX E

MATLAB CODE OF THE OPTIMIZATION ALGORITHM

```
%% ENERGY OPTIMAL PATH PLANNING OF AN UNMANNED SOLAR POWERED
AIRCRAFT %%
% Version 3 %
% Release 1 %
clc
clear all

%% INITIAL VARIABLES %%
IP_LAT          =           (0/180)*pi;
%initial lattitude [rad]
IP_TIME         =           4;
%initial solar time [hour]
exp_deg_tp      =           3;
%exponential degree of time penalty
day             =           79;
%day number(n=79 is 20th of March)(n=171 is 20th of June)
%(n=265 is 22nd of September)(n=355 is 21st of December)

%% SYSTEM CONSTRAINTS & BOUNDARIES %%

% DEFINE SYSTEM BOUNDARIES %

% INITIAL POINT %
IP_X            =           0;
%initial point -x- [m]
IP_Y            =           0;
%initial point -y- [m]
% FINAL POINT %
FP_X            =           250000;
%final point -x- [m]
FP_Y            =           250000;
%final point -y- [m]

% ROLL BOUNDARIES %
IP_ROLL         =           -30;
%initial roll [rad]
FP_ROLL         =           30;
%final roll [rad]

% GRID LENGTH %
GRD_LEN_XY      =           2000;
%grid length -X- and -Y- [m]
GRD_LEN_ROLL    =           10;
%grid roll [rad]
```

```
%% CALCULATE GRIDS %%
grd_X       =           (FP_X-IP_X)/GRD_LEN_XY+1;
%number of grids -X-
grd_Y       =           (FP_Y-IP_Y)/GRD_LEN_XY+1;
%number of grids -X-
grd_ROLL    =           ((FP_ROLL-IP_ROLL)/GRD_LEN_ROLL)+1;
%number of grids -ROLL-

%% DEFINE LOOPS %%
X           =           zeros(1,grd_X);
%define -X-
Y           =           zeros(1,grd_Y);
%define -Y-
ROLL        =           zeros(1,grd_ROLL);
%define -ROLL-
dd          =           zeros(grd_X,grd_Y,3);
%define direct distance
beta        =           zeros(1,grd_ROLL);
%define surface slope of the central wing
beta_l      =           zeros(1,grd_ROLL);
%define surface slope of the left wing
beta_r      =           zeros(1,grd_ROLL);
%define surface slope of the right wing
lat         =           zeros(1,grd_Y);
%define lattitude
rt          =           zeros(1,grd_ROLL);
%define turning radius
rep_time    =           zeros(1,grd_ROLL);
%define repeating number
yaw_rate    =           zeros(1,grd_ROLL);
%define rate of yaw
alfa        =           zeros(grd_X,grd_Y,3,grd_ROLL);
%define angle of alfa
arc_len     =           zeros(grd_X,grd_Y,3,grd_ROLL);
%define length of arc
total_length=           zeros(grd_X,grd_Y,3,grd_ROLL);
%define total length
cl          =           zeros(1,grd_ROLL);
%define coefficient of the lift
cd_ind      =           zeros(1,grd_ROLL);
%define induced drag coefficient
cd          =           zeros(1,grd_ROLL);
%define coefficient of the drag
drag        =           zeros(1,grd_ROLL);
%define drag
thrust      =           zeros(1,grd_ROLL);
%define thrust
TIME        =           zeros(grd_X,grd_Y,3,grd_ROLL);
%define time
yaw         =           zeros(grd_X,grd_Y,3,grd_ROLL);
%define yaw
w           =           zeros(grd_X,grd_Y);
%define hour angle
theta1      =           zeros(grd_Y,grd_ROLL);
%define agent1 of theta angle of central wing
theta2      =           zeros(grd_X,grd_Y,3,grd_ROLL);
%define agent2 of theta angle of central wing
theta3      =           zeros(grd_X,grd_Y,3,grd_ROLL);
```

```
%define agent3 of theta angle of central wing
theta4      =           zeros(grd_X,grd_Y,3,grd_ROLL);
%define agent4 of theta angle of central wing
theta5      =           zeros(grd_X,grd_Y,3,grd_ROLL);
%define agent5 of theta angle of central wing
theta       =           zeros(grd_X,grd_Y,3,grd_ROLL);
%define theta angle of central wing
theta1_l    =           zeros(grd_Y,grd_ROLL);
%define agent1 of theta angle of left wing
theta2_l    =           zeros(grd_X,grd_Y,3,grd_ROLL);
%define agent2 of theta angle of left wing
theta3_l    =           zeros(grd_X,grd_Y,3,grd_ROLL);
%define agent3 of theta angle of left wing
theta4_l    =           zeros(grd_X,grd_Y,3,grd_ROLL);
%define agent4 of theta angle of left wing
theta5_l    =           zeros(grd_X,grd_Y,3,grd_ROLL);
%define agent5 of theta angle of left wing
theta_l     =           zeros(grd_X,grd_Y,3,grd_ROLL);
%define theta angle of left wing
theta1_r    =           zeros(grd_Y,grd_ROLL);
%define agent1 of theta angle of right wing
theta2_r    =           zeros(grd_X,grd_Y,3,grd_ROLL);
%define agent2 of theta angle of right wing
theta3_r    =           zeros(grd_X,grd_Y,3,grd_ROLL);
%define agent3 of theta angle of right wing
theta4_r    =           zeros(grd_X,grd_Y,3,grd_ROLL);
%define agent4 of theta angle of right wing
theta5_r    =           zeros(grd_X,grd_Y,3,grd_ROLL);
%define agent5 of theta angle of right wing
theta_r     =           zeros(grd_X,grd_Y,3,grd_ROLL);
%define theta angle of right wing
gama        =           zeros(grd_X,grd_Y,3,grd_ROLL);
%define surface azimuth
inc1        =           zeros(1,grd_ROLL);
%define second agent of the incl. angle
inc2        =           zeros(grd_X,grd_Y,3,grd_ROLL);
%define first agent of the incl. angle
inc         =           zeros(grd_X,grd_Y,3,grd_ROLL);
%define inclination angle
E_in        =           zeros(grd_X,grd_Y,3,grd_ROLL);
%define energy in
E_out       =           zeros(grd_X,grd_Y,3,grd_ROLL);
%define energy out
TIME_PENALTY=           zeros(grd_X,grd_Y,3,grd_ROLL);
%define time penalty
COST        =           zeros(grd_X,grd_Y,3,grd_ROLL);
%define nodal cost
FC          =           zeros(grd_X,grd_Y);
%define final cost
cost1       =           zeros((grd_X-1),1,1,grd_ROLL);
%define inner cost1
cost2       =           zeros(1,(grd_Y-1),1,grd_ROLL);
%define inner cost1
roll_id1    =           zeros(1,grd_X);
%define indices of optimum roll 1
roll_id2    =           zeros(1,grd_Y);
%define indices of optimum roll 2
GL_ID       =           zeros(grd_X,grd_Y);
```

```
%define indices of optimum route
cost3       =           zeros(grd_X,grd_Y,1,grd_ROLL);
%define inner cost3
cost4       =           zeros(grd_X,grd_Y,1,grd_ROLL);
%define inner cost4
cost5       =           zeros(grd_X,grd_Y,1,grd_ROLL);
%define inner cost5
GL_ROLL_ID  =           zeros(grd_X,grd_Y);
%define indices of optimum roll
mat_cost3   =           zeros(grd_ROLL,grd_X,grd_Y);
%define matrix of inner cost 3
mat_cost4   =           zeros(grd_ROLL,grd_X,grd_Y);
%define matrix of inner cost 4
mat_cost5   =           zeros(grd_ROLL,grd_X,grd_Y);
%define matrix of inner cost 5
mat_time_lin=           zeros(grd_ROLL,grd_X,grd_Y);
%define matrix of time
mat_E_out   =           zeros(grd_X,grd_Y);
%define matrix of energy consumption
mat1_E_in   =           zeros(grd_X,grd_Y);
%define agent1 for matrix of energy income
mat2_E_in   =           zeros(grd_X,grd_Y);
%define agent2 for matrix of energy income
mat_E_in    =           zeros(grd_X,grd_Y);
%define matrix of energy income

%% ENVIRONMENTAL PARAMETERS %%
g           =           9.782;
%gravitional acceleration at 9000m,[m/s^2]
rho         =           0.47;
%air density at 9000m, -46deg, 5% relative humidity [kg/m^3]

%% WING & FUSELAGE STRUCTURE %%
ar          =           12.9;
%aspect ratio
b           =           3.2;
%span [m2]
m_ac        =           2.55;
%total mass of the a/c [kg]
a_sc        =           0.58;
%area of the solar cells [m2]
wing_slope  =           (7/180)*pi;
%slope of the outer wings

%% EFFICIENCIES %%
eff_osw     =           0.9;
%Oswald efficiency factor
eff_sc      =           0.169;
%efficiency of the solar cells
eff_cbr     =           0.9;
%efficiency of the curved solar panels
eff_pr      =           0.85;
%efficiency of the propeller
eff_mot     =           0.85;
%efficiency of the motor
eff_grb     =           0.97;
%efficiency of the gearbox
```

```
%% SOLAR CONSTANTS %%
Imax        =           950;
%maximum irradiance [W/m2]

%% AERODYNAMIC CONSTANTS %%
cd_afl      =           0.013;
%airfoil drag coefficient
cd_par      =           0.006;
%parasitic drag coefficient

%% OTHER CONSTANTS %%
v_aver      =           10;
%average velocity of the a/c [m/s]

%% INITIAL CALCULATIONS %%
k_ar        =           1/(eff_osw*pi*ar);
%aerodynamic ratio
s           =           (b^2)/ar;
%area of the wings [m2]
w_ac        =           m_ac*g;
%total weight of the a/c [N]
delta       =           23.45*sind(360*(284+day)/365)*(pi/180);
%delta is the declination of the sun [radians]
grd_len_time=           GRD_LEN_XY/v_aver;
%grid time length of global time [s]
w_sr_ss     =           acos(-tan(IP_LAT)*tan(delta));
%solar sunrise and susnset time [rad]
w_sr        =           -w_sr_ss;
%solar sunrise [rad]
w_ss        =           w_sr_ss;
%solar sunset [rad]

%% OBTAINING STATES %%

tic
for i=1:grd_X
    for j=1:grd_Y
        for k=1:grd_ROLL
     X(i)       =       (i-1)*GRD_LEN_XY;
     Y(j)       =       (j-1)*GRD_LEN_XY;
     ROLL(k)    =       (k-ceil(grd_ROLL/2))*GRD_LEN_ROLL*(pi/180);
        end
    end
end
% states of -x-, -y- and roll angle

%% TIME INDEPENDENT SIMULATION %%

for i=1:grd_X
    for j=1:grd_Y
        for k=1:grd_ROLL
        if i==grd_X && j==grd_Y
                dd(i,j,1)=0;
                dd(i,j,2)=0;
                dd(i,j,3)=0;
        elseif  i==grd_X && j<grd_Y
                dd(i,j,1)=0;
                dd(i,j,2)=0;
```

```
                dd(i,j,3)=Y(j+1)-Y(j);
        elseif  j==grd_Y && i<grd_X
                dd(i,j,1)=X(i+1)-X(i);
                dd(i,j,2)=0;
                dd(i,j,3)=0;
        else
                dd(i,j,1)=X(i+1)-X(i);
                dd(i,j,2)=sqrt((X(i+1)-X(i))^2+(Y(j+1)-Y(j))^2);
                dd(i,j,3)=Y(j+1)-Y(j);
        end
% calculation of direct distances between the nodes [m]

%% FLIGHT MECHANICS %%

lat(j)              =       IP_LAT+Y(j).*(1/111000)*(1/180)*pi;
%lattitude [rad]
beta(k)             =       ROLL(k);
%surface slope of the central wing [rad]
beta_l(k)           =       ROLL(k)+wing_slope;
%surface slope of the left wing [rad]
beta_r(k)           =       ROLL(k)-wing_slope;
%surface slope of the right wing [rad]
rt(k)               =       v_aver^2/(g*tan(ROLL(k)));
%turning radius [m]
rep_time(k)         =       abs(GRD_LEN_XY./(2*rt(k)));
%repeat of roll
yaw_rate(k)         =       g*tan(ROLL(k))/v_aver;
%yaw rate[rad/s]

% ANGLE OF ALFA %
alfa(i,j,:,k)       =       acos(1-
((dd(i,j,:).^2)./(2.*rt(k).^2)));
        if alfa(i,j,:,k)<pi
            alfa(i,j,:,k)=alfa(i,j,:,k);
        elseif alfa(i,j,:,k)>=pi
            alfa(i,j,:,k)=pi;
        end
        alfa(i,j,:,k)=real(alfa(i,j,:,k));
%alfa angle [rad/s]

% ARC LENGTH %
arc_len(i,j,1,k)    =       abs(alfa(i,j,1,k)*rt(k));
arc_len(i,j,2,k)    =       arc_len(i,j,1,k)*sqrt(2);
arc_len(i,j,3,k)    =       abs(alfa(i,j,3,k)*rt(k));
%arc length [m]

% TOTAL LENGTH %
        if alfa(i,j,:,k)<pi
            total_length(i,j,:,k)=arc_len(i,j,:,k);
        else
            total_length(i,j,:,k)=arc_len(i,j,:,k).*rep_time(k);
        end
%total length [m]

% AERODYNAMICS FORCES %
cl(k)               =
(2*w_ac)./(rho*(v_aver^2)*s.*cos(ROLL(k)));
%coefficient of the lift
```

```
cd_ind(k)           =       k_ar*(cl(k).^2);
%induced drag
cd(k)               =       cd_afl+cd_par+cd_ind(k);
%coefficient of the drag
drag(k)             =       (0.5)*rho*((v_aver)^2)*s.*cd(k);
%drag force [N]
thrust(k)           =       drag(k);
%thrust force [N]

% FLIGHT ANGLES %
yaw(i,j,1,k)        =       0;
yaw(i,j,2,k)        =       45*pi/180;
yaw(i,j,3,k)        =       90*pi/180;
%yaw angle [rad]
gama(i,j,:,k)       =       -yaw(i,j,:,k);
%gama ise the surface azimuth [rad]

% GRID TIME %
        if ROLL(k)==0
            TIME(i,j,:,k)   =       dd(i,j,:)./v_aver;
        else
            TIME(i,j,:,k)   =       total_length(i,j,:,k)./v_aver;
        end
        end
    end
end
%time between grid points [s]

%% TIME DEPENDENT SIMULATION %%

% TIME PENALTY CONSTANTS %
tp_coef                             =        0.00004;
extra_tp                            =        10;
penalty_max                         =        max(grd_X,grd_Y);

% OPTIMIZATION LOOPS %
for i=1:grd_X
    for j=1:grd_Y
        for k=1:grd_ROLL
        if i==1 && j==1
            w(i,j)                  =       (IP_TIME-
12)*15*(pi/180);
            FC(i,j)                 =       0;
            E_in(i,j,:,:)           =       0;
            E_out(i,j,:,:)          =       0;
            TIME_PENALTY(i,j,:,:)   =       0;
            COST(i,j,:,k)           =       0;

        elseif i>1 && j==1

% INCIDENCE ANGLE %
% Central Wing %
theta1(j,k)         =       sin(delta).*sin(lat(j)).*cos(beta(k));
theta2(i,j,:,k)     =
sin(delta).*cos(lat(j)).*sin(beta(k)).*cos(gama(i,j,:,k));
theta3(i,j,:,k)     =
cos(delta).*cos(lat(j)).*cos(beta(k)).*cos(w(i-1,j));
```

```
theta4(i,j,:,k)     =
cos(delta).*sin(lat(j)).*sin(beta(k)).*cos(gama(i,j,:,k)).*cos(w(i-
1,j));
theta5(i,j,:,k)     =
cos(delta).*sin(beta(k)).*sin(gama(i,j,:,k)).*sin(w(i-1,j));
theta(i,j,:,k)      =       acos(theta1(j,k)-
theta2(i,j,:,k)+theta3(i,j,:,k)+...
                            theta4(i,j,:,k)+theta5(i,j,:,k));
% Left Wing %
theta1_l(j,k)       =
sin(delta).*sin(lat(j)).*cos(beta_l(k));
theta2_l(i,j,:,k)   =
sin(delta).*cos(lat(j)).*sin(beta_l(k)).*cos(gama(i,j,:,k));
theta3_l(i,j,:,k)   =
cos(delta).*cos(lat(j)).*cos(beta_l(k)).*cos(w(i-1,j));
theta4_l(i,j,:,k)   =
cos(delta).*sin(lat(j)).*sin(beta_l(k)).*cos(gama(i,j,:,k)).*cos(w(
i-1,j));
theta5_l(i,j,:,k)   =
cos(delta).*sin(beta_l(k)).*sin(gama(i,j,:,k)).*sin(w(i-1,j));
theta_l(i,j,:,k)    =       acos(theta1_l(j,k)-
theta2_l(i,j,:,k)+theta3_l(i,j,:,k)+...
                            theta4_l(i,j,:,k)+theta5_l(i,j,:,k));
% Right Wing %
theta1_r(j,k)       =
sin(delta).*sin(lat(j)).*cos(beta_r(k));
theta2_r(i,j,:,k)   =
sin(delta).*cos(lat(j)).*sin(beta_r(k)).*cos(gama(i,j,:,k));
theta3_r(i,j,:,k)   =
cos(delta).*cos(lat(j)).*cos(beta_r(k)).*cos(w(i-1,j));
theta4_r(i,j,:,k)   =
cos(delta).*sin(lat(j)).*sin(beta_r(k)).*cos(gama(i,j,:,k)).*cos(w(
i-1,j));
theta5_r(i,j,:,k)   =
cos(delta).*sin(beta_r(k)).*sin(gama(i,j,:,k)).*sin(w(i-1,j));
theta_r(i,j,:,k)    =       acos(theta1_r(j,k)-
theta2_r(i,j,:,k)+theta3_r(i,j,:,k)+...
                            theta4_r(i,j,:,k)+theta5_r(i,j,:,k));

% ENERGY IN %
        if theta(i,j,:,k)<=pi/2
E_in(i,j,1,k)       =
(1/3).*eff_cbr.*eff_sc.*Imax.*a_sc.*cos(theta(i,j,1,k)).*TIME(i-
1,j,1,k)+...

(1/3).*eff_cbr.*eff_sc.*Imax.*a_sc.*cos(theta_l(i,j,1,k)).*TIME(i-
1,j,1,k)+...

(1/3).*eff_cbr.*eff_sc.*Imax.*a_sc.*cos(theta_r(i,j,1,k)).*TIME(i-
1,j,1,k);
E_in(i,j,2,k)       =       0;
E_in(i,j,3,k)       =       0;
        else
E_in(i,j,:,k)       =       0;

        end
% ENERGY OUT %
```

```
E_out(i,j,1,k)      =       TIME(i-
1,j,1,k).*(v_aver.*thrust(k)).(eff_pr*eff_mot*eff_grb);
E_out(i,j,2,k)      =       0;
E_out(i,j,3,k)      =       0;

% TIME PENALTY %
        for p=1:penalty_max
        if i==j
TIME_PENALTY(i,j,1,k)       =
E_out(i,j,1,k)*tp_coef*extra_tp;
TIME_PENALTY(i,j,2,k)       =       E_out(i,j,2,k)*tp_coef;
TIME_PENALTY(i,j,3,k)       =
E_out(i,j,3,k)*tp_coef*extra_tp;
        elseif abs(i-j)==p
TIME_PENALTY(i,j,1,k)       =       ((abs(i-
j)+1)^exp_deg_tp)*(E_out(i,j,1,k)*tp_coef*extra_tp);
TIME_PENALTY(i,j,2,k)       =       (abs(i-
j)^exp_deg_tp)*(E_out(i,j,2,k)*tp_coef);
TIME_PENALTY(i,j,3,k)       =       ((abs(i-
j)+1)^exp_deg_tp)*(E_out(i,j,3,k)*tp_coef*extra_tp);
        end
        end

% COST FUNCTION %
COST(i,j,:,k)               =       E_in(i,j,:,k)-E_out(i,j,:,k)-
abs(TIME_PENALTY(i,j,:,k));
cost1(i,j,1,k)              =       COST(i,j,1,k);
mat_cost1                   =       (squeeze(cost1)).';
max_cost1                   =       (max(mat_cost1)).';
% ID1 %
[id_val1 roll_id1]          =       (max(mat_cost1));
GL_ID(i,j)                  =       1;
% NODAL COST %
FC(i,j)                     =       FC(i-1,j)+max_cost1(i,j);
% HOUR ANGLE %
w(i,j)                      =       w(i-1,j)+(TIME(i-
1,j,1,roll_id1(j,i))/3600)*15*(pi/180);

        elseif i==1 && j>1

% INCIDENCE ANGLE %
% Central Wing %
theta1(j,k)                 =
sin(delta).*sin(lat(j)).*cos(beta(k));
theta2(i,j,:,k)             =
sin(delta).*cos(lat(j)).*sin(beta(k)).*cos(gama(i,j,:,k));
theta3(i,j,:,k)             =
cos(delta).*cos(lat(j)).*cos(beta(k)).*cos(w(i,j-1));
theta4(i,j,:,k)             =
cos(delta).*sin(lat(j)).*sin(beta(k)).*cos(gama(i,j,:,k)).*cos(w(i,
j-1));
theta5(i,j,:,k)             =
cos(delta).*sin(beta(k)).*sin(gama(i,j,:,k)).*sin(w(i,j-1));
theta(i,j,:,k)              =       acos(theta1(j,k)-
theta2(i,j,:,k)+theta3(i,j,:,k)+...

theta4(i,j,:,k)+theta5(i,j,:,k));
% Left Wing %
```

```
theta1_l(j,k)                =
sin(delta).*sin(lat(j)).*cos(beta_l(k));
theta2_l(i,j,:,k)            =
sin(delta).*cos(lat(j)).*sin(beta_l(k)).*cos(gama(i,j,:,k));
theta3_l(i,j,:,k)            =
cos(delta).*cos(lat(j)).*cos(beta_l(k)).*cos(w(i,j-1));
theta4_l(i,j,:,k)            =
cos(delta).*sin(lat(j)).*sin(beta_l(k)).*cos(gama(i,j,:,k)).*cos(w(
i,j-1));
theta5_l(i,j,:,k)            =
cos(delta).*sin(beta_l(k)).*sin(gama(i,j,:,k)).*sin(w(i,j-1));
theta_l(i,j,:,k)             =       acos(theta1_l(j,k)-
theta2_l(i,j,:,k)+theta3_l(i,j,:,k)+...

theta4_l(i,j,:,k)+theta5_l(i,j,:,k));
% Right Wing %
theta1_r(j,k)                =
sin(delta).*sin(lat(j)).*cos(beta_r(k));
theta2_r(i,j,:,k)            =
sin(delta).*cos(lat(j)).*sin(beta_r(k)).*cos(gama(i,j,:,k));
theta3_r(i,j,:,k)            =
cos(delta).*cos(lat(j)).*cos(beta_r(k)).*cos(w(i,j-1));
theta4_r(i,j,:,k)            =
cos(delta).*sin(lat(j)).*sin(beta_r(k)).*cos(gama(i,j,:,k)).*cos(w(
i,j-1));
theta5_r(i,j,:,k)            =
cos(delta).*sin(beta_r(k)).*sin(gama(i,j,:,k)).*sin(w(i,j-1));
theta_r(i,j,:,k)             =       acos(theta1_r(j,k)-
theta2_r(i,j,:,k)+theta3_r(i,j,:,k)+...

theta4_r(i,j,:,k)+theta5_r(i,j,:,k));

% ENERGY IN %
        if theta(i,j,:,k)<=pi/2
E_in(i,j,1,k)                =       0;
E_in(i,j,2,k)                =       0;
E_in(i,j,3,k)                =
(1/3).*eff_cbr.*eff_sc.*Imax.*a_sc.*cos(theta(i,j,3,k)).*TIME(i,j-
1,3,k)+...

(1/3).*eff_cbr.*eff_sc.*Imax.*a_sc.*cos(theta_l(i,j,3,k)).*TIME(i,j
-1,3,k)+...

(1/3).*eff_cbr.*eff_sc.*Imax.*a_sc.*cos(theta_r(i,j,3,k)).*TIME(i,j
-1,3,k);
        else
E_in(i,j,:,k)                =       0;
        end

% ENERGY OUT %
E_out(i,j,1,k)               =       0;
E_out(i,j,2,k)               =       0;
E_out(i,j,3,k)               =       TIME(i,j-
1,3,k).*(v_aver.*thrust(k))./(eff_pr*eff_mot*eff_grb);

% TIME PENALTY %
        for p=1:penalty_max
        if i==j
```

```
TIME_PENALTY(i,j,1,k)       =
E_out(i,j,1,k)*tp_coef*extra_tp;
TIME_PENALTY(i,j,2,k)       =       E_out(i,j,2,k)*tp_coef;
TIME_PENALTY(i,j,3,k)       =
E_out(i,j,3,k)*tp_coef*extra_tp;
        elseif abs(i-j)==p
TIME_PENALTY(i,j,1,k)       =       ((abs(i-
j)+1)^exp_deg_tp)*(E_out(i,j,1,k)*tp_coef*extra_tp);
TIME_PENALTY(i,j,2,k)       =       (abs(i-
j)^exp_deg_tp)*(E_out(i,j,2,k)*tp_coef);
TIME_PENALTY(i,j,3,k)       =       ((abs(i-
j)+1)^exp_deg_tp)*(E_out(i,j,3,k)*tp_coef*extra_tp);
        end
        end

% COST FUNCTION %
COST(i,j,:,k)               =       E_in(i,j,:,k)-E_out(i,j,:,k)-
abs(TIME_PENALTY(i,j,:,k));
cost2(i,j,1,k)              =       COST(i,j,3,k);
mat_cost2                   =       squeeze(cost2).';
max_cost2                   =       (max(mat_cost2));
%ID2%
[id_val2 roll_id2]          =       (max(mat_cost2));
GL_ID(i,j)                  =       3;
%NODAL COST%
FC(i,j)                     =       FC(i,j-1)+max_cost2(i,j);
%GLOBAL TIME
w(i,j)                      =       w(i,j-1)+(TIME(i,j-
1,3,roll_id2(i,j))/3600)*15*(pi/180);
        else

% INCIDENCE ANGLE %
% Central Wing %
theta1(j,k)                 =
sin(delta).*sin(lat(j)).*cos(beta(k));
theta2(i,j,1,k)             =
sin(delta).*cos(lat(j)).*sin(beta(k)).*cos(gama(i,j,1,k));
theta2(i,j,2,k)             =
sin(delta).*cos(lat(j)).*sin(beta(k)).*cos(gama(i,j,2,k));
theta2(i,j,3,k)             =
sin(delta).*cos(lat(j)).*sin(beta(k)).*cos(gama(i,j,3,k));
theta3(i,j,1,k)             =
cos(delta).*cos(lat(j)).*cos(beta(k)).*cos(w(i-1,j));
theta3(i,j,2,k)             =
cos(delta).*cos(lat(j)).*cos(beta(k)).*cos(w(i-1,j-1));
theta3(i,j,3,k)             =
cos(delta).*cos(lat(j)).*cos(beta(k)).*cos(w(i,j-1));
theta4(i,j,1,k)             =
cos(delta).*sin(lat(j)).*sin(beta(k)).*cos(gama(i,j,1,k)).*cos(w(i-
1,j));
theta4(i,j,2,k)             =
cos(delta).*sin(lat(j)).*sin(beta(k)).*cos(gama(i,j,2,k)).*cos(w(i-
1,j-1));
theta4(i,j,3,k)             =
cos(delta).*sin(lat(j)).*sin(beta(k)).*cos(gama(i,j,3,k)).*cos(w(i,
j-1));
theta5(i,j,1,k)             =
cos(delta).*sin(beta(k)).*sin(gama(i,j,1,k)).*sin(w(i-1,j));
```

```
theta5(i,j,2,k)             =
cos(delta).*sin(beta(k)).*sin(gama(i,j,2,k)).*sin(w(i-1,j-1));
theta5(i,j,3,k)             =
cos(delta).*sin(beta(k)).*sin(gama(i,j,3,k)).*sin(w(i,j-1));
theta(i,j,:,k)              =       acos(theta1(j,k)-
theta2(i,j,:,k)+theta3(i,j,:,k)+...

theta4(i,j,:,k)+theta5(i,j,:,k));
% Right Wing %
theta1_r(j,k)               =
sin(delta).*sin(lat(j)).*cos(beta_r(k));
theta2_r(i,j,1,k)           =
sin(delta).*cos(lat(j)).*sin(beta_r(k)).*cos(gama(i,j,1,k));
theta2_r(i,j,2,k)           =
sin(delta).*cos(lat(j)).*sin(beta_r(k)).*cos(gama(i,j,2,k));
theta2_r(i,j,3,k)           =
sin(delta).*cos(lat(j)).*sin(beta_r(k)).*cos(gama(i,j,3,k));
theta3_r(i,j,1,k)           =
cos(delta).*cos(lat(j)).*cos(beta_r(k)).*cos(w(i-1,j));
theta3_r(i,j,2,k)           =
cos(delta).*cos(lat(j)).*cos(beta_r(k)).*cos(w(i-1,j-1));
theta3_r(i,j,3,k)           =
cos(delta).*cos(lat(j)).*cos(beta_r(k)).*cos(w(i,j-1));
theta4_r(i,j,1,k)           =
cos(delta).*sin(lat(j)).*sin(beta_r(k)).*cos(gama(i,j,1,k)).*cos(w(
i-1,j));
theta4_r(i,j,2,k)           =
cos(delta).*sin(lat(j)).*sin(beta_r(k)).*cos(gama(i,j,2,k)).*cos(w(
i-1,j-1));
theta4_r(i,j,3,k)           =
cos(delta).*sin(lat(j)).*sin(beta_r(k)).*cos(gama(i,j,3,k)).*cos(w(
i,j-1));
theta5_r(i,j,1,k)           =
cos(delta).*sin(beta_r(k)).*sin(gama(i,j,1,k)).*sin(w(i-1,j));
theta5_r(i,j,2,k)           =
cos(delta).*sin(beta_r(k)).*sin(gama(i,j,2,k)).*sin(w(i-1,j-1));
theta5_r(i,j,3,k)           =
cos(delta).*sin(beta_r(k)).*sin(gama(i,j,3,k)).*sin(w(i,j-1));
theta_r(i,j,:,k)            =       acos(theta1_r(j,k)-
theta2_r(i,j,:,k)+theta3_r(i,j,:,k)+...

theta4_r(i,j,:,k)+theta5_r(i,j,:,k));
% Left Wing %
theta1_l(j,k)               =
sin(delta).*sin(lat(j)).*cos(beta_l(k));
theta2_l(i,j,1,k)           =
sin(delta).*cos(lat(j)).*sin(beta_l(k)).*cos(gama(i,j,1,k));
theta2_l(i,j,2,k)           =
sin(delta).*cos(lat(j)).*sin(beta_l(k)).*cos(gama(i,j,2,k));
theta2_l(i,j,3,k)           =
sin(delta).*cos(lat(j)).*sin(beta_l(k)).*cos(gama(i,j,3,k));
theta3_l(i,j,1,k)           =
cos(delta).*cos(lat(j)).*cos(beta_l(k)).*cos(w(i-1,j));
theta3_l(i,j,2,k)           =
cos(delta).*cos(lat(j)).*cos(beta_l(k)).*cos(w(i-1,j-1));
theta3_l(i,j,3,k)           =
cos(delta).*cos(lat(j)).*cos(beta_l(k)).*cos(w(i,j-1));
```

```
theta4_l(i,j,1,k)           =
cos(delta).*sin(lat(j)).*sin(beta_l(k)).*cos(gama(i,j,1,k)).*cos(w(
i-1,j));
theta4_l(i,j,2,k)           =
cos(delta).*sin(lat(j)).*sin(beta_l(k)).*cos(gama(i,j,2,k)).*cos(w(
i-1,j-1));
theta4_l(i,j,3,k)           =
cos(delta).*sin(lat(j)).*sin(beta_l(k)).*cos(gama(i,j,3,k)).*cos(w(
i,j-1));
theta5_l(i,j,1,k)           =
cos(delta).*sin(beta_l(k)).*sin(gama(i,j,1,k)).*sin(w(i-1,j));
theta5_l(i,j,2,k)           =
cos(delta).*sin(beta_l(k)).*sin(gama(i,j,2,k)).*sin(w(i-1,j-1));
theta5_l(i,j,3,k)           =
cos(delta).*sin(beta_l(k)).*sin(gama(i,j,3,k)).*sin(w(i,j-1));
theta_l(i,j,:,k)            =       acos(theta1_l(j,k)-
theta2_l(i,j,:,k)+theta3_l(i,j,:,k)+...

theta4_l(i,j,:,k)+theta5_l(i,j,:,k));

% ENERGY IN %
        if theta(i,j,:,k)<=pi/2
E_in(i,j,1,k)               =
(1/3).*eff_cbr.*eff_sc.*Imax.*a_sc.*cos(theta(i,j,1,k)).*TIME(i-
1,j,1,k)+...

(1/3).*eff_cbr.*eff_sc.*Imax.*a_sc.*cos(theta_l(i,j,1,k)).*TIME(i-
1,j,1,k)+...

(1/3).*eff_cbr.*eff_sc.*Imax.*a_sc.*cos(theta_r(i,j,1,k)).*TIME(i-
1,j,1,k);
E_in(i,j,2,k)               =
(1/3).*eff_cbr.*eff_sc.*Imax.*a_sc.*cos(theta(i,j,2,k)).*TIME(i-
1,j-1,2,k)+...

(1/3).*eff_cbr.*eff_sc.*Imax.*a_sc.*cos(theta_l(i,j,2,k)).*TIME(i-
1,j-1,2,k)+...

(1/3).*eff_cbr.*eff_sc.*Imax.*a_sc.*cos(theta_r(i,j,2,k)).*TIME(i-
1,j-1,2,k);
E_in(i,j,3,k)               =
(1/3).*eff_cbr.*eff_sc.*Imax.*a_sc.*cos(theta(i,j,3,k)).*TIME(i,j-
1,3,k)+...

(1/3).*eff_cbr.*eff_sc.*Imax.*a_sc.*cos(theta_l(i,j,3,k)).*TIME(i,j
-1,3,k)+...

(1/3).*eff_cbr.*eff_sc.*Imax.*a_sc.*cos(theta_r(i,j,3,k)).*TIME(i,j
-1,3,k);
        else
E_in(i,j,:,k)               =       0;
        end

% ENERGY OUT %
E_out(i,j,1,k)              =       TIME(i-
1,j,1,k).*(v_aver.*thrust(k))./(eff_pr*eff_mot*eff_grb);
E_out(i,j,2,k)              =       TIME(i-1,j-
1,2,k).*(v_aver.*thrust(k))./(eff_pr*eff_mot*eff_grb);
```

```
E_out(i,j,3,k)              =       TIME(i,j-
1,3,k).*(v_aver.*thrust(k))./(eff_pr*eff_mot*eff_grb);

% TIME PENALTY %
        for p=1:penalty_max
        if i==j
TIME_PENALTY(i,j,1,k)       =
E_out(i,j,1,k)*tp_coef*extra_tp;
TIME_PENALTY(i,j,2,k)       =       E_out(i,j,2,k)*tp_coef;
TIME_PENALTY(i,j,3,k)       =
E_out(i,j,3,k)*tp_coef*extra_tp;
        elseif abs(i-j)==p
TIME_PENALTY(i,j,1,k)       =       ((abs(i-
j)+1)^exp_deg_tp)*(E_out(i,j,1,k)*tp_coef*extra_tp);
TIME_PENALTY(i,j,2,k)       =       (abs(i-
j)^exp_deg_tp)*(E_out(i,j,2,k)*tp_coef);
TIME_PENALTY(i,j,3,k)       =       ((abs(i-
j)+1)^exp_deg_tp)*(E_out(i,j,3,k)*tp_coef*extra_tp);
        end
        end

% COST FUNCTION %
COST(i,j,:,k)               =       E_in(i,j,:,k)-E_out(i,j,:,k)-
abs(TIME_PENALTY(i,j,:,k));
%COST3%
cost3(:,:,1,k)              =       COST(:,:,1,k);
cost3(:,1,1,k)              =       0;
mat_cost3(k,:,:)            =       cost3(:,:,1,k);
[max_cost3 roll_id3_1]      =       max(mat_cost3);
sq_max_cost3                =       squeeze(max_cost3);
%ID3%
roll_id3                    =       squeeze(roll_id3_1);
%COST4%
cost4(:,:,1,k)              =       COST(:,:,2,k);
mat_cost4(k,:,:)            =       cost4(:,:,1,k);
[max_cost4 roll_id4_1]      =       max(mat_cost4);
sq_max_cost4                =       squeeze(max_cost4);
%ID4%
roll_id4                    =       squeeze(roll_id4_1);
%COST5%
cost5(:,:,1,k)              =       COST(:,:,3,k);
cost5(1,:,:,k)              =       0;
mat_cost5(k,:,:)            =       cost5(:,:,1,k);
[max_cost5 roll_id5_1]      =       max(mat_cost5);
%ID5%
roll_id5                    =       squeeze(roll_id5_1);
sq_max_cost5                =       squeeze(max_cost5);
%TOTAL COST
[FC(i,j) GL_ID(i,j)]        =       max([(FC(i-
1,j)+sq_max_cost3(i,j));...
                                    (FC(i-1,j-
1)+sq_max_cost4(i,j));...
                                    (FC(i,j-
1)+sq_max_cost5(i,j))]);
            if GL_ID(i,j)==1
                w(i,j)=w(i-1,j)+(TIME(i-
1,j,1,roll_id3(i,j))/3600)*15*(pi/180);
            elseif GL_ID(i,j)==2
```

```
                w(i,j)=w(i-1,j-1)+(TIME(i-1,j-
1,2,roll_id4(i,j))/3600)*15*(pi/180);
            else
                w(i,j)=w(i,j-1)+(TIME(i,j-
1,3,roll_id5(i,j))/3600)*15*(pi/180);
            end
        end
        end
    end
end

%% DESCRIBING THE ROUTE %%

% GLOBAL COORDINATE ID %
for l=grd_X:-1:1
    for m=grd_Y:-1:1
        if GL_ID(l,m)==1
            GL_ID(l,1:(m-1))                =           0;
        elseif GL_ID(l,m)==3
            GL_ID(1:(l-1),m)                =           0;
        elseif GL_ID(l,m)==2
            GL_ID(l,1:(m-1))                =           0;
            GL_ID(1:(l-1),m)                =           0;
        end

% GLOBAL ROLL ID %
        if GL_ID(l,m)== 0
            GL_ROLL_ID(l,m)                 =           0;
        elseif l>1 && m>1 && GL_ID(l,m)==1
            GL_ROLL_ID(l,m)                 =
roll_id3(l,m);
        elseif l>1 && m>1 && GL_ID(l,m)==2
            GL_ROLL_ID(l,m)                 =
roll_id4(l,m);
        elseif l>1 && m>1 && GL_ID(l,m)==3
            GL_ROLL_ID(l,m)                 =
roll_id5(l,m);
        elseif l>1 && m==1
            GL_ROLL_ID(l,m)                 =
roll_id1(1,l);
        elseif l==1 && m>1
            GL_ROLL_ID(l,m)                 =
roll_id2(1,m);
        end
    end
end

 % ENERGY OUTPUTS %
 for i=1:grd_X
    for j=1:grd_Y

% Time Matrix Linearization %
        if GL_ID(i,j)== 0
        mat_time_lin(i,j )                  =           0;
        elseif GL_ID(i,j)== 3 && j>1
            mat_time_lin(i,j)               =           TIME(i,j-
1,GL_ID(i,j),GL_ROLL_ID(i,j));
        elseif GL_ID(i,j)== 1 && i>1
```

```
            mat_time_lin(i,j)                =           TIME(i-
1,j,GL_ID(i,j),GL_ROLL_ID(i,j));
        else
            mat_time_lin(i,j)                =           TIME(i-1,j-
1,GL_ID(i,j),GL_ROLL_ID(i,j));
        end
        vect_mat_time_lin1                   =
mat_time_lin(:)';
        vect_mat_time_lin2                   =
nonzeros(vect_mat_time_lin1);
        vect_mat_time_lin                    =
cumsum(vect_mat_time_lin2);
        vect_solar_time                      =
IP_TIME+(vect_mat_time_lin/3600);


% Energy Loss %
        if GL_ID(i,j)== 0
            mat_E_out(i,j)                   =           0;
        elseif GL_ID(i,j)== 3 && j>1
            mat_E_out(i,j)                   =
E_out(i,j,GL_ID(i,j),GL_ROLL_ID(i,j));
        elseif GL_ID(i,j)== 1 && i>1
            mat_E_out(i,j)                   =
E_out(i,j,GL_ID(i,j),GL_ROLL_ID(i,j));
        else
            mat_E_out(i,j)                   =
E_out(i,j,GL_ID(i,j),GL_ROLL_ID(i,j));
        end
        vect_mat_E_out                       =
mat_E_out(:)';
        vect_mat_E_out                       =
(nonzeros(vect_mat_E_out))./vect_mat_time_lin2;

% Energy Gain %
        if GL_ID(i,j)== 0
            mat1_E_in(i,j)                   =           0;
        elseif GL_ID(i,j)== 3 && j>1
            mat1_E_in(i,j)                   =           E_in(i,j-
1,GL_ID(i,j),GL_ROLL_ID(i,j));
        elseif GL_ID(i,j)== 1 && i>1
            mat1_E_in(i,j)                   =           E_in(i-
1,j,GL_ID(i,j),GL_ROLL_ID(i,j));
        else
            mat1_E_in(i,j)                   =           E_in(i-1,j-
1,GL_ID(i,j),GL_ROLL_ID(i,j));
        end
        if mat_E_out(i,j)==0
            mat2_E_in(i,j)=0;
        else
            mat2_E_in(i,j)=0.000000001;
        end
        mat_E_in(i,j)                        =
mat1_E_in(i,j)+mat2_E_in(i,j);
        vect_mat_E_in                        =
mat_E_in(:)';
        vect_mat_E_in                        =
(nonzeros(vect_mat_E_in))./vect_mat_time_lin2;
```

```
% Energy Balance %
        vect_mat_E_bal                          =
vect_mat_E_in-vect_mat_E_out;

    end
 end

%% PLOTTING THE RESULTS %%
% PLOT ROLL ID %
vect_GL_ROLL_ID                                 =
GL_ROLL_ID(:)';
vect_GL_ROLL_ID                                 =
nonzeros(vect_GL_ROLL_ID);
vect_GL_ROLL_DEG                                =
(vect_GL_ROLL_ID-ceil(grd_ROLL/2))*GRD_LEN_ROLL;
fs                                              =           28;
%fontsize

% PLOT ENERGY %
figure(1)
stairs(vect_solar_time,vect_mat_E_in,...
    '-.g','Linewidth',2,...
    'MarkerEdgeColor','k',...
    'MarkerFaceColor','g',...
    'MarkerSize',4)
hold on
stairs(vect_solar_time,vect_mat_E_out,...
    '--r','Linewidth',2,...
    'MarkerEdgeColor','k',...
    'MarkerFaceColor','g',...
    'MarkerSize',4)
hold on
stairs(vect_solar_time,vect_mat_E_bal,...
    'b','Linewidth',2,...
    'MarkerEdgeColor','k',...
    'MarkerFaceColor','g',...
    'MarkerSize',4)
ylabel('[ Watt ]','fontsize',fs)
xlabel('Time [h]','fontsize',fs)
hleg=legend('Power Generated','Power Consumption','Net Power');
set(hleg,'Location','NorthEast','fontsize',20);
grid minor

% PLOT ROLL ANGLE %
fig2=figure(2);
stairs(vect_solar_time,vect_GL_ROLL_DEG,...
    '-.cyans','Linewidth',2,...
    'MarkerEdgeColor','k',...
    'MarkerFaceColor','g',...
    'MarkerSize',5)
ylabel('Optimal Roll Angle [deg]','fontsize',fs)
xlabel('Time [h]','fontsize',fs)
grid minor

% PLOT ROUTE %
[ind_X_GL_ID,ind_Y_GL_ID,logical_GL_ID]=find(GL_ID>0);
fig3=figure(3);
```

```
plot(ind_X_GL_ID*GRD_LEN_XY,ind_Y_GL_ID*GRD_LEN_XY,...
    '--ro','LineWidth',2,...
    'MarkerEdgeColor','k',...
    'MarkerFaceColor','g',...
    'MarkerSize',5)
ylabel('coordinate -Y- [m]','fontsize',fs)
xlabel('coordinate -X- [m]','fontsize',fs)
grid on

% INSET PLOT%
[h_m h_i]=inset(fig3,fig2);
%set(h_i,'xtick','xlim')

%% CALCULATING THE OPTIMIZATION TIME %%
process_time=toc;
```

APPENDIX F

CALCULATION LOAD

Table F.1 Effect of the number of nodes on calculation load of the optimization process

Number of Nodes	Process Time [s]	CPU Used [%]	Memory Used [MB]
16	1.3	18	222
961	5.7	18	260
15876	375.1	35	290
63001	6221	45	380

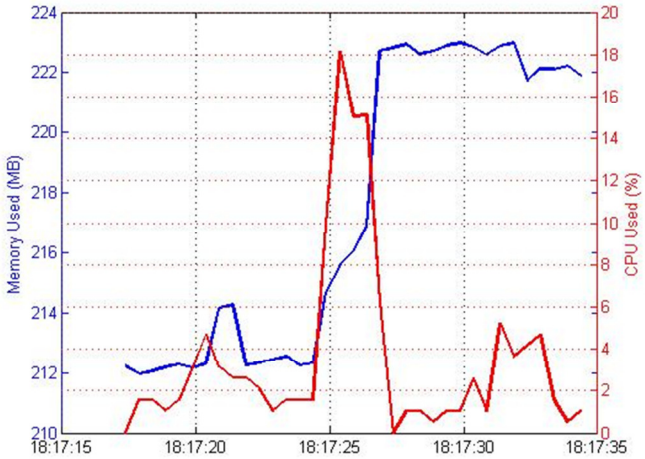

Figure F.1 Memory and CPU used for a grid formed from 16 nodes

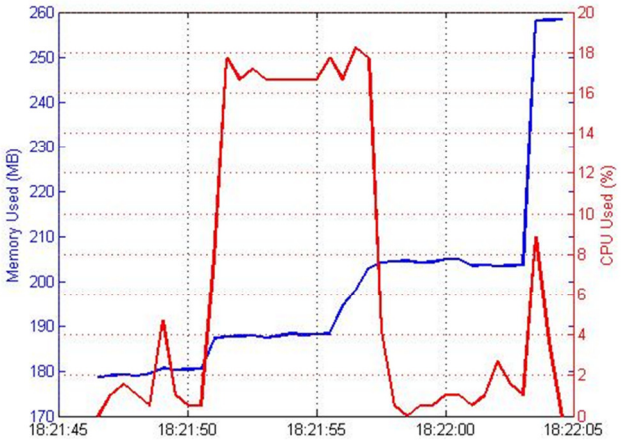

Figure F.2 Memory and CPU used for a grid formed from 961 nodes

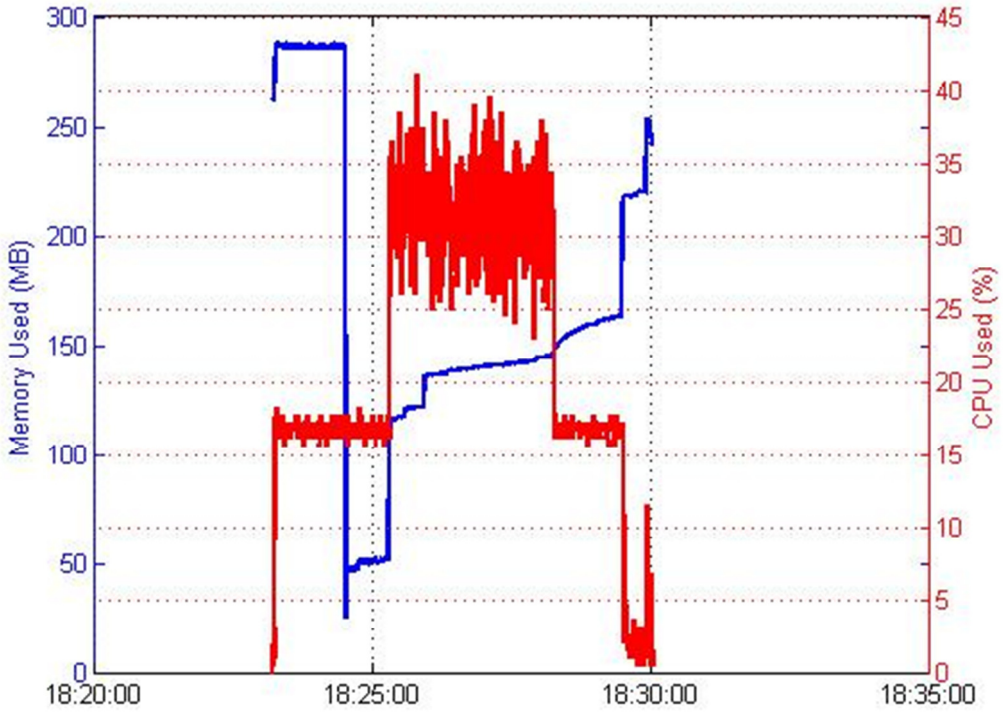

Figure F.3 Memory and CPU used for a grid formed from 15876 nodes

Figure F.4 Memory and CPU used for a grid formed from 63001 nodes